ELLIPTICAL METASURFACES FOR CLOAKING AND ANTENNA APPLICATIONS AT MICROWAVE AND TERAHERTZ FREQUENCIES

A Thesis
presented in partial fulfillment of requirements
for the degree of Master of Science
in the Department of Electrical Engineering
with Emphasis in Electromagnetics
The University of Mississippi

by

HOSSEIN MEHRPOURBERNETY

August 2015

ABSTRACT

One of the interesting applications of metamaterials is the phenomenon of electromagnetic invisibility and cloaking, which implies the suppression of bistatic scattering width of a given object, independent of incident and observation angles. In this regard, diverse techniques have been proposed to analyze and design electromagnetic cloak structures, including transformation optics, anomalous resonance methods, transmission-line networks, and plasmonic cloaking, among others. A common drawback of all these methods is that they rely on bulk materials, which are difficult to realize in practice. To overcome this issue, the mantle cloaking method has been proposed, which utilizes an ultrathin metasurface that provides anti-phase surface currents to reduce the scattering dominant mode of a given object. Recently, an analytical model has been proposed to cloak dielectric and conducting cylindrical objects realized with printed and slotted arrays at microwave frequencies. At low-terahertz (THz) frequencies, one of the promising materials to realize the required metasurface is graphene. In this regard, a graphene monolayer, characterized by inductive reactance, has been proposed to cloak dielectric planar and cylindrical objects. Then, it has been shown that a metasurface made of graphene nanopatches owns dual capacitive/inductive inductance and can be used to cloak both dielectric and conducting cylindrical objects at low-THz frequencies.

So far, planar and cylindrical dielectric and conducting structures have been studied. In our study, we have extended the concept and presented an accurate analytical approach to investigate

the cloaking of two-dimensional (2-D) elliptical objects including infinite dielectric elliptical cylinders using graphene monolayer; metallic elliptical cylinders, and also, as a special case, 2-D metallic strips using a nanostructured graphene patch array at low-THz frequencies. We have also obtained the results for cloaking of ellipses at microwave frequencies.

In this work, we propose a novel approach to reduce the mutual coupling between two closely spaced strip dipole antennas with the elliptical metasurfaces formed by conformal printed arrays of sub-wavelength periodic elements. We show that by covering each strip with the metasurface cloak, the antennas become invisible to each other and their radiation patterns are restored as if they were isolated. The electromagnetic scattering analysis pertained to the case of antennas with the frequencies far from each other is shown to be as a good approximation of a 2-D metallic strip scattering cancellation problem solved by expressing the incident and scattered fields in terms of radial and angular Mathieu functions, with the use of sheet impedance boundary conditions at the metasurface.

In addition, we extend the novel approach based on the concept of mantle cloaking in order to reduce the mutual near-field and far-field coupling between planar antennas in printed technology. To present the idea, we consider two microstrip-fed monopole antennas resonating at slightly different frequencies and show that by cloaking the radiating part of each antenna, the antennas become invisible to each other, and thus, the mutual coupling between the antennas is suppressed drastically. The cloak structure is realized by a conformal elliptical metasurface formed by confocal printed arrays of sub-wavelength periodic elements, partially embedded in the substrate. The presence of the metasurfaces leads to the restoration of the radiation patterns of the antennas as if they were isolated.

DEDICATION

This work is dedicated to my loving wife Atefeh, my parents, and my sister, whose never ending support and encouragement have sustained me throughout the completion of my studies and this research.

ACKNOWLEDGMENTS

I would like to thank my advisor Professor Alexander B. Yakovlev for his guidance and support throughout my graduate studies and research at the University of Mississippi. I express my deep gratitude to him for sharing his knowledge in electromagnetics as well as his personal time, invaluable suggestions, and constant support that made this work possible.

I would also like to thank Dr. Ramanarayanan "Vish" Viswanathan, the Chair of the Electrical Engineering Department, and Dr. Paul Goggans, Professor of Electrical Engineering, for serving as the members of the examining committee and for their helpful advice and assistance.

I take this opportunity to thank all of the Department of Electrical Engineering faculty members especially Dr. Richard Gordon, Associate Professor of Electrical Engineering, and Dr. Elliot Hutchcraft, Associate Professor of Electrical Engineering, for their help and support. Also, I am thankful to all fellow graduate students in the Department of Electrical Engineering, who have been friendly and helpful.

Finally, last but not least, I am most grateful to my wife, my parents, and my sister for their patience and love and to all my friends for their incessant encouragement and support all these years.

Hossein Mehrpourbernety

TABLE OF CONTENTS

LIST OF FIGURES

FIGURE PAGE

CHAPTER I

CLOAKING OF ELLIPTICAL CYLINDERS AND STRIPS

1.1 Introduction

In recent years, electromagnetic invisibility has caught researchers' attention and interest. This phenomenon makes it possible to suppress the bistatic scattering width of a given object, independently of the incident and observation angles. Cloaking technology provides various interesting applications such as camouflaging, non-invasive probing [1, 2], low-interference communications [3, 4], and imaging, among others. In this regard, different methods have been proposed in order to analyze and design cloak structures such as transformation optics [5–9], which is sensitive to tiny perturbations in practice [10], anomalous resonance method [11], and transmission-line networks [12–14]. Another technique to mention is the plasmonic cloaking method [15] which is based on the use of the exotic properties of bulk isotropic low or negative index materials to suppress the dominant scattering mode of the object to be cloaked [1, 3, 16–20]. All the methods mentioned above rely on bulk volumetric metamaterials, which in practice have a thickness comparable to the size of the object to be cloaked, and their realization is not an easy task. Recently, in order to overcome this common drawback, a different cloaking method has been proposed [21–28] based on the concept of mantle cloaking to make planar, cylindrical, and spherical objects invisible. In this method, an infinitesimally thin metasurface is used to create anti-phase surface currents in order to suppress the dominant electromagnetic scattering mode of

a moderately sized object, and thus to make the object invisible to the incoming electromagnetic wave. To implement the technique at microwave frequencies, an analytical model has been presented in [26], wherein practical cloaks composed of one-dimensional (1-D) horizontal and vertical metallic strips and two-dimensional (2-D) conformal printed (patches, Jerusalem crosses, and cross dipoles) and slotted (meshes, slot-Jerusalem crosses, and slot-cross dipoles) arrays of sub-wavelength periodic elements have been proposed. By properly designing the metasurface, the required average surface reactance is tailored, and thus, a drastic electromagnetic scattering reduction is achieved. However, at higher frequencies such as terahertz (THz), infrared (IR), and optical frequencies, the realization of the mantle cloak metasurface is more difficult due to the increase of losses in metallic elements. In this regard, one of the promising materials to implement the mantle cloaking method at low-THz frequencies is graphene.

Graphene is a single layer of carbon atoms in a honeycomb lattice [29], which is particularly interesting due to its unique thermal, mechanical, and electrical properties that makes it useful in various electronic and electromagnetic applications [30–34]. In order to analyze and consider graphene for electromagnetic applications, a model has been proposed for its complex surface conductivity based on the Kubo formula [35],

$$\sigma_s(\omega, \mu_c, \tau, T) = \frac{-je^2(\omega + j\tau^{-1})}{\pi\hbar^2}$$

$$\times \left[\frac{1}{(\omega+j\tau^{-1})^2}\int_0^\infty \left(\frac{\partial f_d(\varepsilon)}{\partial \varepsilon} - \frac{\partial f_d(-\varepsilon)}{\partial \varepsilon}\right)\varepsilon d\varepsilon - \int_0^\infty \frac{f_d(-\varepsilon)-f_d(\varepsilon)}{(\omega+j\tau^{-1})^2-4(\varepsilon/\hbar)^2}d\varepsilon\right] \quad (1.1)$$

where $-e$ is the charge of an electron, ω is the radian frequency, $\hbar$ is the reduced Planck's constant, $f_d(\varepsilon) = -(e^{(\varepsilon-\mu_c)/k_BT} + 1)^{-1}$ is the Fermi-Dirac distribution, k_B is Boltzmann's constant, T is temperature, ε is the energy, μ_c is the chemical potential, and τ is the momentum relaxation time.

It should be mentioned that in our calculations it is assumed $T = 300$ K and $\tau = 1.5$ ps. The first term in equation (1.1) is related to the intraband contribution and can be obtained in closed form by [35]:

$$\sigma_{\text{intra}} = j\frac{e^2 k_B T}{\pi\hbar^2(\omega + j\tau^{-1})}\left[\frac{\mu_c}{k_B T} + 2\ln\left(e^{-\frac{\mu_c}{k_B T}} + 1\right)\right]. \quad (1.2)$$

The second term is related to the interband contribution and in case of $k_B T \ll |\mu_c|,\ \hbar\omega$ can be approximated by [35]

$$\sigma_{\text{inter}} = \frac{je^2}{4\pi\hbar}\ln\left(\frac{2|\mu_c| - (\omega + j\tau^{-1})\hbar}{2|\mu_c| + (\omega + j\tau^{-1})\hbar}\right). \quad (1.3)$$

It should be noted that in the low-THz region, up to 15 THz, the intraband contribution dominates the interband contribution; nevertheless we take into account both terms in our calculations.

Recently, it has been shown that an atom thick homogeneous graphene monolayer enables a drastic scattering reduction for dielectric planar and cylindrical objects at low-THz frequencies [36]. In this frequency range, the ultrahigh mobility of graphene monolayer (more than 20000 cm^2 V^{-1} S^{-1}) [36] makes it possible to achieve a nearly imaginary surface conductivity, and consequently, a low-loss inductive metasurface. However, it should be noted that in case of a metallic cylinder, a capacitive reactance is needed and graphene monolayer cannot be used for cloaking. It has been shown that a metasurface formed by a periodic array of sub-wavelength graphene nanopatches possesses a dual capacitive/inductive surface reactance at low-THz frequencies [37]. In [38], this property of graphene nanopatches has been taken into consideration in order to cloak both dielectric and conducting cylindrical objects by properly tuning the surface impedance of graphene metasurface. However, so far, the mantle cloaking method with the use of

graphene (and graphene metasurface) has been studied only for symmetric geometries such as dielectric and metallic circular cylinders and spheres.

In this chapter, we extend the idea of the mantle cloaking method and the scattering cancellation concept to cloak elliptical structures, which possess non-symmetric geometries unlike circular cylinders, by using confocal and conformal elliptically shaped graphene metasurfaces. It is worth noting that since elliptical cylinders have non-symmetric cross-sections, the use of cylindrical metasurfaces of circular cross-section will no longer provide efficient cloaking. In this regard, here we propose a novel analytical approach in order to cloak two-dimentional elliptical objects, including an infinitely long dielectric elliptical cylinder with a graphene monolayer and a metasurface formed by graphene nanopatches; a metallic elliptical cylinder with the same metasurface, and as a special case, a 2-D metallic strip with a nanostructured graphene patch array at low-THz frequencies. The novel approach presented in this chapter is based on the fact that the electromagnetic scattering cancellation from cloaked elliptical objects and strips is ruled by the elliptical modes that can be formulated and represented by even and odd radial and angular Mathieu functions [39]. We show that the use of confocal and conformal elliptically shaped metasurfaces is indispensable in providing an anti-phase surface current based on the concept of mantle cloaking, and consequently, in order to reduce the dominant elliptical scattering mode. A special case pertains to a 2-D metallic strip as a degenerated metallic elliptical cylinder, which can be cloaked by placing the focal points of the metasurface at the edges of the strip. Recently, we have presented one of the applications of cloaking metallic strips at microwave frequencies [40], in which elliptical cloak metasurfaces formed by periodic arrays of sub-wavelength elements have been utilized in order to reduce the mutual coupling between strip dipole antennas. A similar

concept may be used for reducing the destructive mutual coupling between strip antennas at THz frequencies. Besides, closed-form expressions for the optimum surface reactance of metasurfaces have been derived for dielectric and metallic elliptical cylinders under a transverse magnetic (TM) polarized plane-wave incidence in the quasi-static limit. In addition to all mentioned, we extend the idea of cloaking a single elliptical object to multiple elliptical cylinders and strips which form a cluster of closely spaced, intersecting, and merging elliptical objects with a size comparable to the wavelength at the design frequency.

The chapter is organized as follows. Section 1.2 concerns the proposed analytical model for the analysis of cloaking of 2-D dielectric and metallic elliptical cylinders, and a metallic strip as a special case. In Section 1.3, we present the numerical results for cloaking of single and multiple elliptical structures. Section 1.4 is allocated to the conclusions. A time dependence of the form $e^{-j\omega t}$ is assumed and suppressed.

1.2 Formulation of the Scattering Problem

Here, we present the mathematical formulation to analyze the scattering problem for the cases of a dielectric elliptical cylinder covered with a graphene monolayer (Figure 1.1(a)) and a nanostructured graphene metasurface (Figure 1.1(b)); a metallic elliptical cylinder coated with the same nanostructured graphene metasurface (Figure 1.1(c)) and a 2-D strip covered by an elliptically shaped dielectric spacer and a metasurface (Figure 1.1(d)). The analysis of the problem is based on the method of separation of variables to solve the 2-D wave equation in the elliptical coordinates $(u,\ v,\ z)$, and consequently, to solve the well-known angular and radial Mathieu equations. It should be mentioned that the solution provided here is related to the case of an infinitely long elliptical metallic cylinder covered by a metasurface (the scattering problems for

other structures shown in Figure 1.1 are omitted for the sake of brevity).

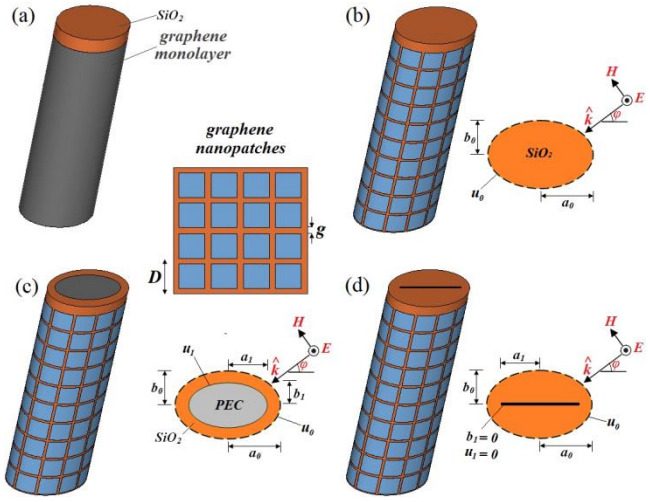

Figure 1.1 Schematic representation of elliptical objects with a TM-polarized plane wave at normal incidence: (a) dielectric elliptical cylinder cloaked with graphene monolayer, (b) the same cylinder with graphene nanopatches, (c) metallic elliptical cylinder with the same graphene metasurface, and (d) metallic strip with graphene nanopatches.

Then, we express the incident, scattered, and transmitted electric and magnetic fields in terms of even and odd angular and radial Mathieu functions in the elliptical coordinates. In this regard, the incident electric field, which is related to the free-space region $u > u_0$ ($u_0 = \tanh^{-1}(b_0/a_0)$) can be represented as follows [41]:

$$E_z^i = \sqrt{8\pi}\sum_n j^{-n}\frac{J_{pm}(q_0,u,n)}{N_{pm}(q_0,n)}S_{pm}(q_0,v,n)\,S_{pm}(q_0,\varphi,n) \tag{1.4}$$

where $J_{pm}(q_0,u,n)$ is the radial Mathieu function of the first kind, $S_{pm}(q_0,v,n)$ is the angular Mathieu function, $N_{pm}(q_0,n)$ is the normalization constant, u is the radial parameter, v is the angular parameter, and $q_0 = k_0^2F^2/4$ (k_0 is the wave number in free space and F is the focus of the ellipse or strip). The scattered electric field pertained to the region $u > u_0$ can be written as:

$$E_z^s = \sqrt{8\pi}\sum_n j^{-n}a_{pm}^{(n)}\,H_{pm}^{(1)}(q_0,u,n)S_{pm}(q_0,v,n)\,S_{pm}(q_0,\varphi,n) \tag{1.5}$$

where $H_{pm}^{(1)}(q_0,u,n)$ is the radial Mathieu function of the third kind, which indicates the outgoing

wave, and $a_{pm}^{(n)}$ are the unknown coefficients to be determined. Similarly, the transmitted electric field inside the dielectric spacer $u_1 < u < u_0$ can be expressed as:

$$E_z^t = \sqrt{8\pi}\sum_n j^{-n}[b_{pm}^{(n)} J_{pm}(q_1,u,n) + c_{pm}^{(n)} Y_{pm}(q_1,u,n)]\, S_{pm}(q_1,v,n)\, S_{pm}(q_0,\varphi,n) \quad (1.6)$$

where $Y_{pm}(q_0,u,n)$ is the radial Mathieu function of the second kind, $b_{pm}^{(n)}$ and $c_{pm}^{(n)}$ are the unknown transmitted field expansion coefficients, and $q_1 = k_1^2F^2/4$ (k_1 is the wave number in the dielectric spacer). It should be noted that p and m denote either even or odd functions.

The incident, scattered, and transmitted magnetic fields can be obtained by using Maxwell equations as follows:

$$H_v^i = \frac{j}{\omega\mu h}\sqrt{8\pi}\ \sum_n j^{-n}\frac{J'_{pm}(q_0,u,n)}{N_{pm}(q_0,n)} S_{pm}(q_0,v,n)\, S_{pm}(q_0,\varphi,n) \quad (1.7.1)$$

$$H_v^s = \frac{j}{\omega\mu h}\sqrt{8\pi}\ \sum_n j^{-n} a_{pm} H_{pm}^{(1)'}(q_0,u,n)\, S_{pm}(q_0,v,n)\, S_{pm}(q_0,\varphi,n) \quad (1.7.2)$$

$$H_v^t = \frac{j}{\omega\mu h}\sqrt{8\pi}\sum_n j^{-n}[b_{pm} J'_{pm}(q_1,u,n) + c_{pm} Y'_{pm}(q_1,u,n)]$$
$$\times S_{pm}(q_1,v,n)\, S_{pm}(q_0,\varphi,n) \quad (1.7.3)$$

where $h = F\sqrt{\cosh^2 u - \cos^2 v}$ is the scalar factor in the elliptical coordinate system. It should be noted that the prime indicates the derivative of the functions with respect to the variable u.

The unknown coefficients in equations (1.5) and (1.6) can be determined by imposing the boundary condition at $u_1 = \tanh^{-1}(b_1/a_1)$, which is the surface of the metallic elliptical cylinder ($u_1 = 0$ for the strip case), the boundary conditions at the metasurface, and also, by applying the orthogonality property of angular Mathieu functions. It should be mentioned that the tangential components of the electric fields are continuous across the metasurface while the use of an impedance surface results in the discontinuity of the tangential components of magnetic fields

($H_v^{\tan}$). Hence, the boundary conditions can be written as:

$$E_z^t|_{u=u_1} = 0 \tag{1.8.1}$$

$$E_z^i\big|_{u=u_0^+} + E_z^s|_{u=u_0^+} = E_z^t|_{u=u_0^-} \tag{1.8.2}$$

$$E_z^t|_{u=u_0^-} = Z_s\left[H_v^i\big|_{u=u_0^+} + H_v^s|_{u=u_0^+} - H_v^t|_{u=u_0^-}\right] \tag{1.8.3}$$

where Z_s is the surface impedance of the metasurface. The bistatic scattering width can be reduced drastically for all the incident angles by choosing an appropriate value for Z_s. For a metasurface realized by nanostructured graphene patch array, as shown in Fig. 1, the surface impedance can be expressed as [37]:

$$Z_s = R_s - jX_s = \frac{D}{\sigma_s(D-g)} + j\frac{\pi}{2\omega\varepsilon_0\left(\frac{\varepsilon_r+1}{2}\right)D\ln\left[\csc\left(\frac{\pi g}{2D}\right)\right]} \tag{1.9}$$

where σ_s is the complex surface conductivity of graphene calculated using the Kubo formula in equation (1.1), with the analytical representations for the intraband and interband contributions as shown in equations (1.2) and (1.3), respectively, R_s is the surface resistance per unit cell related to the conduction losses, and X_s is the surface reactance per unit cell; D and g are the periodicity and gap size, respectively, ε_r is the relative permittivity of the dielectric elliptical cylinder or the spacer for the conducting elliptical cylinder. The first term in equation (1.9) accounts for the kinetic inductance and resistance per unit cell of graphene nanopatches, and the second term corresponds to the capacitance of graphene patch array.

The unknown coefficients have been determined by applying the boundary conditions mentioned above and solving the matrix equation presented in Appendix. Then, the bistatic scattering width ($\sigma_{2\mathrm{D}}$) for a TM-polarized plane-wave excitation can be obtained by using the asymptotic form of the radial Mathieu function of the third kind at the desired frequency as follows:

$$\frac{\sigma_{2D}}{\lambda} = \left|\sum_n \sqrt{8\pi}\, j^{-2n} a_{pm}\, S_{pm}(q_0, v, n) S_{pm}(q_0, \varphi, n)\right|^2. \quad (1.10)$$

Also, the total scattering width as a quantitative measure of the overall visibility of the object can be obtained by taking the average of the bistatic scattering width with respect to the observation angle (v) as follows:

$$\sigma_{\text{total}} = \frac{1}{2\pi}\int_0^{2\pi} \sigma_{2D}(v)\, dv\ . \quad (1.11)$$

Now, in order to be able to reduce the scattering cross-section of any given elliptical object drastically at the desired frequency, we present the closed-form conditions for both dielectric and metallic elliptical cylinders. These conditions have been obtained by setting the coefficients $a_{pm}^{(n)}$ to zero. It is also informative to analyze how the cloaking condition can be expressed in the quasi-static limit, for which $q_0,\ q_1 \ll 1$. In this case, the required optimum surface reactance to cloak dielectric elliptical cylinders shown in Figure 1.1(a or b) for a TM-polarized plane-wave incidence has been derived as:

$$X_{\text{diel}} = -\omega\mu F \frac{1 - q_1 \sinh^2 u_0}{2(q_0 - q_1)\ \sinh u_0}\ . \quad (1.12)$$

For a metallic elliptical cylinder with a relatively thin dielectric spacer and permittivity ε_r, the closed-form required optimum surface reactance in the quasi-static limit has been obtained as:

$$X_{\text{PEC}} = -\omega\mu F \frac{(u_0 - u_1)\ \cosh u_0}{1 + \left(q_0(u_0 - u_1) + q_1\left(u_1 + \frac{1}{2}\ln q_1\right)\right)\ \sinh 2u_0}. \quad (1.13)$$

It should be mentioned that by appropriately balancing the capacitance of the patch array and the kinetic inductance of graphene, the same elliptically shaped metasurface formed by graphene nanopatches can be utilized in order to meet both required surface reactances, and consequently, cloak both dielectric and metallic elliptical cylinders at low-THz frequencies.

The optimum required surface reactances for the dielectric and metallic elliptical cylinders

and the strips shown in Figure 1.1, calculated based on equations (1.12) and (1.13) are plotted versus frequency in Figure 1.2. The detailed values for the parameters of each geometry at the design frequency $f = 3$ THz are provided in Section 1.3. Also, the frequency dispersion of the surface reactance for each cloak metasurface including (i) a graphene monolayer with $\mu_c = 0.6158$ eV, (ii) a graphene-nanopatch metasurface with $\mu_c = 0.2672$ eV, $D = 5.064$ μm, and $g = 0.524$ μm, (iii) the same metasurface with $\mu_c = 0.55$ eV, and (iv) a metasurface formed by graphene nanopatches with $\mu_c = 0.9$ eV, $D = 5.29$ μm, and $g = 0.6$ μm, is depicted in Figure 1.2. It clearly shows that how the optimum surface reactance required for cloaking of each structure can be realized by tuning the parameters of the respective metasurface.

It is also worth noting that the dual capacitive/inductive behavior of the array of graphene nanopatches makes it possible to use the same metasurface in order to cloak both dielectric and conducting elliptical cylinders.

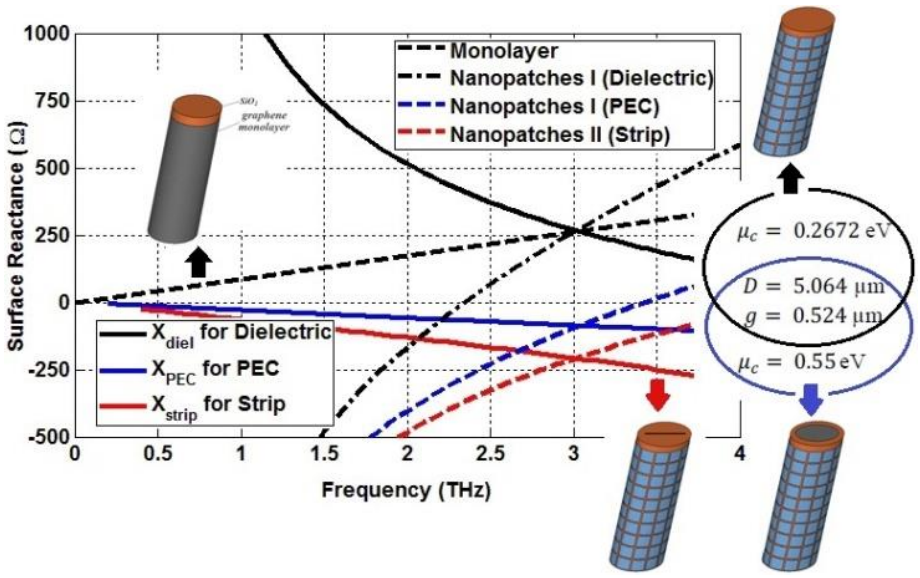

Figure 1.2 Surface Reactance of a graphene monolayer and a graphene-nanopatch metasurface (Nanopatches I) for the dielectric elliptical cylinder, and the same metasurface for the conducting elliptical cylinder, and a metasurface formed by an array of graphene nanopatches (Nanopatches II) for the strip.

1.3 Results and Discussions

In this section, we consider several elliptical objects cloaked by confocal elliptically shaped metasurfaces in order to present the applicability and effectiveness of the proposed analytical approach. The cloaking is studied for single elliptical objects, and then the cases of multiple objects and clusters are presented. The results of our analytical approach are compared and confirmed by full-wave numerical simulations with CST Microwave Studio [42].

1.3.1 Cloaking of Elliptical Cylinders and Strips

1.3.1.1 Dielectric Elliptical Cylinder Cloaked by a Graphene Monolayer

In order to reduce the electromagnetic scattering from a dielectric cylinder, it was shown that a mantle cloak with inductive surface reactance is required [36]. Following the idea and due to the fact that a single atom thick graphene monolayer provides an inductive reactance at low-

THz frequencies, a dielectric elliptical cylinder can be cloaked once the required surface reactance is found and by choosing appropriate parameters for the graphene monolayer. In this regard, for a given infinitely long dielectric elliptical cylinder shown in Fig. 1(a) with the relative permittivity $\varepsilon_r = 4$ (silicon dioxide), $a_0 = 12.5$ μm $(\lambda_0/8)$, $b_0 = 10$ μm $(\lambda_0/10)$, the required surface reactance is found to be $X_s = 260\ \Omega$ based on (12) with $\mu_c = 0.6158$ eV for the design frequency of $f = 3$ THz. To visualize this scattering reduction, the bistatic scattering widths for both uncloaked (with no cover) and cloaked (covered by the graphene monolayer) cases with different angles of incidence (φ) are shown in Figure 1.3(a). In Figure 1.3(b), the polar representation of the bistatic scattering width obtained by analytical and full-wave simulation results is shown for $\varphi = 45°$. Also, the total scattering width, as a quantitative measure of its overall visibility for all observation angles, is shown in Figure 1.4 with respect to the incident angle of $\varphi = 45°$. The analytical results are validated by using numerical full-wave simulations obtained with CST Microwave Studio. In addition, Figure 1.5 illustrates the snapshots of electric field distributions for both cloaked and uncloaked cases with $\varphi = 45°$. It can be clearly observed that in the absence of the graphene monolayer the electric field distribution is intensely disturbed while in case of its presence the electric field distribution is uniform, which indicates that the object does not exist seemingly in the electromagnetic field.

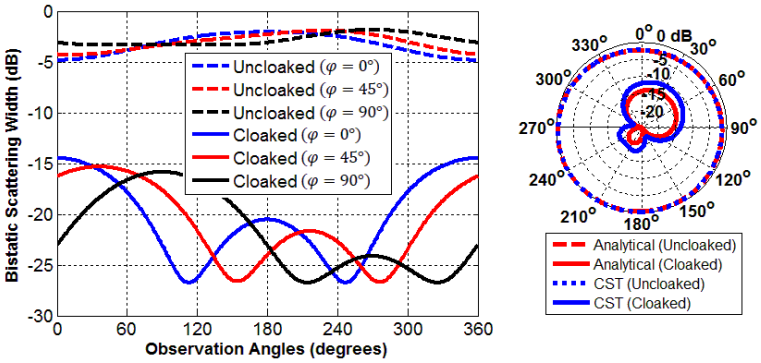

(a) (b)

Figure 1.3 (a) Bistatic scattering widths for uncloaked and cloaked (with graphene monolayer) cases with respect to different incident angles in the $x-y$ plane, and (b) analytical and full-wave total scattering widths for uncloaked and cloaked cases with $\varphi = 45°$.

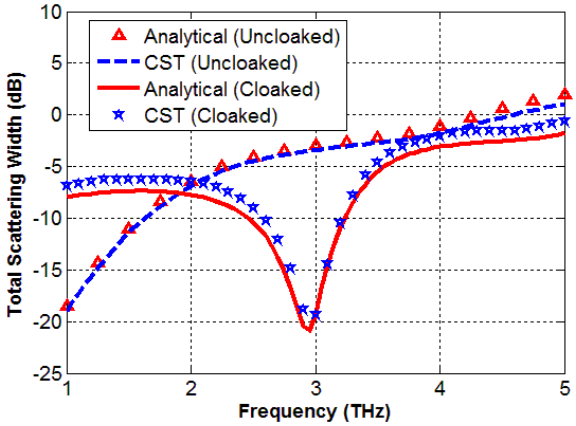

Figure 1.4 Analytical and full-wave total scattering widths for uncloaked and cloaked cases with the incident angle of $\varphi = 45°$.

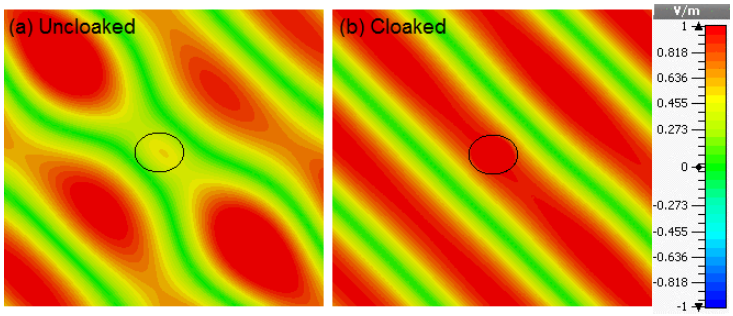

Figure 1.5 Snapshots of the electric field distribution for uncloaked and cloaked (with graphene monolayer) infinitely long dielectric elliptical cylinder illuminated by a TM-polarized plane wave at normal incidence with $\varphi = 45°$.

1.3.1.2 Dielectric Elliptical Cylinder Cloaked by a Metasurface

Here, we consider the same dielectric elliptical cylinder, however, instead of a graphene monolayer we employ a cloak metasurface formed by an array of graphene nanopatches. As mentioned in Section 1.3.1.1, the required surface reactance is $X_s = 260\ \Omega$ at the design frequency of $f = 3$ THz. In order to realize the metasurface, according to equation (1.9), the parameters of the graphene-nanopatch metasurface are found: $D = 5.064$ μm, $g = 0.524$ μm, and $\mu_c = 0.2672$ eV. It should be noted that the graphene-nanopatch metasurface requires a chemical potential much lower than that of the uniform graphene monolayer discussed in Section 1.3.1.1. The polar representations of the bistatic scattering width of the structure for both uncloaked and cloaked cases are plotted in Figure 1.6 with the incident angles of $\varphi = 0°$, $\varphi = 45°$, and $\varphi = 90°$, respectively. The figure illustrates that the bistatic scattering width of the dielectric elliptical cylinder is reduced remarkably for all the incident and observation angles. Also, the calculated and simulated total scattering widths of the object with $\varphi = 90°$ are shown in Figure 1.7. The analytical results agree well with the full-wave simulation results, confirming a drastic reduction of the total scattering width. In addition, as shown in Figure 1.8, it can be clearly seen that the wavefronts of the electric field are restored by wrapping the suitable graphene metasurface around the object, while in the absence of the mantle cloak, the electric field is strongly disturbed.

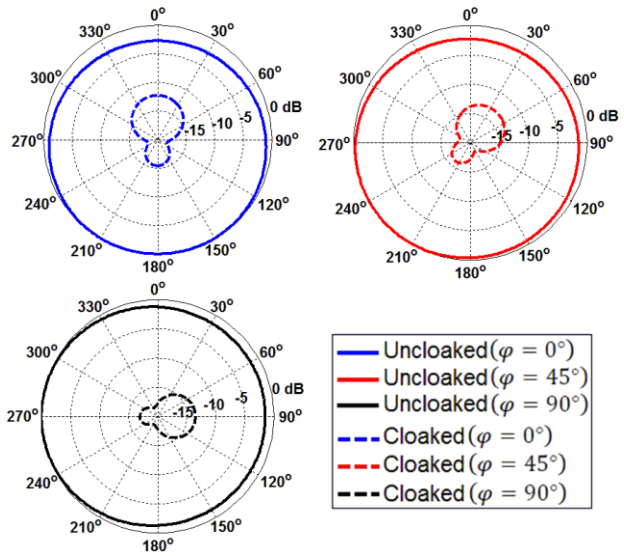

Figure 1.6 Polar representations of the bistatic scattering widths of the object in the $x - y$ plane with the incident angles of $\varphi = 0°$, $\varphi = 45°$, and $\varphi = 90°$.

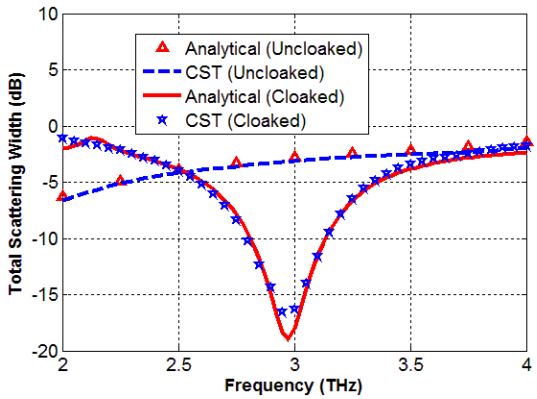

Figure 1.7 Analytical and full-wave total scattering widths for uncloaked and cloaked cases with the incident angle of $\varphi = 90°$.

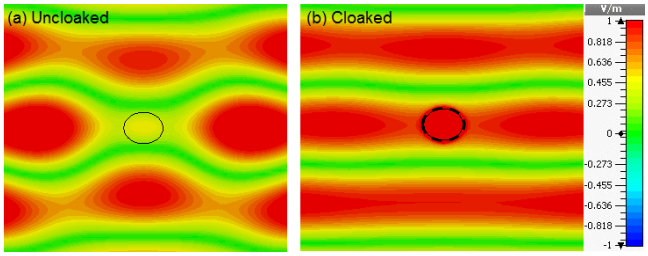

Figure 1.8 Snapshots of the electric field distribution for uncloaked and cloaked (with graphene nanopatches) infinitely long dielectric elliptical cylinder illuminated by a TM-polarized plane wave at normal incidence with $\varphi = 90°$.

1.3.1.3 Metallic Elliptical Cylinder

Consider the metallic elliptical rod shown in Figure 1.1(c), with the dimensions $a_1 = 10.04$ μm ($\lambda_0/9.96$), $b_1 = 6.67$ μm ($\lambda_0/15$), $a_0 = 12.5$ μm ($\lambda_0/8$), $b_0 = 10$ μm ($\lambda_0/10$), and the dielectric spacer with relative permittivity $\varepsilon_r = 4$ (silicon dioxide). As it is mentioned above, a capacitive reactance is required for cloaking the metallic ellipse. In this regard, the same metasurface mentioned in Section 1.3.1.2 is considered. Here, the chemical potential is set to $\mu_c = 0.55$ eV in order to realize the required surface reactance of $X_s = -83.45\ \Omega$ based on the optimum surface reactance provided in equation (1.13). The total scattering width of this cloak design is illustrated in Figure 1.9, which confirms that the scattering width is significantly reduced at the design frequency of $f = 3$ THz for different incident angles. Also, the analytical and full-wave results of the total scattering widths for a TM-polarized plane-wave incidence with $\varphi = 0°$ are shown in Figure 1.10. The snapshots of the electric field and the vector power-flow distributions are shown in Figure 1.11 for cloaked and uncloaked cases illustrating the effective cloaking, which illustrates how the presence of the metasurface resolves the perturbation of the electric field and the power.

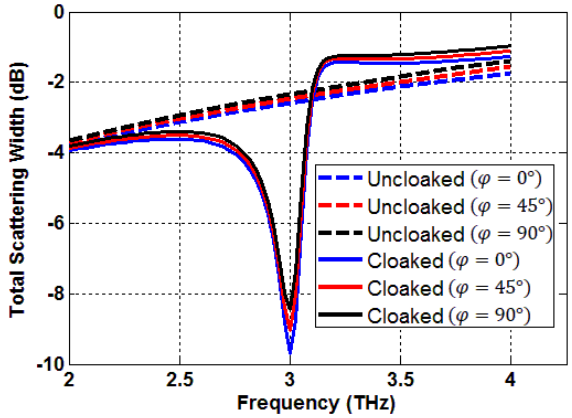

Figure 1.9 Total scattering widths for uncloaked and cloaked cases with the different incident angles of $\varphi = 0°$, $\varphi = 45°$, and $\varphi = 90°$.

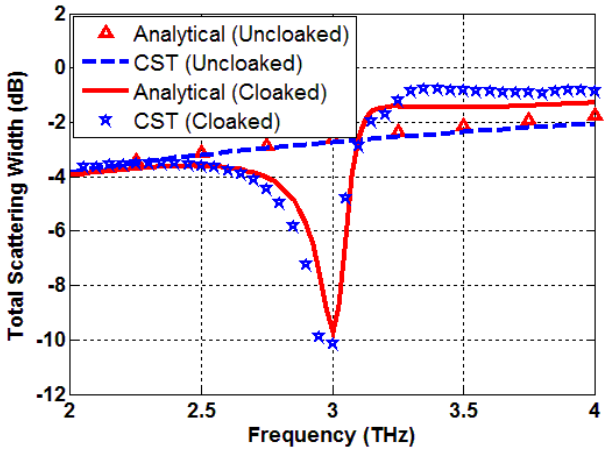

Figure 1.10 Analytical and full-wave results for the total scattering widths of uncloaked and cloaked cases with the incident angle of $\varphi = 0°$.

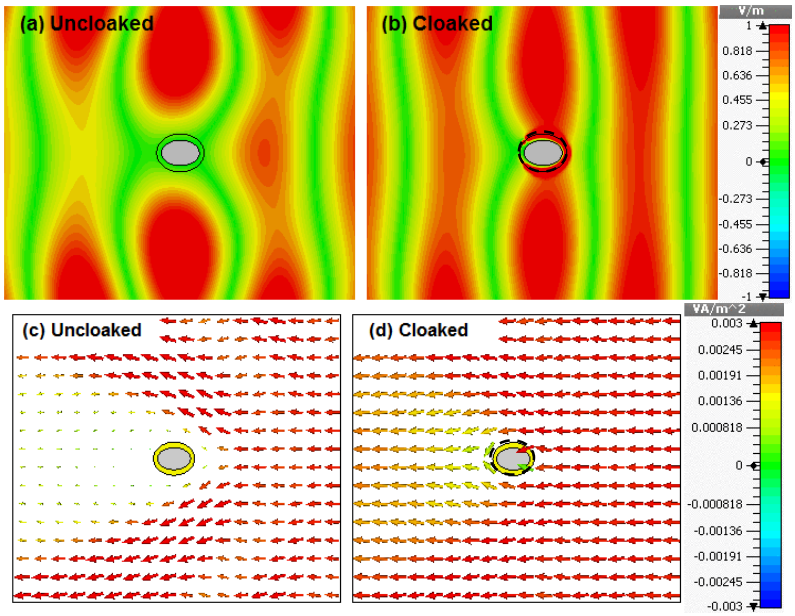

Figure 1.11 Snapshots of the electric field distribution for (a) uncloaked and (b) cloaked (with graphene nanopatches) infinite metallic elliptical cylinder. Vector power-flow distribution for (c) uncloaked and (d) cloaked cases, illuminated by a TM-polarized plane wave at normal incidence with $\varphi = 0°$.

1.3.1.4 Metallic Strip

Now, we consider a special case of a 2-D metallic strip as a degenerated metallic elliptical cylinder ($b_1 = 0$). In order to cancel the scattering waves from a strip, an elliptical metasurface

has been utilized. The optimum scattering reduction is achieved by placing the focal points of the elliptically shaped cloak metasurface at the edges of the strip. Figure 1.1(d) shows a strip with an elliptical metasurface formed by an array of graphene nanopatches wrapped around the dielectric spacer with the relative permittivity $\varepsilon_r = 4$. The dimensions of the structure are: $a_0 = 10.04$ µm ($\lambda_0/9.96$), $b_0 = 6.67$µm ($\lambda_0/15$), $a_1 = 7.5 = F$ µm ($\lambda_0/13.33$), and $b_1 = 0$ µm. Here, the required surface reactance is determined analytically to be $X_s = -69.5\ \Omega$ based on the optimum surface reactance presented in (13), which can be realized by choosing the parameters of the graphene-nanopatch metasurface as $D = 5.29$ µm, $g = 0.6$ µm, and $\mu_c = 0.9$ eV. The analytical results for the total scattering width of the metallic strip with various angles of incidence and both uncloaked and cloaked cases are shown in Figure 1.12. Also, comparisons between the analytical and full-wave simulation results of the total and bistatic scattering widths of the strip are presented in Figures 1.13(a) and 13(b), respectively. In addition, the electric field snapshots for both uncloaked and cloaked cases are shown in Figure 1.14. It confirms the fact that the fields are not disturbed in case of using the metasurface and the strip is hidden from the incoming wave. Figure 1.15 depicts the far-field scattering pattern of the metallic strip on the same scale for uncloaked and cloaked cases.

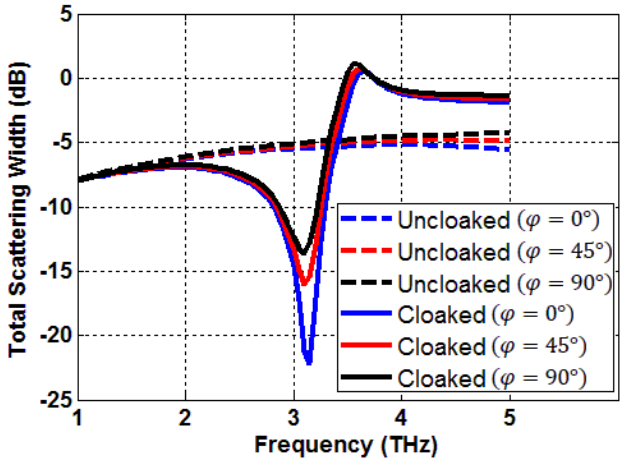

Figure 1.12 Total scattering widths for the metallic 2-D strip with different incident angles of $\varphi = 0°$, $\varphi = 45°$, and $\varphi = 90°$.

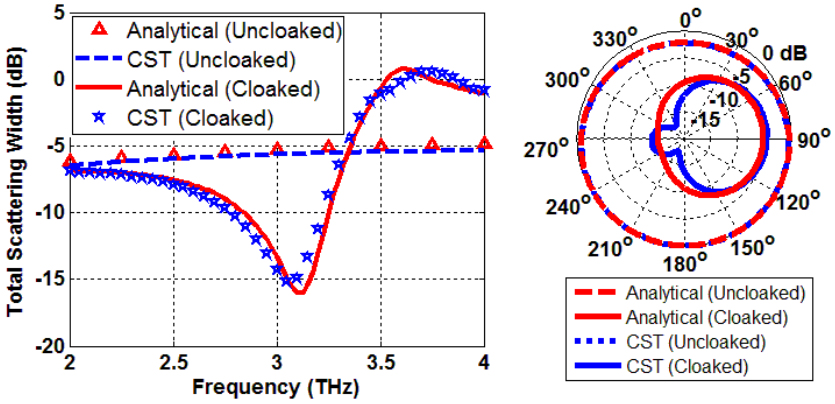

(a) (b)

Figure 1.13 Analytical and full-wave results for (a) total scattering widths and (b) bistatic scattering widths, for uncloaked and cloaked cases with the incident angle of $\varphi = 45°$ in the $x - y$ plane.

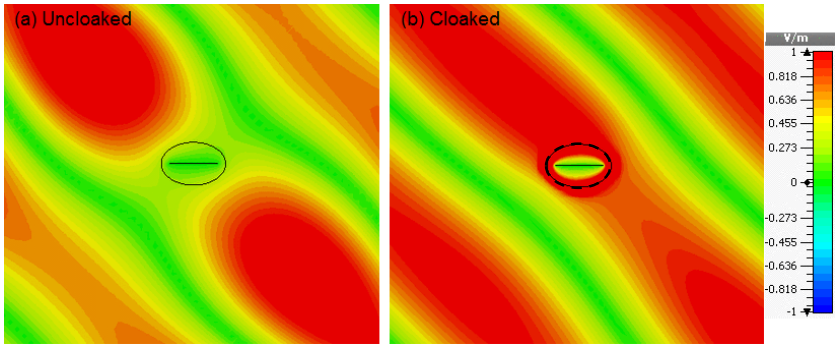

Figure 1.14 Snapshots of the electric field distribution for uncloaked and cloaked (with graphene nanopatches) infinite metallic 2-D strip illuminated by a TM-polarized plane wave at normal incidence with $\varphi = 45°$.

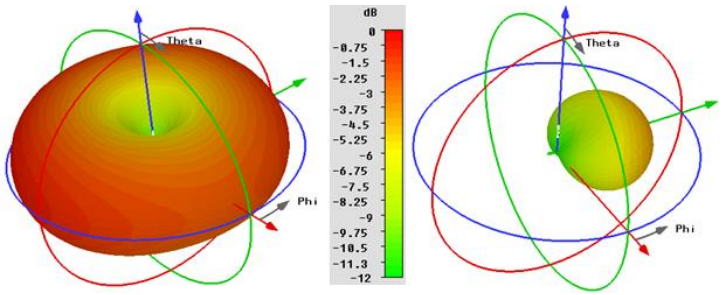

(a) (b)

Figure 1.15 Far-field scattering patterns of the metallic strip for (a) uncloaked and (b) cloaked cases, plotted on the same scale with the incident angle of $\varphi = 45°$.

1.3.2 Cloaking a Cluster of Elliptical Objects

Following our analytical approach discussed in the previous section to cloak various single dielectric and conducting objects at low-THz frequencies, here we extend the idea and present the cloaking of multiple elliptical objects which form a cluster. It has been shown in [43] that plasmonic covers may cloak multiple impenetrable spherical objects. However, the proposed cover is made of a material with a combination of plasmonic properties and with a magnetic permeability higher than that of the free space ($\mu = 5.1\,\mu_0$), which is difficult to realize in practice. As shown in Section 1.3.1.1, an ultrathin uniform graphene monolayer can be used to reduce the total scattering width of a dielectric elliptical cylinder more than 17 dB. Regarding this very low scattering cross-section and considering the fact that no higher order modes exist in case of using a graphene monolayer, we expect to be able to reduce the scattering width of a cluster of several dielectric elliptical cylinders even if they are located very close to each other. Similarly, the cloak metasurface can lower the coupling between metallic strips, and thus, reduce the scattering cross-section of metallic strips.

1.3.2.1 Cluster of Dielectric Elliptical Cylinders Cloaked by a Graphene Monolayer

Based on the design presented in Section 1.3.1.1 for the cloaking of a single dielectric elliptical cylinder covered by a graphene monolayer, here, we consider different cases of closely spaced, merging, and overlapping configurations.

First, we consider two touching (Figure 1.16(b)) and two overlapping (Figure 1.16(c)) dielectric elliptical cylinders. The total lengths of the structures are $l = 50$ μm ($\lambda_0/2$) and $l = 48$ μm ($\lambda_0/2.083$), respectively. The full-wave simulation results for the total Radar Cross-Section (RCS) of these configurations are plotted versus frequency in Figure 1.16(a). It can be clearly seen that the minimum scattering width is achieved for two touching dielectric elliptical cylinders at $f = 3$ THz, the same frequency as the case of a single one. The simulation results show that although the structures are touching, each graphene monolayer cloaks its respective ellipse at the same frequency of $f = 3$ THz as if they were separated, and no singular or nonlocal behavior of electromagnetic field is observed. In case of two overlapping ellipses, it is observed that the scattering cross-section is reduced drastically at a frequency less than the desired cloaking frequency. It implies that due to merging the ellipses, the optimum required surface reactance is not the same as for a single ellipse. This frequency shift can be compensated easily by modifying the chemical potential of the graphene monolayer. In Figure 1.16(d), the snapshots of the electric field distribution are shown with respect to $f = 2.8$ THz for the two overlapping elliptical cylinders. It clearly presents the invisibility of the given object in front of the incoming TM-polarized plane wave.

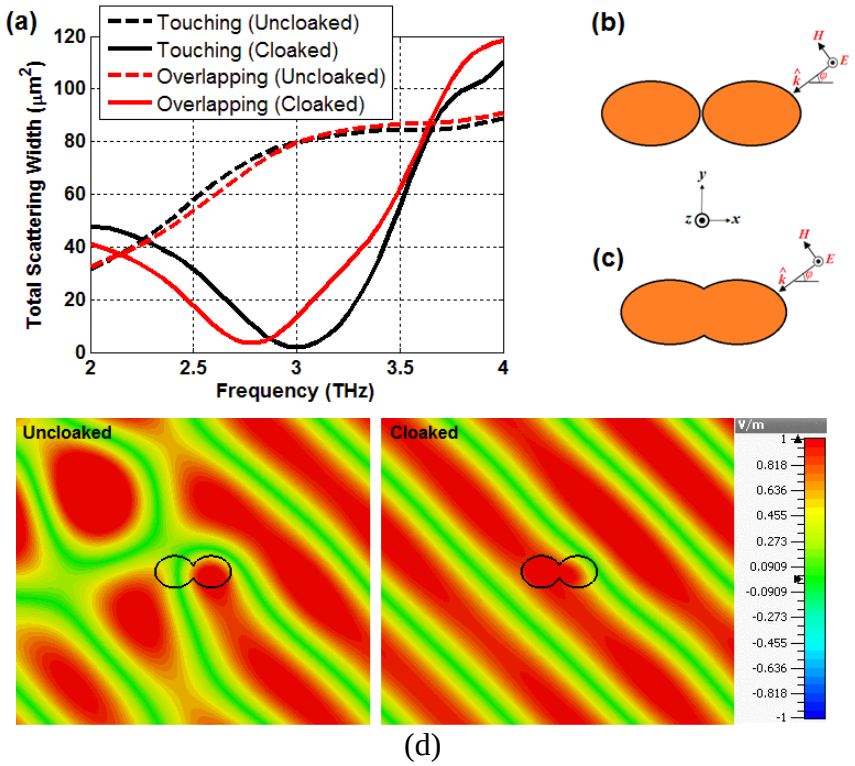

(d)

Figure 1.16 (a) Total scattering widths of uncloaked and cloaked cases for two touching and overlapping dielectric elliptical cylinders with the schematic representation of the 2-D cross-sections shown in (b) and (c), respectively. (d) Snapshots of the electric field distribution at $f = 2.8$ THz for two overlapping dielectric elliptical cylinders under a TM-polarized plane-wave incidence with $\varphi = 45°$.

Now, we consider the case of a cluster formed by several dielectric elliptical cylinders with four and nine ellipses shown in Figure 1.17(b) and Figure 1.17(c), respectively. It should be mentioned that despite the large size of the whole cluster, due to the negligible coupling among elements, the metasurface used for cloaking of a single ellipse can be employed again with no change in its parameters to reduce the scattering width at the same frequency of $f = 3$ THz, as illustrated in Figure 1.17(a). In order to clarify further, the time snapshots of the electric field distribution in the $x - y$ plane are shown in Figure 1.17(d) for nine ellipses. It can be observed that the presence of the metasurface formed by a uniform graphene monolayer (designed

individually for each dielectric elliptical cylinder) plays an important role in restoring the wavefronts of the electric field, and thus, making the whole cluster invisible. Also, the vector power-flow distribution is shown in Figure 1.17(e) for the cloaked and uncloaked cluster of nine ellipses confirming the effective cloaking.

Also, we have studied a chain of six overlapping infinitely long dielectric elliptical cylinders with the total length of $l = 140$ μm ($1.4\ \lambda_0$) at $f = 3$ THz as shown in Figure 1.18(b). Here, the total RCS is minimized at $f = 2.8$ THz as depicted in Figure 1.18(a). It implies that the graphene monolayer wrapped around the surface of this chain is able to provide cloaking for each elliptical cylinder individually, and consequently, can lower the scattering cross-section of the whole chain. To provide further clarification, the snapshots of the electric field distribution are shown in Figure 1.18(c), and also, the vector power-flow of the TM-polarized plane wave with $\varphi = 45°$ is illustrated in Figure 1.18(d). It can be observed that unlike the uncloaked case, in which the chain scatters most of the impinging power to all directions, the tunneling of the plane wave takes place through the chain with a uniform power distribution. Figure 1.18(e) depicts the far-field scattering patterns of the whole structure for the uncloaked and cloaked cases on the same scale, showing a remarkable reduction of RCS for all observation angles.

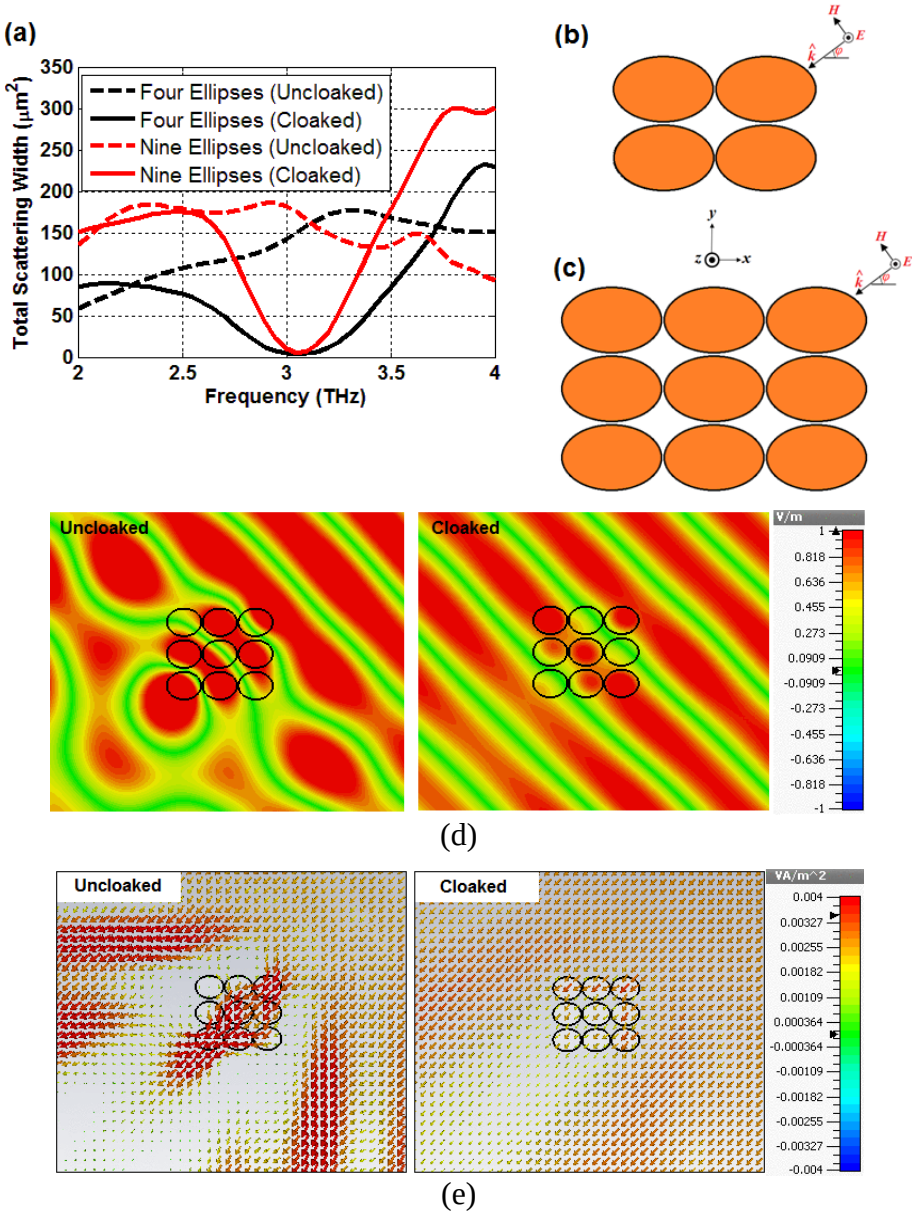

Figure 1.17 (a) Total scattering widths of uncloaked and cloaked cases for four touching and nine touching dielectric elliptical cylinders with the schematic representation of the 2-D cross-sections shown in (b) and (c), respectively. (d) Snapshots of the electric field distribution and (e) vector power-flow distribution at $f = 3$ THz for nine touching dielectric elliptical cylinders under a TM-polarized plane-wave incidence with $\varphi = 45°$.

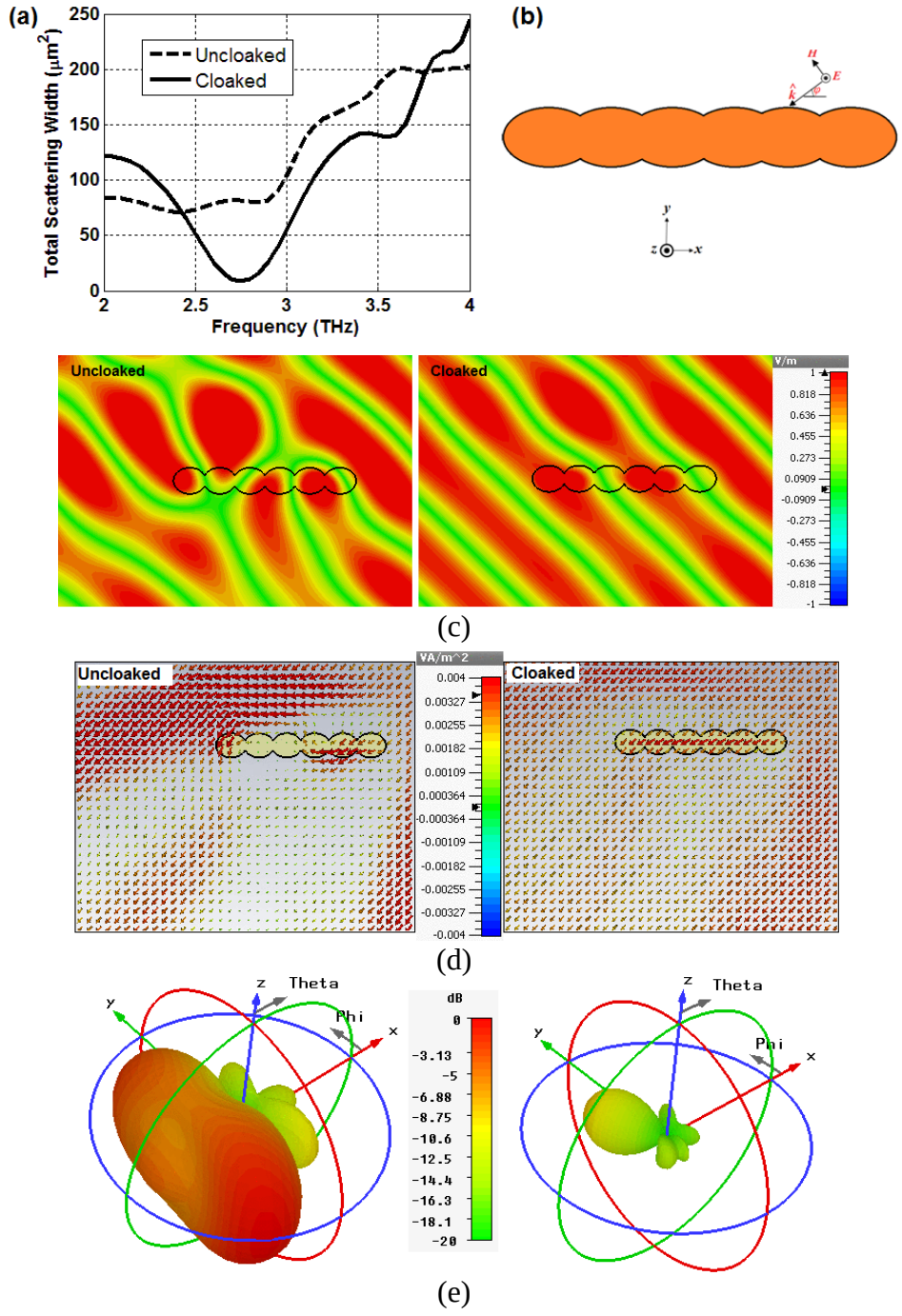

Figure 1.18 (a) Total scattering widths of uncloaked and cloaked cases for the chain of six overlapping dielectric elliptical cylinders with the schematic representation of the 2-D cross-section shown in (b). (c) Snapshots of the electric field distribution for uncloaked and cloaked cases, (d) vector power-flow distribution of the chain for uncloaked and cloaked cases with $\varphi = 45°$, and (e) far-field scattering patterns of the structure for uncloaked (left-sided) and cloaked cases (right-sided), plotted on the same scale with the incident angle of $\varphi = 45°$.

1.3.2.2 Metallic Strips Cloaked by a Nanostructured Graphene Metasurface

In this section, we present a study of cloaking two metallic strips for the different cases of horizontally spaced, vertically spaced, overlapped spacers, and connected. The parameters of each elliptically shaped cloak metasurface are the same as the ones used previously to cloak the single metallic strip mentioned in Section 1.3.1.4. Figure 1.19(a) presents the full-wave simulation results of the total scattering widths of the structures shown in Figures 1.19(b) and 1.19(c). The invisibility of the metallic strips can also be confirmed by comparing the vector power-flow representation of the uncloaked and cloaked cases depicted in Figure 1.19(d). It can be observed that, in the absence of the cloak metasurface, the power is scattered in different directions which can be sensed easily by any bistatic sensor. However, when the graphene-nanopatch metasurface is employed, the power distribution is uniform in the direction of excitation, which indicates that the whole structure is hidden from the incoming plane wave. It is worth noting that to have the cloaking behavior exactly at the desired frequency, the cloak structures should be separated at least one period (D) [27]. Here in our case, the metasurfaces are touching, which results only in a slight frequency shift for the minimum scattering of the whole structure obtained at the frequency of $f = 2.95$ THz. Also, for the metallic strips located vertically to each other (Figure 1.19(c)), the far-field scattering patterns of the structure are shown in Figure 1.19(e) for both uncloaked and cloaked cases on the same scale with the incident angle of $\varphi = 45°$ (with respect to the x axis). As shown, the RCS is decreased significantly, thereby hiding the metallic strips from the incoming wave and achieving the desired transparency.

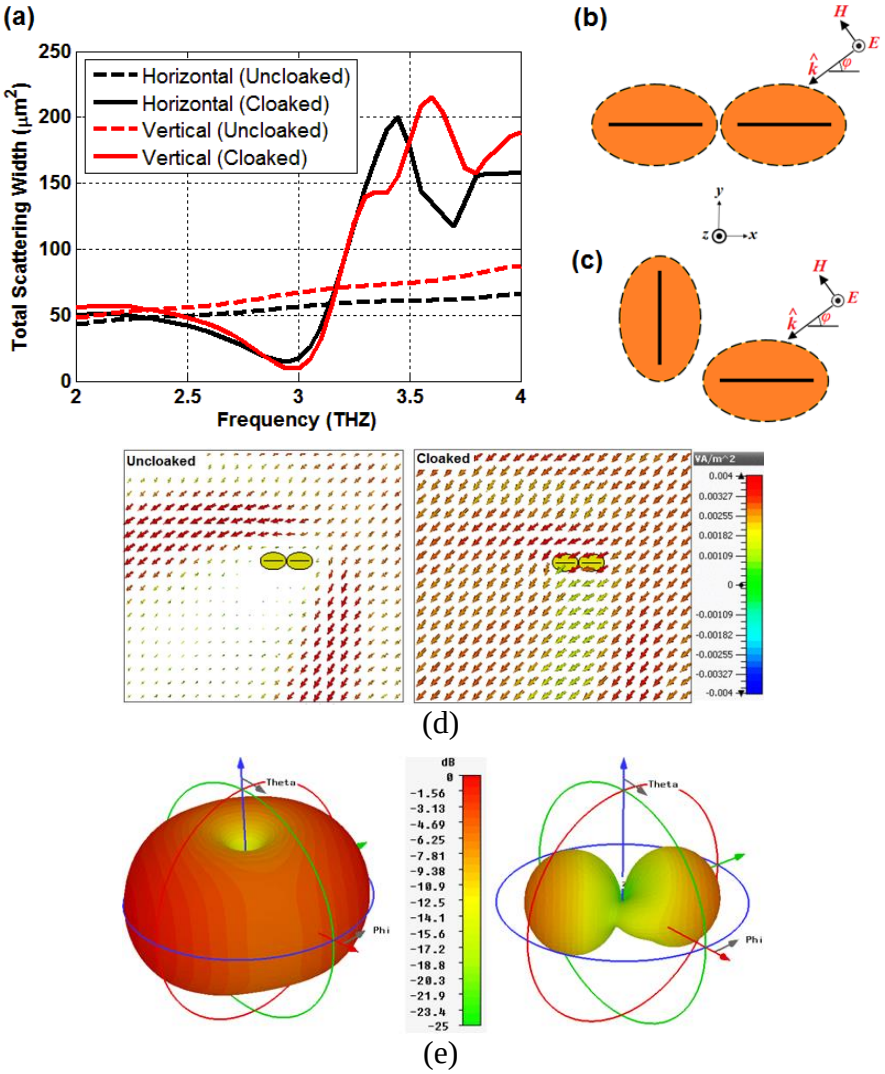

Figure 1.19 (a) Total scattering widths of uncloaked and cloaked cases for two horizontally and vertically spaced metallic strips with the schematic representation of the 2-D cross-sections shown in (b) and (c), respectively. (d) Vector power-flow distribution of the horizontally spaced strips, and (e) far-field scattering patterns of the vertically spaced strips, for uncloaked and cloaked cases under a TM-polarized plane wave at normal incidence with $\varphi = 45°$.

Here, in order to explain the availability of generalizing the cloaking of a single metallic strip to other scenarios, we consider two other cases shown in Figures 1.20(b) and 20(c). It should be noted that the geometric parameters of the metasurface and the chemical potential of graphene are the same as the ones mentioned in Section 1.3.1.4. Figure 1.20(a) shows the total RCS of these

structures versus frequency. The figure conveys the fact that the cloak cover lowers the scattering cross-section of the structure in Figure 1.20(b) remarkably again at $f = 3$ THz until the strips are not united as a wider strip. It is worth noting that if the same cloak metasurface is used in case of two connected strips, the cloaking frequency will be slightly shifted from $f = 3$ THz to $f = 2.8$ THz, which can be easily compensated by optimizing the chemical potential of graphene. Figures 1.20(d) and 1.20(e) show the time snapshots of the electric field distributions of both uncloaked and cloaked cases for the structures shown in Figures 1.20(b) and 1.20(c), respectively. The results confirm that the electric fields are not disturbed in case of using the metasurfaces and the structures become hidden from the incoming TM-polarized plane wave. Also, Figure 1.20(f) depicts the 3-D far-field scattering pattern of the two connected strips for uncloaked and cloaked cases. It can be observed that the scattering cross-section is lowered significantly.

In addition to all mentioned above, as an interesting consequence, it should be stressed that the use of the proposed cloak structure formed by the overlapping spacers and two joint elliptically shaped metasurfaces, opens up the possibility of cloaking wider metallic strips (for example, here, the total width is equal to $l = 30$ μm ($\lambda_0/3.33$)). Hence, the overlapping elliptical metasurfaces outperform the use of one single cloak metasurface in terms of cloaking larger strips.

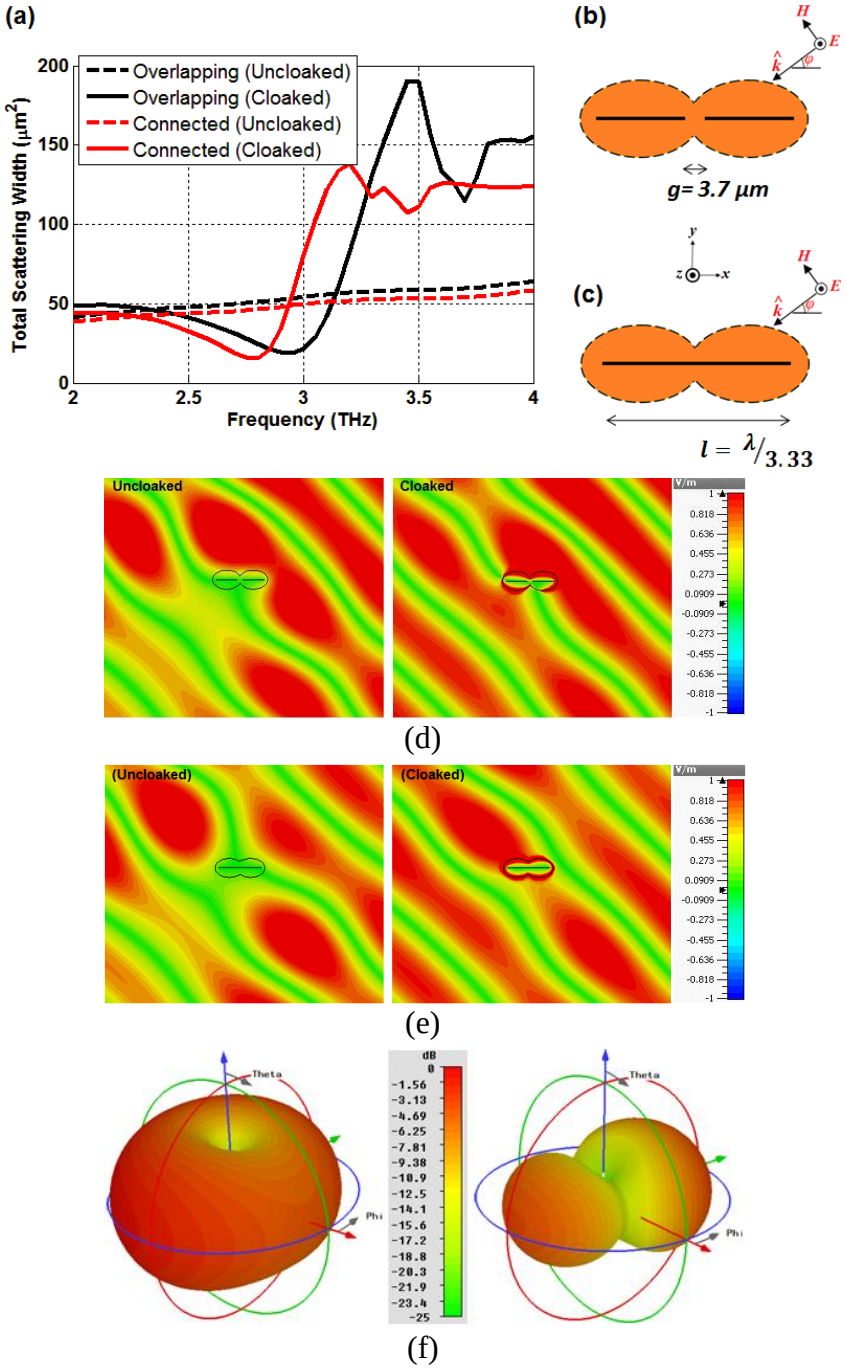

Figure 1.20 (a) Total scattering widths of uncloaked and cloaked cases for two metallic strips with overlapping spacers and for two connected strips with the schematic representation of the 2-D cross-sections shown in (b) and (c), respectively. Snapshots of the electric field distributions of uncloaked and cloaked cases for (d) two metallic strips with overlapping spacers at $f = 3$ THz, and (e) for two connected metallic strips at $f = 2.8$ THz, and (f) far-field scattering patterns of the two connected strips at $f = 2.8$ THz. A TM-polarized plane wave at normal incidence with $\varphi = 45°$ is considered for all the results.

1.4 Conclusion

In this chapter, we have proposed a novel analytical approach in order to cloak dielectric and metallic elliptical cylinders and metallic strips realized by conformal and confocal elliptically shaped cloak metasurfaces, including a graphene monolayer and a nanostructured graphene patch array at low-terahertz frequencies. The analytical approach is based on the solution of the scattering problem in terms of elliptical waves represented by the radial and angular Mathieu functions, with the use of sheet impedance boundary conditions at the metasurface. It is shown that scattering cancellation can be achieved for all incident and observation angles. The idea has been also extended in order to cloak a cluster of elliptical objects for different cases of dielectric elliptical cylinders and metallic strips. This provides more possibility for cloaking larger dielectric objects and wider metallic strips.

CHAPTER II

REDUCTION OF MUTUAL COUPLING IN STRIP DIPOLE ANTENNAS

2.1 Introduction

Recently, there has been a remarkable interest in the study of the phenomenon of electromagnetic invisibility and cloaking, which implies the suppression of the bistatic scattering width of a given object, independently of the incident and observation angles. To analyze and design cloak structures, different methods have been proposed such as transformation optics [5], [7], which is based on the principle of bending electromagnetic waves around the object to be cloaked, anomalous resonance method [11], transmission-line networks [12], [14], and plasmonic cloaking [15] that utilizes bulk isotropic low or negative index materials in order to suppress the dominant scattering mode [19], [20], [45]–[46]. A common drawback of all these methods is that they rely on bulk volumetric metamaterials, which have a finite thickness usually comparable with the size of the object to be cloaked, and are difficult to realize in practice. In [47], a solution has been proposed to cloak surface waves, in which the cloak design is realized by utilizing curved geometries combined with graded index media to make the curvature of a surface invisible. In [48], a thin cloak ($\lambda/40$) based on microwave networks, which is composed of microstrip-connected metallic patches, was presented to provide cloaking by coupling electromagnetic fields into the cloaking layer and transferring around the object. In [49], minimum scattering has been achieved by covering a metallic rod with a high permittivity conventional dielectric.

Recently, a different cloaking technique has been presented based on the concept of mantle cloaking to reduce the scattering width of various types of planar, cylindrical, and spherical objects [21]–[28], which utilizes an ultrathin metasurface that provides anti-phase surface currents to reduce the dominant scattering mode of a given object. In [24], active frequency-selective conformal cloaks have been introduced based on non-Foster metasurfaces in order to broaden the cloaking bandwidth. Also, a wideband conformal cloak structure, which is based on width-modulated microstrip lines, has been presented and verified experimentally in [25] in order to cloak single and multiple cylindrical objects. In [26], an analytical model has been proposed to cloak dielectric and conducting cylindrical objects using 1-D and 2-D conformal printed and slotted arrays of sub-wavelength periodic elements at microwave frequencies. Also, it was shown that the analytical grid impedance expressions derived for the planar arrays of sub-wavelength elements can be used to describe the surface reactance of cylindrical conformal mantle cloaks. The mantle cloaking method has also been implemented at low-THz frequencies by using a graphene monolayer and a nanostructured graphene patch array [36], [38]. Recently, the idea of mantle cloaking has been extended and an analytical framework for the analysis of the electromagnetic cloaking of dielectric and metallic elliptical cylinders and 2-D metallic strips has been presented in [50]–[53], where the cloak structures are realized by a graphene monolayer and a nanostructured graphene patch array at low-THz frequencies, and also, by conformal arrays of sub-wavelength periodic elements at microwave frequencies. However, all the techniques mentioned above are designed to cloak passive structures.

An interesting and critical antenna application of electromagnetic cloaking is the reduction of the mutual coupling between antennas. Indeed, the destructive mutual coupling effect has

always been an important unavoidable issue in antenna designs and applications. The presence of a passive element influences the radiation pattern and matching characteristics of a radiating antenna. Several articles have been proposed in order to reduce the blockage effect by passive elements in front of antennas. For instance, in [54], hard surfaces have been used to reduce the forward scattering from cylindrical objects such as struts and masts. Also, in [55], low scattering struts covered by the hard surface, realized by metallic strips printed on a thin low dielectric permittivity layer, have been introduced to improve the performance of center-fed reflector antennas. In [56], an electromagnetic cloak design, which consists of periodical conical plates, has been used to hide passive metallic cylinders placed near a commercial horn antenna, and in [57], a transmission-line cloak structure has been used to demonstrate the antenna blockage reduction. The purpose of these designs has been on reducing the mutual coupling effect of passive elements placed directly in front of an antenna.

On the other hand, it is not a facile task to suppress the mutual coupling between two antennas. The reason is that the cloak structure for an antenna is needed to be designed in a way that provides drastic scattering reduction, and at the same time, preserve the electromagnetic performance of the antenna. In this regard, in [58], a mushroom-like electromagnetic band-gap (EBG) structure has been proposed in the design of microstrip antenna arrays in order to reduce the strong mutual coupling caused by the thick and high permittivity substrates. In [3], the concept of cloaking a sensor (a short dipole antenna) without affecting its ability to receive an incoming signal has been presented. However, the proposed method relies on plasmonic cloaking which requires bulk materials. Also, [59] proposes a semi-analytical method to reduce the scattered field from an infinite two-dimensional planar microstrip antenna by using a superstrate with low or

negative index materials (carpet cloaking). It should be stressed that although the use of low or negative index materials based on plasmonic cloaking is favorable, their experimental realization is difficult. On the other hand, it has been shown in [60] that plasmonic cloaks are more appropriate for the antennas with the length less than a quarter wavelength than self-resonating antennas. Recently, in [61] and [62], the mantle cloaking method has been applied to reduce the mutual blockage effects between two wire dipole antennas resonating at close frequencies.

In this chapter, we propose the use of the mantle cloaking method realized by conformal and confocal elliptical printed sub-wavelength structures in order to make resonating elements invisible, not only in front of a plane-wave illumination but also in case of radiating in close electrical vicinity of other resonating elements. The novelty of our approach is the use of elliptically shaped metasurface cloaks in order to cancel the dominant elliptical scattering mode from strip dipole antennas, which are involved in many applications such as microstrip technology, RFID tags, and on-chip realizations, and extending the idea to reduce the mutual coupling between two strip dipole antennas located in close proximity of each other. In other words, to create an anti-phase surface current and reduce the dominant elliptical scattering mode of a strip dipole antenna based on the concept of mantle cloaking, we have shown that the scattering cancellation can be realized by utilizing confocal and conformal elliptical metasurface cloaks, which result in the reduction of mutual blockage effect, and makes it possible to restore the radiation pattern and impedance characteristics of antennas. To convey the idea, we show how the aforementioned elliptically shaped metasurface cloaks can be utilized to reduce the mutual coupling between two strip dipoles resonating at two different frequencies. Actually, unlike wire dipole antennas, the scattering problem of strip dipole antennas is ruled by the non-symmetric configuration of these

antennas, which makes the cloaking mechanism more complicated and necessitates the use of an elliptical metasurface [50]–[53]. In addition, we show that if the resonance frequencies of the antennas are far from each other, by using an analytical model, the strip dipole antennas can be cloaked in a way that minimum mutual coupling is achieved. Regarding this, the scattering problem is solved by an analytical approach, in which the incident and scattered fields are expressed in terms of radial and angular even and odd Mathieu functions [39 and references therein], with the use of sheet impedance boundary conditions at the metasurface, and by placing the focal points of the cloak at the edges of each strip dipole. In [61], the antennas were covered by vertical metallic strips, which provide inductive response, to be hidden from each other. In this chapter, we show that the applicability of vertical strips (inductive response) or horizontal rings (capacitive response) [26] is dependent on the difference between the resonance frequencies of the antennas. Therefore, appropriate confocal elliptically shaped mantle cloaks, wrapped around elliptical dielectric spacers, are used to cover two electrically close 3-D resonating strip dipole antennas in order to reduce the mutual coupling drastically, and consequently, restore their radiation patterns and matching characteristics as in the isolated case.

This chapter is organized as follows. Section 2.2 is devoted to our analytical model for the analysis of cloaking of 2-D metallic strips at microwave frequencies covered by sub-wavelength conformal printed elements. In Section 2.3, we discuss the mutual coupling reduction between two strip dipole antennas for two different cases. Section 2.4 is allocated to the conclusion. A time dependence of the form $e^{-j\omega t}$ is assumed and suppressed.

2.2 Cloaking of 2-D Metallic Strips at Microwave Frequencies

Here, we present the mathematical formulation to analyze the scattering problem of 2-D metallic elliptical cylinders and as a special case a 2-D metallic strip. Consider the infinitely long metallic strip shown in Figure 2.1(a), which is illuminated by a transverse magnetic (TM) plane wave at normal incidence ($\theta = 90°$) with an angle φ with respect to the x-axis in the xy-plane. The 2-D cross-section is shown in Figure 2.1(b).

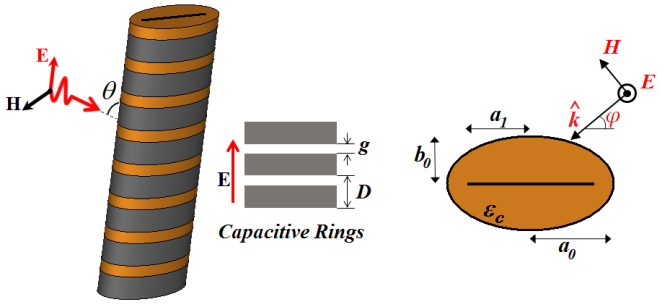

(a) (b)

Figure 2.1 Schematic representation of an infinitely long metallic strip with a TM-polarized plane wave at normal incidence: (a) metallic strip with horizontal capacitive rings and (b) 2-D cross-section of the structure.

In the first step, to realize the cloaking of 2-D metallic strips, we need to formulate the electromagnetic scattering problem. The analysis of the problem is based on the method of separation of variables to solve the 2-D wave equation in the elliptical coordinates (u, v, z), and consequently, to solve the well-known Mathieu equations. Then, we express the incident, scattered, and transmitted electric and magnetic fields in terms of even and odd angular and radial Mathieu functions in the elliptical coordinates. In this regard, the incident electric field, which is related to the free-space region $u > u_0$ ($u_0 = \tanh^{-1}(b_0/a_0)$) (Figure 2.1(b)), can be represented as below [41]:

$$E_z^i = \sqrt{8\pi}\sum_n j^{-n}\frac{J_{\mathrm{pm}}(q_0,u,n)}{N_{\mathrm{pm}}(q_0,n)}S_{\mathrm{pm}}(q_0,v,n)\,S_{\mathrm{pm}}(q_0,\varphi,n) \tag{2.1}$$

where $J_{\mathrm{pm}}(q_0, u, n)$ is the radial Mathieu function of the first kind, $S_{\mathrm{pm}}(q_0, v, n)$ is the angular Mathieu function, $N_{\mathrm{pm}}(q_0, n)$ is the normalization constant, u is the radial parameter in the elliptical coordinate system, v is the angular parameter, and $q_0 = k_0^2 F^2/4$ (k_0 is the wave number in free space and F is the focus of the ellipse or strip). The scattered electric field pertained to the region $u > u_0$ can be written as:

$$E_z^s = \sqrt{8\pi} \times \sum_n j^{-n} a_{pm}^{(n)} H_{pm}^{(1)}(q_0, u, n) S_{pm}(q_0, v, n) S_{pm}(q_0, \varphi, n) \tag{2.2}$$

where $H_{pm}^{(1)}(q_0, u, n)$ is the radial Mathieu function of the third kind, which indicates the outgoing wave, and $a_{pm}^{(n)}$ are the unknown coefficients to be determined. Similarly, the transmitted electric field inside the dielectric spacer region $u_1 < u < u_0$ (Figure 2.1(b)) can be expressed as:

$$E_z^t = \sqrt{8\pi} \sum_n j^{-n} [b_{pm}^{(n)} J_{pm}(q_1, u, n) + c_{pm}^{(n)} Y_{pm}(q_1, u, n)] S_{pm}(q_1, v, n) S_{pm}(q_0, \varphi, n) \tag{2.3}$$

where $Y_{\mathrm{pm}}(q_0, u, n)$ is the radial Mathieu function of the second kind, $b_{pm}^{(n)}$ and $c_{pm}^{(n)}$ are the unknown transmitted field expansion coefficients, and $q_1 = k_1^2 F^2/4$ (k_1 is the wave number in the dielectric spacer). It should be noted that p and m denote either even or odd functions.

The incident, scattered, and transmitted magnetic fields can be obtained by using Maxwell equations as follows [41]:

$$H_v^i = \frac{j}{\omega\mu h} \sqrt{8\pi} \sum_n j^{-n} \frac{J'_{pm}(q_0, u, n)}{N_{pm}(q_0, n)} S_{pm}(q_0, v, n) S_{pm}(q_0, \varphi, n) \tag{2.4.1}$$

$$H_v^s = \frac{j}{\omega\mu h} \sqrt{8\pi} \sum_n j^{-n} a_{pm} H_{pm}^{(1)'}(q_0, u, n) S_{pm}(q_0, v, n) S_{pm}(q_0, \varphi, n) \tag{2.4.2}$$

$$H_v^t = \frac{j}{\omega\mu h} \sqrt{8\pi} \sum_n j^{-n} [b_{pm} J'_{pm}(q_1, u, n) + c_{pm} Y'_{pm}(q_1, u, n)] \times S_{pm}(q_1, v, n) S_{pm}(q_0, \varphi, n) \tag{2.4.3}$$

where $h = F\sqrt{\cosh^2 u - \cos^2 v}$ is the scalar factor in the elliptical coordinate system. It should be noted that the prime indicates the derivative of the functions with respect to the variable u.

The unknown coefficients in equations (2.2) and (2.3) can be determined by imposing the boundary condition at $u_1 = \tanh^{-1}(b_1/a_1)$ ($u_1 = 0$ for the strip case (Figure 2.1(b))), the sheet impedance boundary conditions for the tangential electric and magnetic fields at the metasurface ($u = u_0$), and also, by applying the orthogonality property of angular Mathieu functions. It should be mentioned that the tangential components of the electric fields are continuous across the interfaces while the use of an impedance surface results in the discontinuity of the tangential components of magnetic fields ($H_v^{\tan}$) at the boundary:

$$E^{\tan}|_{u=u_1} = 0 \tag{2.5.1}$$

$$E^{\tan}|_{u=u_0} = Z_s\left[H_v^{\tan}|_{u=u_0^+} - H_v^{\tan}|_{u=u_0^-}\right] \tag{2.5.2}$$

where Z_s is the surface impedance of the metasurface. Actually, the bistatic scattering width can be reduced drastically for all the incident angles by choosing an appropriate value for Z_s. For a metasurface formed by horizontal capacitive rings with a TM-polarized plane-wave incidence, as shown in Figure 2.1(a), the surface impedance can be expressed as [26, 63]:

$$Z_s^{\text{TM,Capacitive}} = \frac{j\eta_0 c\pi}{\omega(\varepsilon_c+1)\, D \ln \csc\left(\frac{\pi g}{2D}\right)} \tag{2.6}$$

where D and g are the periodicity and gap size, respectively, and ε_c is the relative permittivity of the dielectric spacer. The formulas of Z_s for a variety of metasurfaces including arrays of strips, mesh grids/patches, Jerusalem crosses, and crossed dipoles were presented in [26].

Here, to cancel the dominant scattering mode of a 2-D metallic strip, we place the focal points of the cloak structure at the edges of the strip (Figure 2.1(b)). To cloak an infinitely long metallic

strip, we need a capacitive reactance [52]. For example, to cloak the strip with the focus $F = a_1 = 0.075\,\lambda = 7.5$ mm at $f = 3$ GHz, the required reactance is found to be $Z_s = j85.15\ \Omega$, which can be realized by the following parameters of the metasurface: $a_0 = 8.457$ mm $(\lambda_0/11.82)$, $b_0 = 3.908$ mm $(\lambda_0/25.58)$, $\varepsilon_c = 10$, $D = 8.93$ mm, and $g = 0.6$ mm. The results of the bistatic scattering widths for both uncloaked and cloaked cases of the strip with different angles of incidence are shown in Figure 2.2. It can be clearly seen that the bistatic scattering width is significantly reduced for all the incident and observation angles. Also, the total scattering width, as a quantitative measure of its overall visibility for all observation angles, is shown in Figure 2.3 for the incident angle of $\varphi = 90°$, and compared with full-wave simulation results obtained with CST Microwave Studio [42]. In addition, a snapshot of the electric field distribution is illustrated in Figure 2.4 for both uncloaked and cloaked cases. It confirms the fact that fields are not disturbed when the metasurface is used and the strip is invisible to the incoming wave.

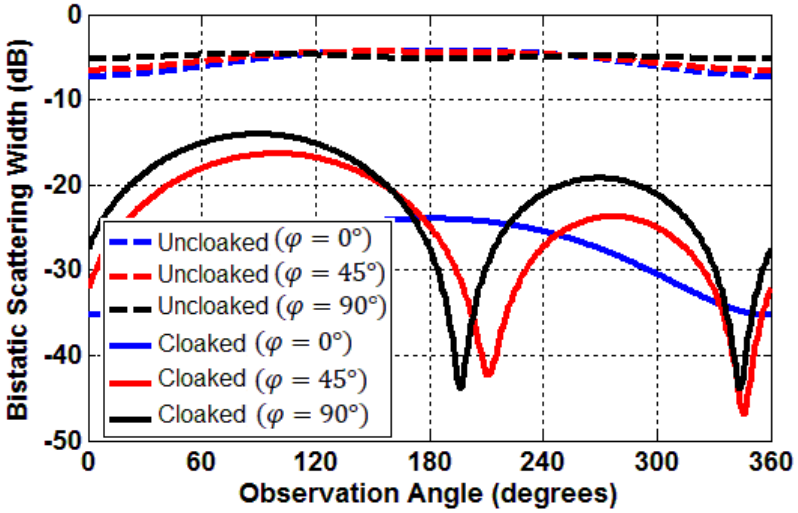

Figure 2.2 Bistatic scattering width of a 2-D metallic strip with different incident angles for uncloaked and cloaked cases.

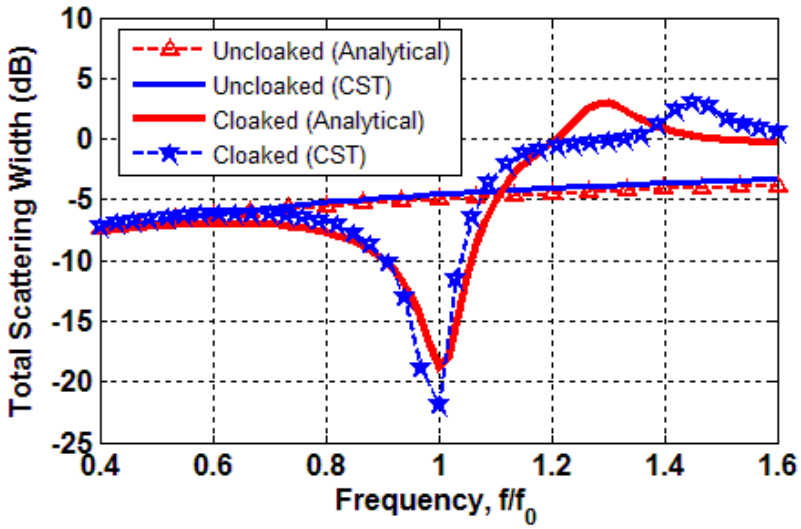

Figure 2.3 Total scattering width of a 2-D metallic strip with $\varphi = 90°$ for uncloaked and cloaked cases.

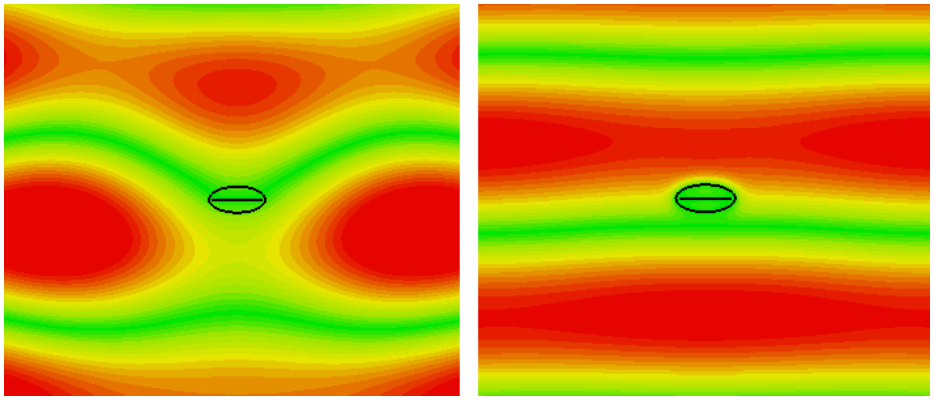

(a) (b)

Figure 2.4 Snapshot of the electric field distribution for at 3 GHz (a) uncloaked, and (b) cloaked 2-D metallic strip illuminated by a TM-polarized plane wave at normal incidence with $\varphi = 90°$.

2.3 Cloaking of Strip Dipole Antennas

In this section, we propose cloak structures to reduce the mutual coupling effect between two strip dipole antennas. Therefore, the obstacle here is no longer a passive element, which affects the operating frequency and radiation characteristics of each of them, and also, deteriorates their performance. In this regard, the cloak metasurfaces are designed to hide the antennas from each other, and also, preserve their characteristics at their resonance frequencies with the performance

similar to the isolated case. Here, to present the applicability of the mantle cloaking method for mutual coupling reduction between two strip dipole antennas, we consider two different designs namely, Case I and Case II. In Case I, we suppose to have two strip dipole antennas resonating at $f_1 = 1$ GHz and $f_2 = 5$ GHz, and in Case II, $f_1 = 3.02$ GHz and $f_2 = 3.33$ GHz.

2.3.1 Case I

Consider two strip dipole antennas shown in Figure 2.5(a); the longer one resonating at $f_1 = 1$ GHz (Antenna I) and the shorter one resonating at $f_2 = 5$ GHz (Antenna II) with the dimensions of $W_1 = W_2 = 4$ mm, $L_1 = 130.5$ mm, and $L_2 = 27.45$ mm. Both antennas are optimized to be matched to a 75-Ω feed and $\Delta = 0.2$ mm. The antennas are in close proximity with the distance of $d = 6$ mm ($\lambda/10$ at $f = 5$ GHz and $\lambda/50$ at $f = 1$ GHz). The radiation patterns of the two antennas are shown in Figure 2.6 for the isolated scenario (Figure 2.6(a) and Figure 2.6(b)) and when the antennas are placed in close proximity (Figure 2.6(c) and Figure 2.6(d)). It can be clearly seen that although Antenna II is electrically so close to Antenna I, its presence does not affect the radiation pattern and scattering characteristics of Antenna I because of its small size in comparison to the wavelength of the resonance frequency of Antenna I ($L_2 \approx \lambda_1/11$). Hence, it can be inferred that if the frequencies of the antennas are far from each other, the radiation properties of the longer antenna is not changed remarkably even in the scenario when they are located so close to each other.

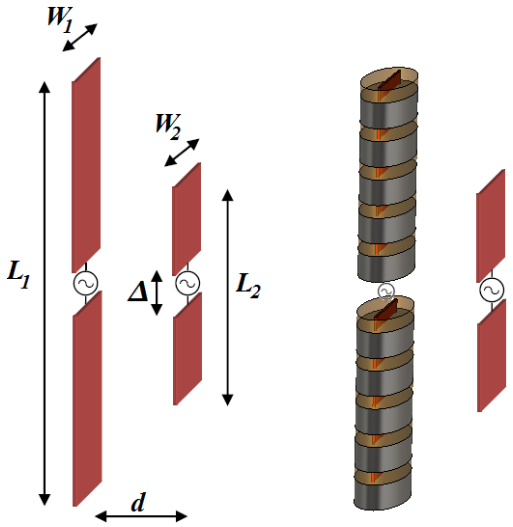

(a) (b)

Figure 2.5 Schematics of (a) uncloaked resonant strip dipole Antenna I (left) at 1 GHz and strip dipole Antenna II (right) at 5 GHz, and (b) cloaked resonant strip dipole Antenna I (left) at 1 GHz and strip dipole Antenna II (right) at 5 GHz.

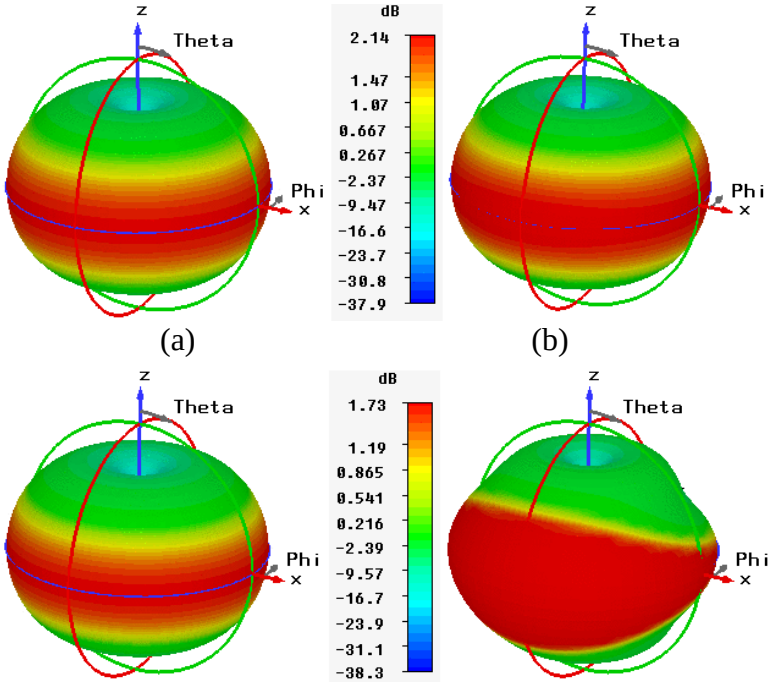

(a) (b)

(c) (d)

Figure 2.6 3-D radiation patterns of (a) the isolated Antenna I at 1 GHz, (b) the isolated Antenna II at 5 GHz, (c) Antenna I in the vicinity of Antenna II at 1 GHz, and (d) Antenna II in the presence of Antenna I at 5 GHz.

On the other hand, the presence of Antenna I affects the radiation properties of Antenna II dramatically in a way that it no longer provides an omni-directional pattern. In Figure 2.7, the S-parameters at the input ports of both antennas are shown for the isolated and coupled scenarios.

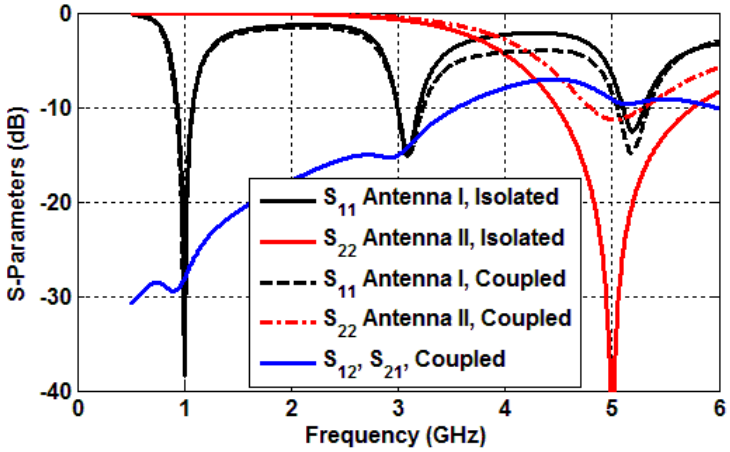

Figure 2.7 S-parameters at the input ports of Antenna I and Antenna II for the isolated and coupled scenarios.

As expected, Antenna II is no longer matched to the source perfectly due to the remarkable mutual coupling at $f = 5$ GHz. The reflection coefficient confirms that Antenna I is not affected by the presence of Antenna II due to the small electrical size of Antenna II at $f = 5$ GHz. Hence, there is no need to cloak Antenna II for the resonance frequency of Antenna I. However, in order to reduce the mutual coupling effect on Antenna II, we need to cover the strip dipole Antenna I with a mantle cloak. Here, the question is that how the cloak structure be realized since the mantle cloaking method, which has been proposed so far, is pertained to the cloaking of 2-D infinitely long dielectric and metallic objects. In [64], a 3-D mantle cloak structure is proposed to cloak a finite-length dielectric rod with the length of $L = 2.2\,\lambda$ at the design frequency of $f = 3.73$ GHz and is verified experimentally. In our case, $L_1 \approx 2.5\,\lambda_2$ and we can consider Antenna I to be long enough with comparison to the wavelength of Antenna II. Therefore, by applying the analytical

approach used to cloak infinite length metallic elliptical cylinders and strips, a good approximation for the parameters of the cloak design can be found. It should be noted that the object to be cloaked in the analytical method is assumed to be under a transverse magnetic (TM) plane-wave excitation, while in our scenario each dipole antenna is excited by the near fields of the other one, which, in principle, is different from an ideal plane-wave excitation. In fact, in spite of this difference, since the radiation of the dipole antenna is dominated by the TM polarization, the cloaking effect is robust to this excitation as well. Here, the required reactance is found to be $Z_s = j28\ \Omega$, which can be realized by the following parameters of the metasurface: $a_0 = 2.2$ mm $(\lambda_0/27.27)$, $b_0 = 0.9165$ mm $(\lambda_0/65.46)$, $\varepsilon_c = 25$, $D = 6.515$ mm, and $g = 1.29$ mm. To calculate the parameters of the metasurface, we consider the infinitely long strip with the dielectric spacer and find the optimum $\mathrm{Z_s}$ with the same process explained in Section 2.2. Here, in our design, based on the mathematical formulation for the infinitely long strip, we have $g = 0.4$ mm for the respective optimum value of $Z_s = j28\ \Omega$, and the optimum value obtained by simulation is found to be $g = 1.29$ mm. In fact, if we use a spacer with bigger semi-axes a_0 and b_0, the difference between these two values will be close to zero, and thus, we can obtain the exact value by mathematical formulation. It should be also noted that if we use a symmetric metasurface with respect to the feed point of the antenna instead of the non-symmetric one shown in Figure 2.5(b), again, we obtain the same cloaking behavior. There will be only a slight frequency shift from 5 GHz to 4.95 GHz for Antenna II (The results are not shown here for the sake of brevity). Figure 2.8 illustrates the total Radar Cross-Section (RCS) of Antenna I illuminated by a TM-polarized plane wave at normal incidence for both uncloaked and cloaked scenarios.

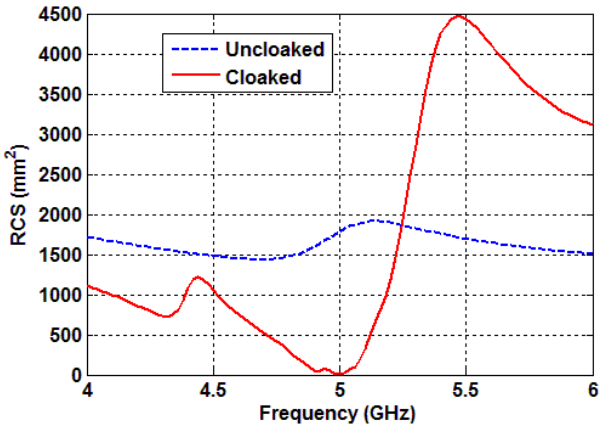

Figure 2.8 Total RCS of Antenna I for the uncloaked and cloaked cases with the TM-polarized plane wave at normal incidence with $\varphi = 90°$.

In the absence of the cloak design, the electric field is intensively disturbed, and consequently, the presence of Antenna I exacerbates the matching characteristics of Antenna II and deforms its omni-directional radiation pattern. On the other hand, the presence of the mantle cloak reduces the total RCS of Antenna I drastically, which results in the invisibility of it in front of Antenna II and leads to the restoration of the matching characteristics and the omni-directional radiation pattern of Antenna II as confirmed by Figures 2.9 and 2.10. Also, Figure 2.11 shows the radiation pattern of the strip dipole antennas in three different scenarios of (i) isolated, (ii) coupled but uncloaked, and (iii) the scenario in which Antenna I is cloaked with respect to the resonance frequency of Antenna II (Figure 2.5(b)) in the H-plane (xy-plane) and E-plane (xz-plane). It is obvious that a remarkable restoration of the original pattern for Antenna II is obtained by applying the capacitive horizontal mantle cloak to Antenna I. Actually, the presence of Antenna I changes the H-plane pattern of Antenna II intensively (Figure 2.11(b)) and forces Antenna II to have a directional pattern with a high gain of 5.69 dB. To compensate this large uncloaked pattern, as mentioned above, Antenna I is cloaked with respect to the resonance frequency of Antenna II,

which results in the restoration of the radiation pattern of Antenna I. In addition, Figure 2.11(c) shows that the radiation pattern of Antenna I is not affected by the presence of Antenna II, not only at its first resonance frequency but also at its second resonance frequency (3 GHz). Therefore, the antennas are invisible to each other.

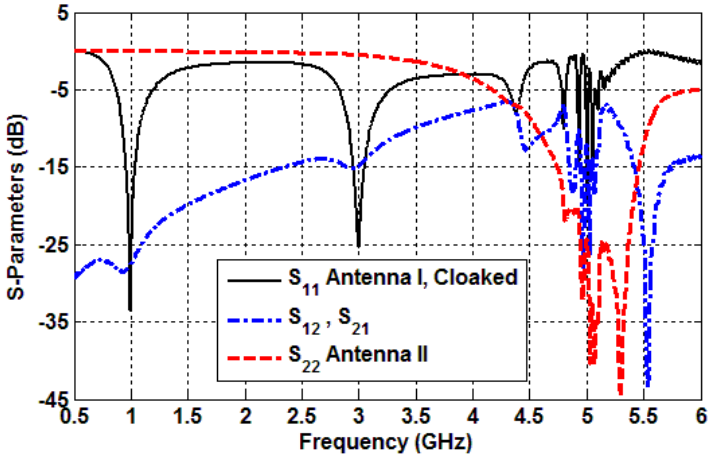

Figure 2.9 S-parameters coefficients at the input ports of Antenna I and Antenna II pertained to the scenario in which Antenna I is cloaked for the resonance frequency of Antenna II and the antennas are in close proximity.

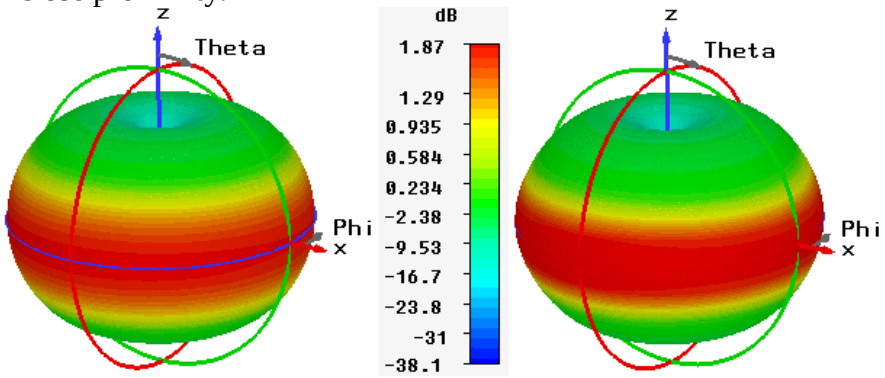

Figure 2.10 3-D radiation patterns of Antenna I at 1 GHz (left) and Antenna II at 5 GHz (right) for the scenario in which Antenna I is cloaked for the resonance frequency of Antenna II and the antennas are in close proximity.

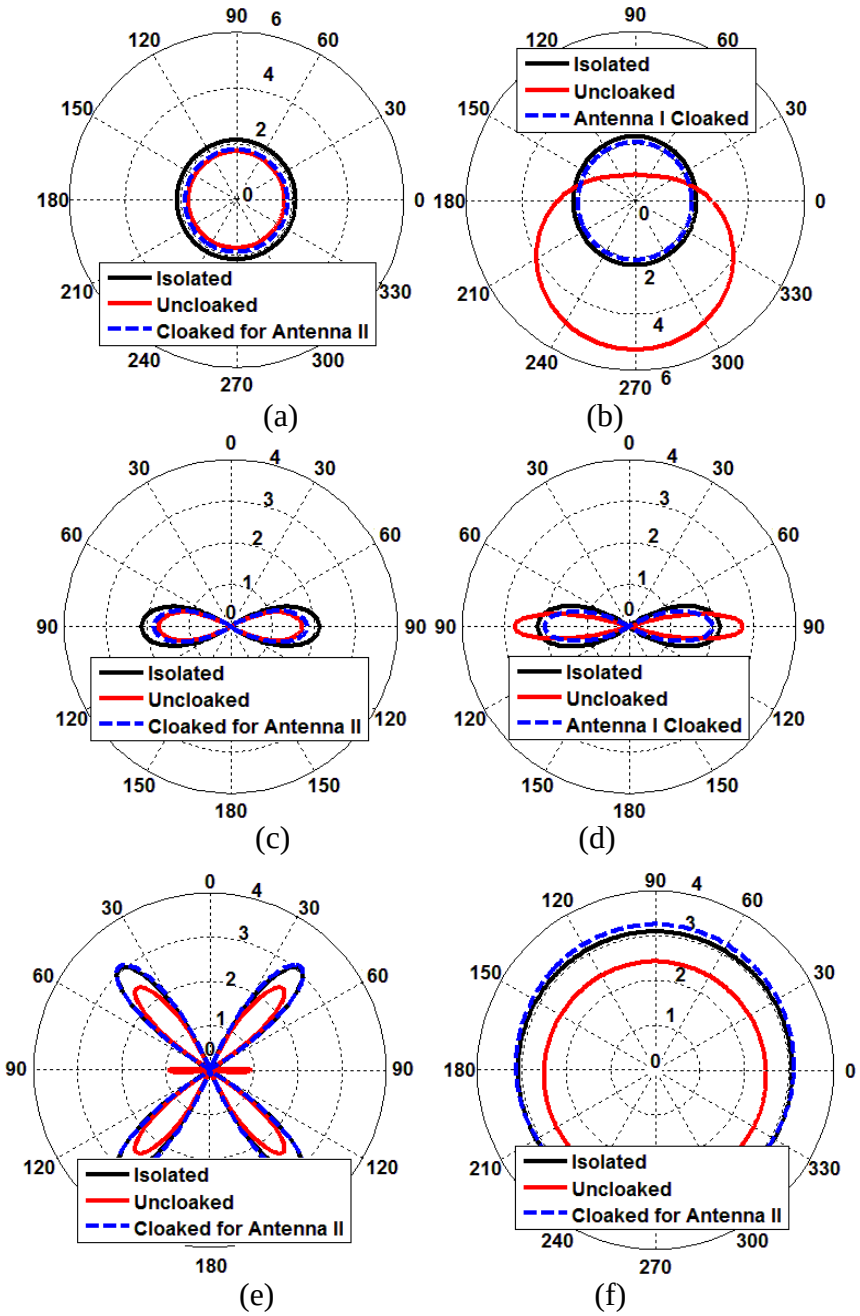

Figure 2.11 Gain patterns of (a) Antenna I at 1 GHz in the H-plane, (b) Antenna II at 5 GHz in the H-plane, (c) Antenna I at 1 GHz in the E-plane, (d) Antenna II at 5 GHz in the E-plane, (e) Antenna I at 3 GHz in the E-plane, and (f) Antenna I at 3 GHz in the H-plane.

2.3.2 Case II

In this section, we consider two strip dipole antennas resonating at slightly different frequencies of $f_1 = 3.02$ GHz and $f_2 = 3.33$ GHz, which are separated with a short distance of $d = \lambda/10$ at $f = 3$ GHz (Figure 2.12). The radiation patterns of the isolated strip dipoles at their respective resonance frequencies are shown in Figures 2.13(a) and 2.13(b). In addition, the reflection coefficient of each antenna at its input port for the isolated scenario is shown in Figure 2.13(c).

Now, the antennas are placed in close proximity to each other. As expected, the presence of each of the antennas affects the radiation pattern of the other one drastically because the near-field distribution is changed, and therefore, the input reactance is changed remarkably, which leads to directive radiation patterns as shown in Figure 2.14.

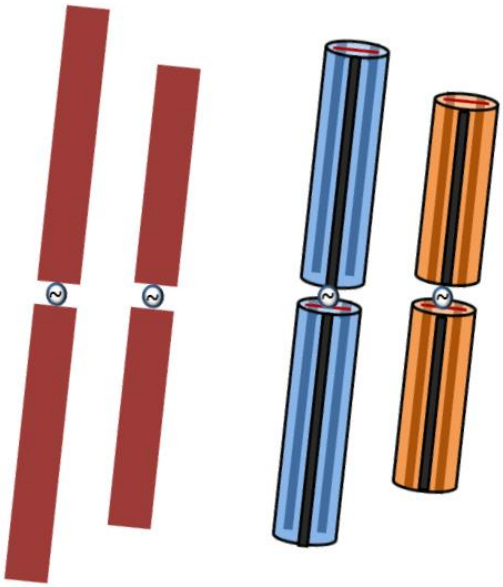

(a) (b)

Figure 2.12 Schematics of (a) uncloaked resonant strip dipole Antenna I (left) at 3.02 GHz and strip dipole Antenna II (right) at 3.33 GHz, and (b) cloaked resonant strip dipole Antenna I (left) at 3.02 GHz and cloaked strip dipole Antenna II (right) at 3.33 GHz.

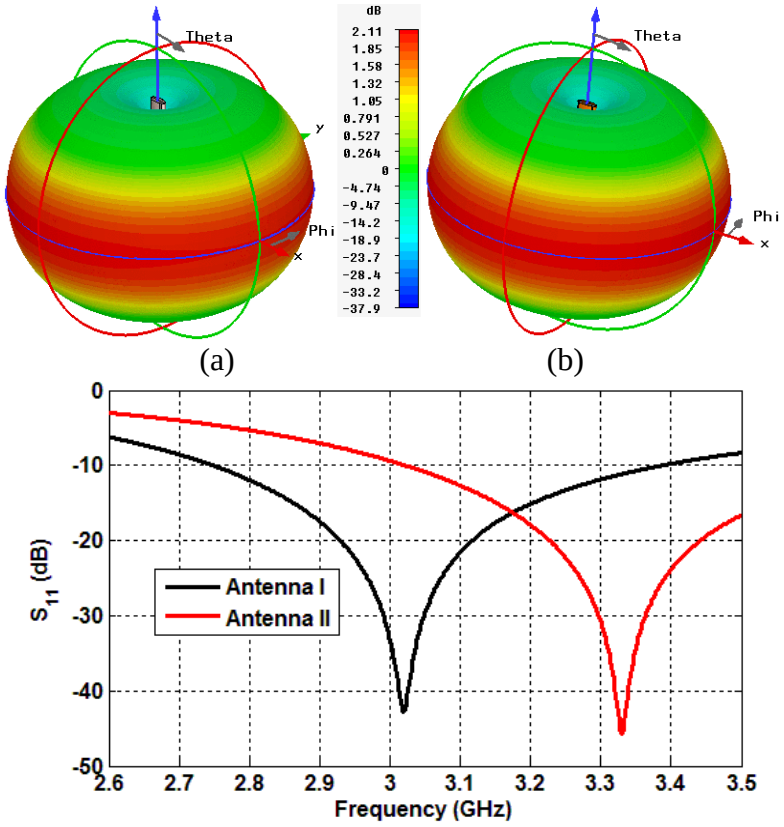

Figure 2.13 3-D radiation patterns of (a) the isolated Antenna I at 3.02 GHz, (b) the isolated Antenna II at 3.33 GHz, and (c) the reflection coefficient of Antenna I and Antenna II.

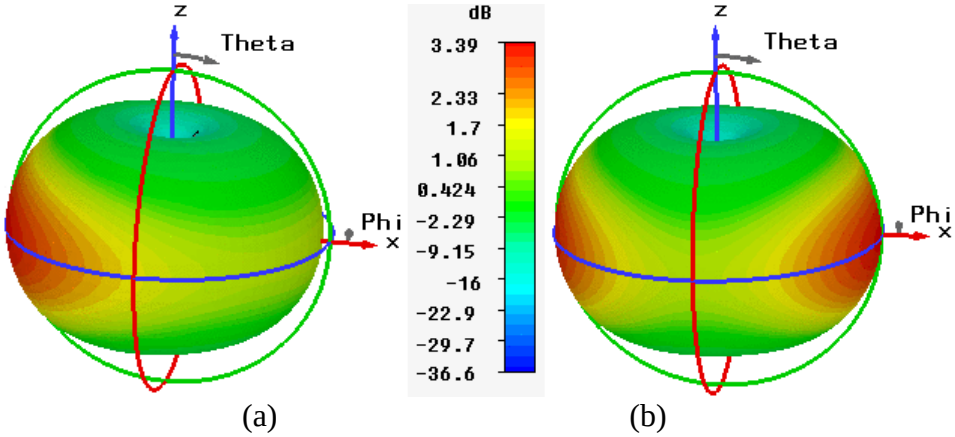

Figure 2.14 3-D radiation patterns of (a) Antenna I in the vicinity of Antenna II at 3.02 GHz and (b) Antenna II in the presence of Antenna I at 3.33 GHz.

To reduce the mutual coupling, we cover each dipole antenna with an elliptically shaped metasurface consisting of inductive vertical strips and a spacer between the strips and the metasurface. The presence of the spacer, and then, the cloak structure, changes the resonance frequency of the antenna in a way that the frequency is shifted to a lower value. Therefore, we reduce the length of each antenna in order to provide good matching at the desired resonance frequency. Here, the length of Antenna I is reduced from $L_1 = 45.8$ mm to $L_1 = 41.4$ mm and the length of Antenna II is reduced from $L_2 = 41.5$ mm to $L_2 = 38.8$ mm.

On the other hand, the parameters of the cloak structure should be chosen in a way that each antenna is invisible at the resonance frequency of the other one. We have performed an appropriate optimization to minimize the 3-D total cross-section of each dipole antenna under the transverse magnetic (TM) plane-wave excitation. To explain the design process, it should be mentioned that, initially, we consider having $N = 3$ as the total number of vertical strips for each antenna, which implies to have the periodicity $D = 3.4034$ mm. Then, we have two parameters in order to tune each metasurface: (i) the widths of the vertical strips and (ii) the permittivity of the dielectric spacer. In the next step, we perform a case study optimization in a way that we fix all the parameters, and also, one of these two parameters and change the other one, and investigate the behavior of the cloak structure and the resonance frequency of each antenna. The careful parametric study for these two parameters leads to optimum values for the design. The reflection coefficients and 3-D radiation pattern of the antennas are shown in Figures 2.15 and 2.16.

It should be mentioned that the parameters of Antenna I and its respective cloak structure are: $W_1 = 4$ mm, $a_0 = 2.2$ mm, $b_0 = 0.9165$ mm, $L_1 = 41.4$ mm, $D = 3.4034$ mm, $w = 0.35$ mm, $\varepsilon_r = 6.15$ and the parameters of Antenna II and its cloak are: $W_2 = 4$ mm, $a_0 = 2.2$ mm, $b_0 = 0.9165$ mm, $L_2 = 41.4$ mm, $D = 3.4034$ mm, $w = 0.3$ mm, $\varepsilon_r = 9.8$.

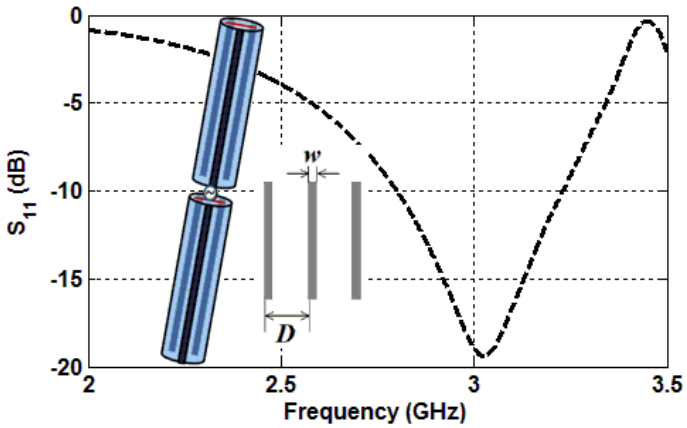

(a)

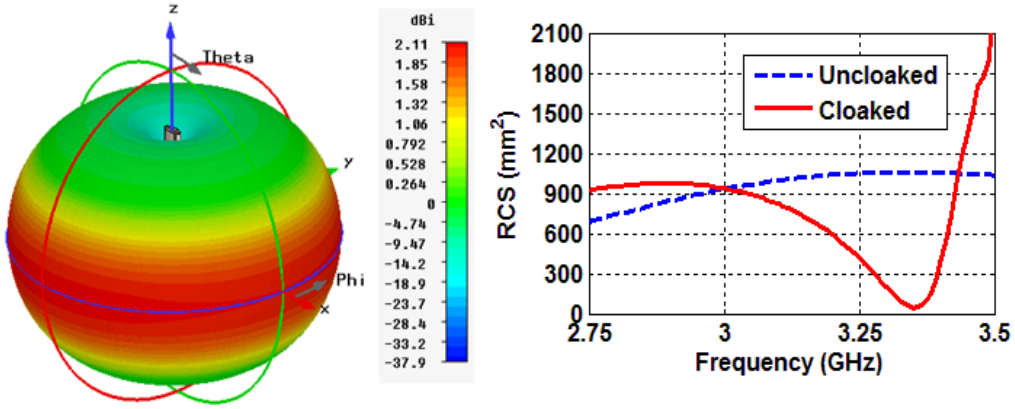

(b)

Figure 2.15 (a) Reflection coefficient of Antenna I after being cloaked, and (b) the radiation pattern of the antenna for the cloaked case (left) at 3.02 GHz and the total scattering width of Antenna I for the uncloaked and cloaked cases (right) with a TM-polarized plane wave at normal incidence with $\varphi = 90°$.

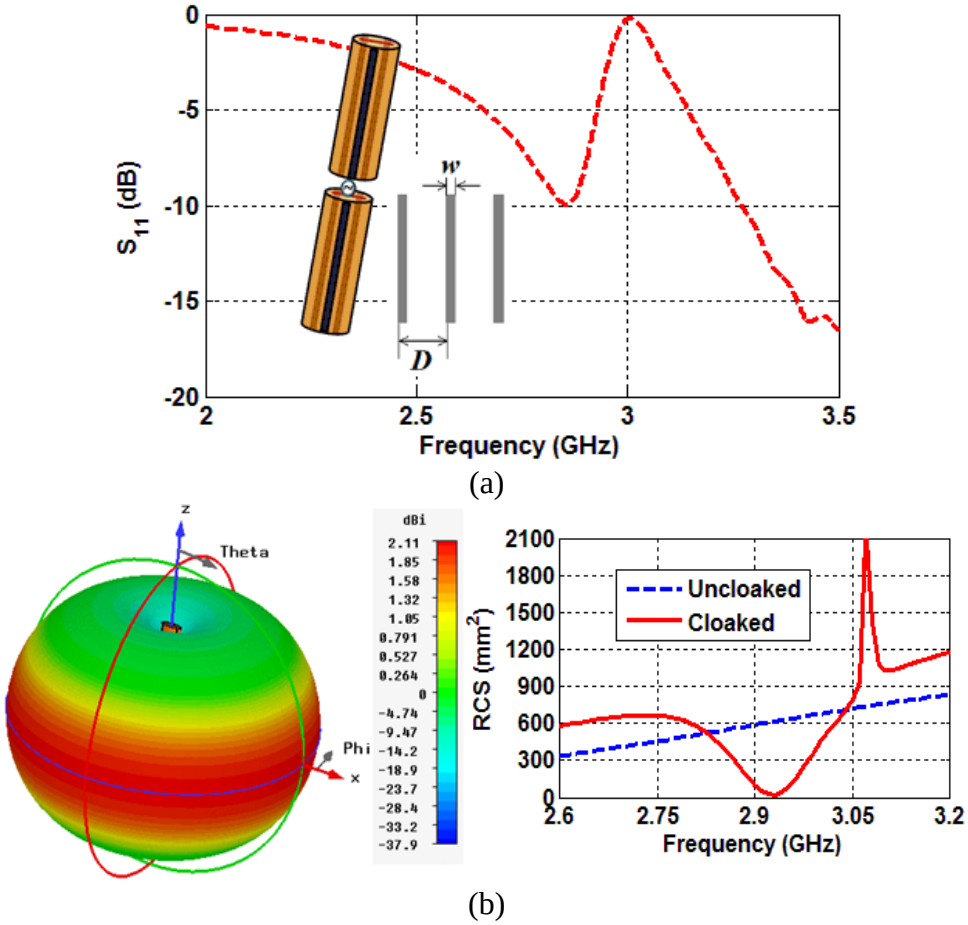

Figure 2.16 (a) The reflection coefficient of Antenna II after being cloaked, and (b) the radiation pattern of the antenna for the cloaked case (left) at 3.33 GHz and the total scattering width of Antenna II for the uncloaked and cloaked cases (right) with a TM-polarized plane wave at normal incidence with $\varphi = 90°$.

Up to now, it has been shown that when two strip dipole antennas, each resonating at a frequency slightly different from the resonance frequency of the other antenna, are put together in very close proximity, their respective reflection coefficient and radiation pattern are totally changed in a way that the antennas are no longer matched to their feed due to the high level of mutual coupling. In order to reduce the mutual coupling in this case, we have utilized inductive vertical strips [61] to cloak each antenna for the resonance frequency of the other one, and at the same time, by optimizing the parameters of the cloak metasurfaces, each of the antennas is matched

to its feed, and its resonance frequency is restored, while they are kept isolated. Now, we expect that the antennas preserve their radiation and matching properties when they are put together with an electrically small distance. The 3-D gain patterns of the antennas and their S-parameters are shown in Figure 2.17. It is evident that by covering the antennas with the elliptical metasurfaces, the original patterns and scattering parameters of the antennas are restored significantly, despite being in very close vicinity of each other. Figure 2.18 shows the gain patterns of Antenna I and Antenna II at $f_1 = 2.9491$ GHz and $f_2 = 3.3515$ GHz, respectively, in the E-plane and H-plane for three different scenarios of (i) isolated, (ii) uncloaked, and (iii) cloaked. In addition, we have also investigated the robustness of the designed metasurface cloaks for different proximity distances; especially for the case they are located further. In Figure 2.19, we show the H-plane radiation patterns of the antennas (E-plane patterns are omitted for the sake of brevity), for the proximity distance of $d = 0.15\,\lambda$ at the resonance frequency of each antenna, and also, at $f = 2.92$ GHz for Antenna I, and $f = 3.37$ GHz for Antenna II. It can be concluded that the optimal designs provide high endurance with respect to the proximity distance, and also, at the frequencies close to the resonance frequency of the antennas.

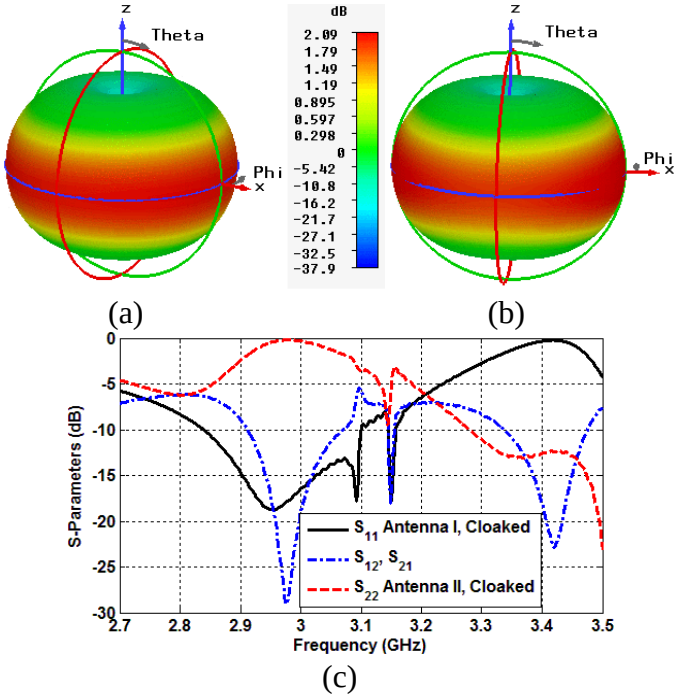

Figure 2.17 3-D radiation patterns of (a) Antenna I at 2.9491 GHz, (b) Antenna II at 3.3515 GHz, and (c) S-parameters at the input ports of Antenna I and Antenna II pertained to the scenario in which each antenna is cloaked for the resonance frequency of the other one and put in very close vicinity of it.

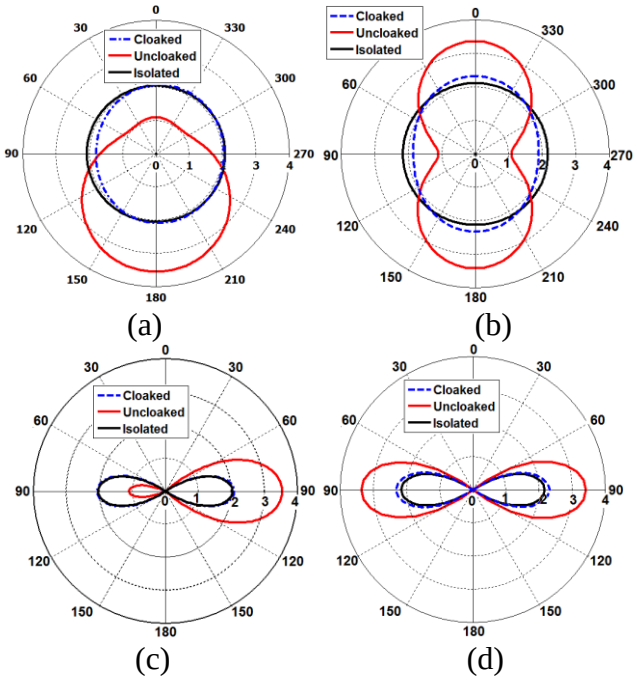

Figure 2.18 Gain patterns of (a) Antenna I at 2.9491 GHz in the H-plane, (b) Antenna II at 3.3515 GHz in the H-plane, (c) Antenna I at 2.9491 GHz in the E-plane, and (d) Antenna II at 3.3515 GHz in the E-plane.

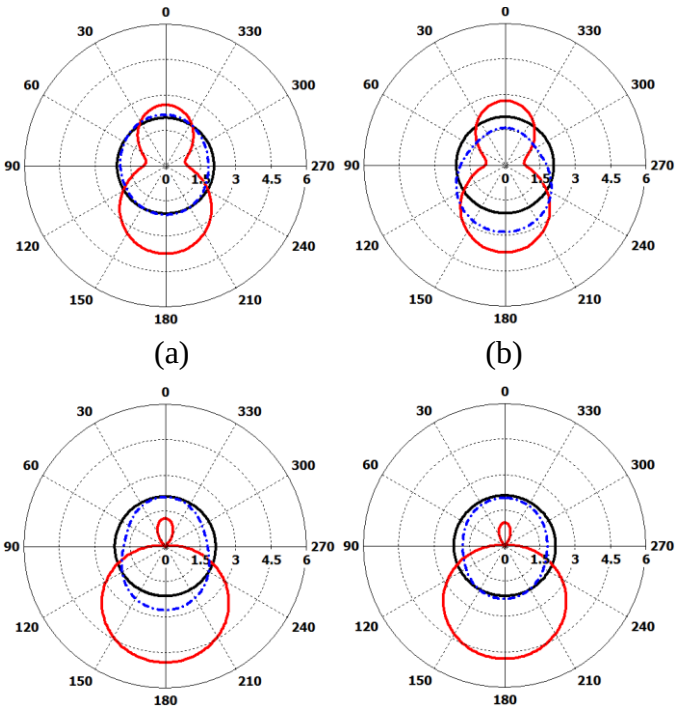

Figure 2.19 Gain patterns of (a) Antenna I at 2.92 GHz (left) and 2.9491 GHz (right) in the H-plane and (b) Antenna II at 3.3515 GHz (left) and 3.37 GHz, in the H-plane for the proximity distance of $d = 0.15\,\lambda$ (The isolated (alone), uncloaked, and cloaked cases are shown by black solid line, red solid line and the dashed blue line, respectively).

2.4 Conclusion

In this chapter, we have proposed to utilize the mantle cloaking method in order to make resonating strip dipole antennas hidden from each other, and consequently, to reduce the mutual coupling between antennas. It has been shown that if the frequencies of the antennas are far from each other, the analytical approach to cloak an infinitely long 2-D strip, considered as a degenerated 2-D elliptical cylinder, can be adopted as a good approximation to provide invisibility for the antenna resonating at the lower frequency. The analytical method is based on the solution of the scattering problem by expressing the incident and scattered fields in terms of Mathieu functions in elliptical coordinates, and also, by using sheet impedance boundary conditions at the metasurface. Also, it has been shown that the matching characteristics and radiation patterns of

two strip dipole antennas resonating at slightly different frequencies can be restored remarkably by covering each antenna with an elliptical metasurface. The numerical results confirm that the radiation properties and matching characteristics of the antennas are recovered in a way that they seem to be unperturbed as they were isolated.

CHAPTER III

REDUCTION OF MUTUAL COUPLING IN PRINTED ANTENNAS

3.1 Introduction

Metamaterials have drawn much attention in recent years and been utilized widely in order to provide electromagnetic invisibility by suppressing both bi-static and total scattering cross-sections (SCS) of the object to be cloaked. In this regard, various methods have been proposed such as transformation optics [5, 7], anomalous resonance method [11], transmission-line networks [12, 14], and plasmonic cloaking [15, 19, 20, 45, 46], among others. These techniques rely on bulk volumetric metamaterials and are difficult to realize in practice. To surmount the issue, a different cloaking technique has been presented based on the concept of mantle cloaking [21]–[28], in which an ultrathin metasurface is used for drastic reduction of the dominant scattering mode of the object to be cloaked. In this method, conformal lightweight cloaks provide anti-phase surface currents to lower the echo width of a given object remarkably. The mantle cloaking method has also been implemented at low-THz frequencies by using a graphene monolayer and a nanostructured graphene patch array [26, 27]. Recently, the idea of mantle cloaking has been extended and an analytical framework for the analysis of the electromagnetic cloaking of dielectric and metallic elliptical cylinders and 2-D metallic strips has been presented in [50, 65], where the cloak structures are realized by a graphene monolayer and a nanostructured graphene patch array at low-THz frequencies, and also, by conformal arrays of sub-wavelength periodic elements at microwave

frequencies.

In addition to non-invasive probing, camouflaging, and imaging, one of the interesting applications of cloaking technology can be considered to be the reduction of mutual coupling between antennas [4]. The destructive mutual coupling effect pertaining to the existence of other elements has always been an important issue in antenna applications and designs. For instance, multiple antennas can be installed in a compact space on complex structures such as shipboards [66] and lowering the coupling levels is highly required. It should be also mentioned that suppressing the mutual coupling caused by the presence of an antenna is more complicated than the case, in which a passive element is present [54]–[57], due to the fact that the cloak structure for an antenna ought to be designed in such a way that provides coupling reduction, and at the same time, preserves the electromagnetic performance of the antenna. Regarding this, recently, the concept of electromagnetic invisibility has been applied [3, 61, 67] to short and half-wavelength dipole antennas. In [3], the plasmonic cloaking method has been used for making a sensor (a short dipole antenna) invisible while being able to receive an incoming signal. In [61], the mantle cloaking method has been utilized to suppress the mutual blockage effects between two cylindrical dipole antennas with close resonance frequencies. In [67], confocal elliptical 1-D printed sub-wavelength elements have been applied to cloak strip dipole antennas in free space, and consequently, led to the restoration of the matching characteristics and radiation patterns of the antennas.

Microstrip antennas are widely used in modern crowded electromagnetic environments such as airborne and wireless communications, wherein demands for high performance, reliability, compactness, and lightweight ought to be met. However, this leads to the increase in mutual

coupling level between closely spaced radiators. The sources of this unwanted destructive effect related to planar microstrip antennas can be classified as: (i) near-field coupling, (ii) far-field coupling, and (iii) surface-wave coupling [68]. The near-field coupling arises when an antenna is located in the near-field zone (Fresnel region) of another antenna, wherein electromagnetic fields are reactive and decrease rapidly as the distance becomes larger. It should be mentioned that this type of coupling will be more pronounced in case of low-permittivity substrates due to the fact that the wavelength in the substrate is very close to that of the free-space, and will deteriorate the radiation properties of antennas drastically. On the other hand, the far-field coupling or the space-wave coupling occurs due to the radiation energy absorbed by an antenna located in the far-field zone (Fraunhofer Region) of another antenna. This type of coupling will be more involved in power interactions between antennas if a thin grounded dielectric substrate is used. Besides these coupling mechanisms, a microstrip antenna typically excites surface waves, which are guided by its dielectric substrate and ground plane. Surface waves are critical only when the thickness of the substrate is large [69] in a way that the ratio of the substrate thickness (h) to the free-space wavelength (λ_0) is equal or greater than $h/\lambda_0 = 0.048/\sqrt{\varepsilon_r}$ (ε_r is the relative permittivity of the substrate) [68].

Various methods have been proposed in several papers in the literature in order to deal with the problem of mutual coupling between printed antennas. In [52], mushroom-like electromagnetic band gap (EBG) structures have been utilized in order to suppress surface waves, caused by thick and high permittivity substrates, for antennas with a separation of $d = 0.75\ \lambda_0$ with the use of unit cells connected to the ground through via. In addition to various EBG designs [70]–[75], defected grounded structures (DGS) [76]–[80], realized by etching the ground plane with a specific shape,

which manipulates the current distribution of an antenna, have been proposed to provide a bandstop effect due to the combination of inductance and capacitance, and thus, lower near-field coupling and surface-wave coupling. This frequency bandgap can be controlled by changing the shape (such as U-shaped [80], circular [81], elliptical [82], and dumbbell [83]), dimension and position of the designed DGS. For instance, in [80], a U-shaped DGS and an inverted U-shaped resonator have been employed to reduce the near-field coupling between two nearby microstrip antennas resonating at slightly different frequencies with a separation of $d = 0.4\,\lambda_1$ (λ_1 is the wavelength related to the antenna with the lower frequency). In [84], an approach based on the idea of field cancellation has been introduced to suppress the mutual coupling (near-field coupling mechanism) between two closely spaced metamaterial-inspired printed monopole antennas. However, it should be mentioned that this method is not applicable for higher frequencies such as the upper WiFi band (5.15–5.8 GHz). Besides, insertion of slits [85] and parasitic elements [86]–[89] are other techniques to be mentioned. It is worth noting that in spite of numerous techniques and designs that have been proposed so far, to establish and develop an efficient method for the reduction of mutual coupling, without affecting antenna characteristics and radiation patterns, is still immensely challenging.

Here, we propose a novel technique to lower the electromagnetic interaction between microstrip antennas and overcome the mutual coupling blockage effect on the basis of the well-known mantle cloaking method [26, 27]. To explicate further, it should be mentioned that, fundamentally, this approach is inspired by the cloaking of 2-D elliptical objects discussed in [65], wherein confocal and conformal elliptically shaped metasurfaces make it possible to provide electromagnetic invisibility for infinitely long metallic elliptical cylinders and strips. Also, in [67],

it has been shown that this concept can be applied to half-wavelength free-standing strip dipole antennas considered as 3-D elliptical objects. In order to extend and link the concept of electromagnetic invisibility (realized by metasurfaces) to the suppression of mutual coupling between printed antennas, it is worth noting that the non-symmetric configuration of metallic strips (in terms of bi-static scattering cross-section) in microstrip technology necessitates the use of elliptical cloak structures [65, 67]. In fact, the cloak designs provided in [61] for free-standing cylindrical dipole antennas cannot be extended to microstrip antennas due to the circular cross-sections of the antennas and their respective metasurface cloaks. To meet the requirements of coupling reduction in printed technology, here we propose the idea of suppressing the electromagnetic interactions between antennas based on the technique presented in [67] and demonstrate that how elliptically shaped metasurfaces can overcome the mutual coupling between microstrip-fed monopole antennas. To convey the novel idea, we consider two microstrip-fed monopole antennas resonating at slightly different frequencies and show that by covering each antenna with a properly designed conformal elliptical metasurface (the foci of each elliptical metasurface coincides with the edges of each strip) formed by printed arrays of sub-wavelength periodic elements, partially embedded in the substrate, the antennas become invisible to each other and their radiation patterns are restored as if they were isolated. Since the mantle cloaking method provides invisibility for small and large distances [27], it should be noted that our proposed cloak structure and the resulting mutual coupling reduction works for both near-field and far-field regions. The surface-wave coupling can be neglected due to the low-permittivity substrate used in our design.

This chapter is organized as follows. Section II is devoted to the design procedure. In

Section III, we introduce the proposed mantle cloak design and we describe how elliptically shaped sub-wavelength conformal printed elements involve in the reduction of near-field coupling and far-field coupling between the microstrip-fed monopole antennas. Section IV is allocated to the conclusion.

3.2 Design Procedure

To clarify the design procedure and discuss the application of elliptically shaped metasurfaces for mutual coupling reduction between the antennas with metallic strip inclusions, first of all, it is worth noting that this type of mantle cloaks is inspired by the analytical approach used for cloaking infinitely long metallic elliptical cylinders and strips, wherein the object to be cloaked is supposed to be under a transverse magnetic (TM) plane-wave excitation [65]. The analytical method is based on the solution of the scattering problem by expressing the incident and scattered fields in terms of Mathieu functions in elliptical coordinates, and also, by using sheet impedance boundary conditions at the metasurface, which implies the fact that the metasurface cloak should be conformal and confocal with respect to the object in order to achieve efficient electromagnetic invisibility. Although elliptical objects have been considered to be infinitely long in this method, recently, in [67], it has been shown that the idea can be generalized to the objects with finite lengths, and it has been illustrated that by covering strip dipole antennas with elliptical metasurfaces, the antennas become invisible to each other, and thus, mutual coupling reduction can be obtained. Here, the question is that how elliptical cloak structures can be realized for the antennas widely used in printed technology.

An interesting feature of the aforementioned metasurface cloaks is that once the optimized parameters for the free-standing dipole antennas are found, these parameters can be applied to

other antenna structures of the same frequency such as free-standing monopole antennas and dipole antennas printed on a low-permittivity substrate. In addition, it should be mentioned that in case of high-permittivity substrates or a substrate with a ground plane, again the same cloak structures are applicable, and can be used by only modifying the permittivity of the dielectric spacer of the cloak, which will be discussed for microstrip-fed monopole antennas in the next section. For example, for the monopole antennas shown in Figure 3.1, namely Antenna I (left) and Antenna II (right), with the parameters: $L_1 = 22.75$ mm, $L_2 = 20.65$ mm, $W = 4$ mm, $\Delta = 0.1$ mm, $D = 3.4034$ mm, $a = 2.2$ mm, $b = 0.9165$ mm, $\varepsilon_{c_1} = 6.15$, $\varepsilon_{c_2} = 9.8$, $w_1 = 0.35$ mm, $w_2 = 0.3$ mm, and a separation of $d = 10$ mm, $f_1 = 3.02$ GHz and $f_2 = 3.33$ GHz, mutual coupling reduction can be obtained by covering the antennas with the same metasurface cloaks formed by inductive vertical strips presented in [67] with no modifications.

Figure 3.2 shows the gain patterns of Antenna I and Antenna II at $f_1 = 2.9$ GHz and $f_2 = 3.3$ GHz, respectively, in the E-plane and H-plane for three different cases of (i) isolated, (ii) uncloaked, and (iii) cloaked. It can be clearly seen that by using the same elliptically shaped metasurface cloaks as the ones provided in [67], the monopole antennas can be hidden from each other, and thus, their radiation patterns are restored. The S-parameters of the antennas are not shown here for the sake of brevity.

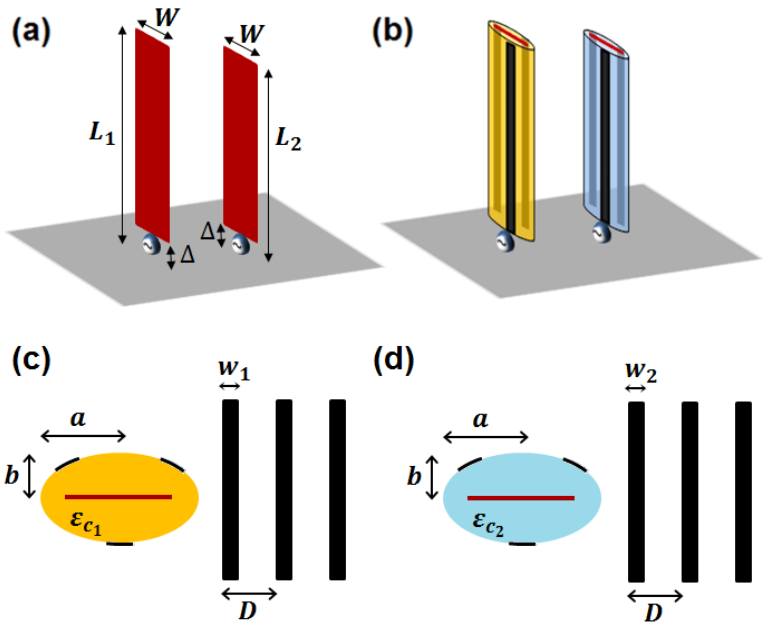

Figure 3.1 Schematics of monopole Antenna I and Antenna II for (a) uncloaked and (b) cloaked cases. Cross-section view of the cloak structure and the metasurface for (c) Antenna I and (d) Antenna II.

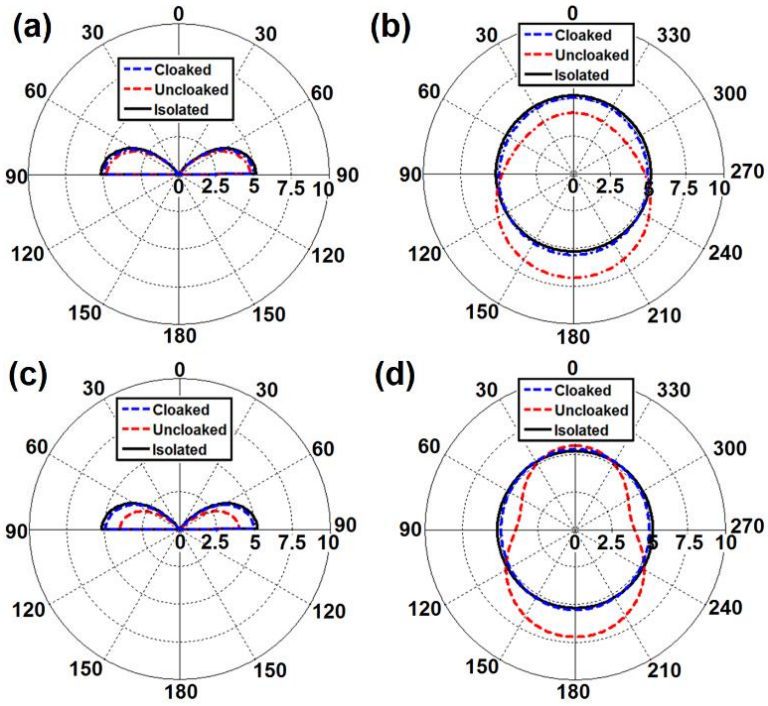

Figure 3.2 Gain patterns of Antenna I at 2.9 GHz (a) in the E-plane and (b) in the H-plane, and Antenna II at 3.3 GHz (c) in the E-plane and (d) in the H-plane.

Here, we present another example in order to verify the fact that the metasurface cloaks designed and optimized for free-standing dipole antennas can be applied to achieve mutual coupling reduction for well-known printed dipole antennas. For instance, consider two dipole antennas resonating at slightly different frequencies printed on a common Rogers RT/duroid 5880 substrate with $\varepsilon_r = 2.2$ and $h = 1.575$ mm as shown in Figure 3.3. We place the dipole antennas close to each other with a short distance of $d = 0.1\,\lambda$ at $f = 3$ GHz. As expected, the presence of each antenna affects the radiation pattern of the other one intensely, and thus, they no longer provide their original radiation patterns. Now, by covering the antennas with the elliptical metasurfaces used for the previous example (as provided in [67]), the mutual near-field coupling between the antennas decreases drastically, and the original patterns of the antennas are restored significantly. Figure 3.4 shows the gain patterns of Antenna I and Antenna II at $f_1 = 2.9$ GHz and $f_2 = 3.3115$ GHz, respectively, in the E-plane and H-plane for isolated, uncloaked, and cloaked cases.

As a summary, to explain the design process for printed antennas, it should be mentioned that similar to the design process in [67], initially, we consider to have a specific value for the total number of vertical strips of the cloak structure, which implies to have a specific value for the periodicity (D) due to the perimeter of the dielectric spacer. Then, we deal with the change in two parameters to tune the properties of each metasurface: i) the widths of the vertical strips and ii) the permittivity of the dielectric spacer (ε_c). Subsequently, we perform a case study optimization in such a way that all the parameters are considered to be constant along with one of these two parameters, and by varying the other one, we examine the cloaking behavior in terms of the mutual scattering parameter (S_{12}) and the change in the resonance frequency of each antenna. This careful

and systematic study leads to finding optimum values for the elliptically shaped metasurface. As discussed in details in [67], for the case of the antennas with the frequencies far from each other, the cloak parameters can be found directly from the analytical approach by solving the scattering problem in terms of Mathiue function, which makes the design process much easier.

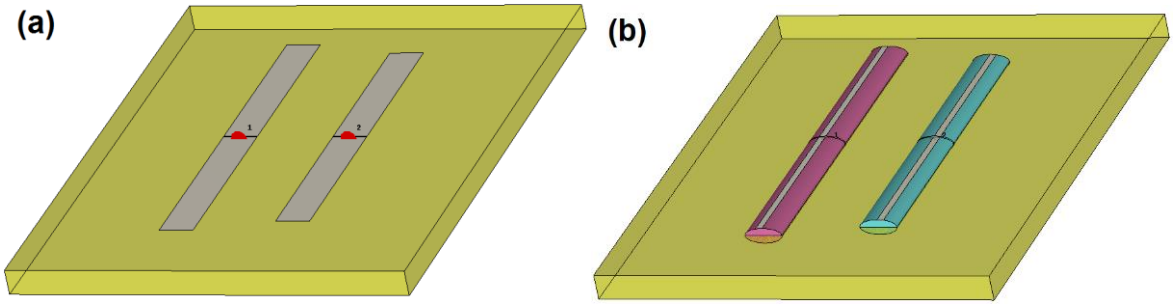

Figure 3.3 Schematics of printed monopole Antenna I and Antenna II for (a) uncloaked and (b) cloaked cases.

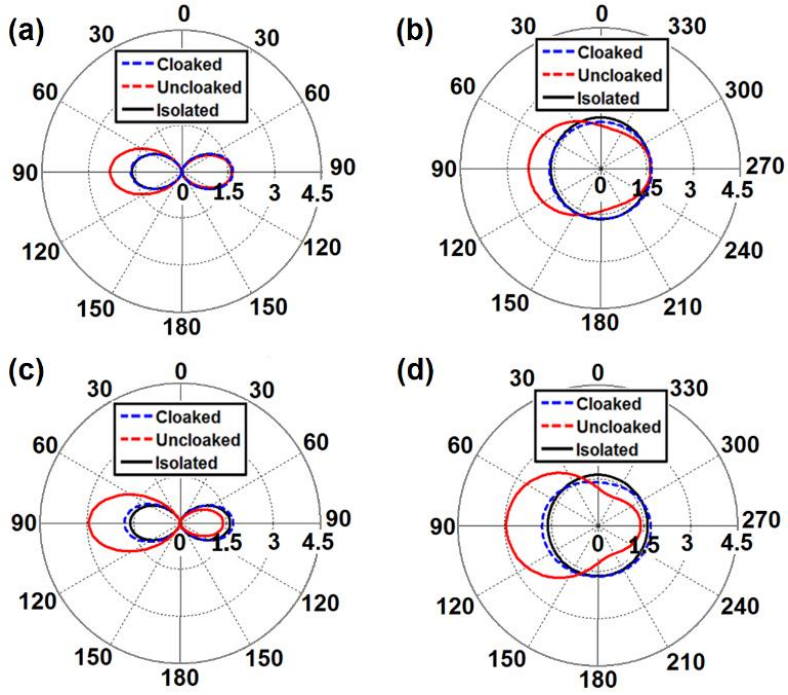

Figure 3.4 Gain patterns of Antenna I at 2.9 GHz (a) in the E-plane and (b) in the H-plane, and Antenna II at 3.3115 GHz (c) in the E-plane and (d) in the H-plane.

3.3 Cloaking of Microstrip-Fed Monopole Antennas and Reduction of Mutual Coupling

Here, we present the mechanism of mutual coupling reduction between two microstrip-fed monopole antennas based on the mantle cloaking method, realized by confocal elliptically shaped metasurfaces. In order to clarify the problem, we consider three different cases of (i) isolated, (ii) uncloaked, and (iii) cloaked. First of all, we study the radiation pattern and reflection coefficient of each antenna in the isolated case, wherein the antennas are supposed to operate while no other object is present. Then, we consider the antennas to be in the proximity of each other with no cloak structures, and investigate the effects of this case, in which the antennas are coupled to each other and exchange power. Finally, we consider the cloaked case, wherein the antennas are covered by appropriately designed elliptical metasurfaces in order to compensate and neutralize the coupling effects, and thus, restore the radiation patterns and impedance characteristics of the antennas as if they were isolated. It is of paramount importance that these elliptical metasurface cloaks should be engineered in such a way that make the antennas invisible to each other, and simultaneously, preserve their impedance characteristics at their resonance frequencies with the performance similar to the isolated case.

Since a low-permittivity substrate has been used here and $h/\lambda_2 < 0.048/\sqrt{\varepsilon_r}$ ($h/\lambda_2 = 0.017$ and $0.048/\sqrt{\varepsilon_r} = 0.032$, and λ_2 is the wavelength of the antenna with the higher frequency), the surface-wave coupling is weakly excited and its effect on the resulting mutual coupling between the antennas can be neglected. Due to this condition, in the upcoming sub-sections, two different scenarios are studied in details in order to suppress the near-field coupling and the far-field coupling between the antennas. In the first scenario, we consider the antennas to be separated in a way that they are in the near-field region of each other, and in the second scenario,

the antennas are located in the far-field region of each other, wherein the near-field and far-field coupling mechanisms are dominant, respectively.

3.3.1 Scenario I – Reduction of Near-Field Coupling

As mentioned in Section I, the presence of a microstrip antenna in the near-field region of the other one results in power exchange between the antennas and this mutual coupling may change the characteristics of each antenna. To present the applicability of the proposed coupling reduction method, first of all, here we consider two microstrip-fed monopole antennas in the isolated case resonating at $f_1 = 3$ GHz (Antenna I) and $f_2 = 3.33$ GHz (Antenna II), each on a Rogers RT/duroid 5880 substrate with $\varepsilon_r = 2.2$ and $h = 1.575$ mm, and a partial ground structure (non-symmetric with respect to the location of the antennas) as shown in Figure 3.5 with the parameters: $L = 55$ mm, $M = 63$ mm, $L_1 = 37.65$ mm, $L_2 = 35.4$ mm, $W = 4$ mm, $s = 19.5$ mm, and $G = 17$ mm. Also, the reflection coefficients and radiation patterns of the antennas related to the isolated case are shown in Figures 3.6 and 3.7, respectively. Full-wave simulations have been performed by using CST Microwave Studio [42].

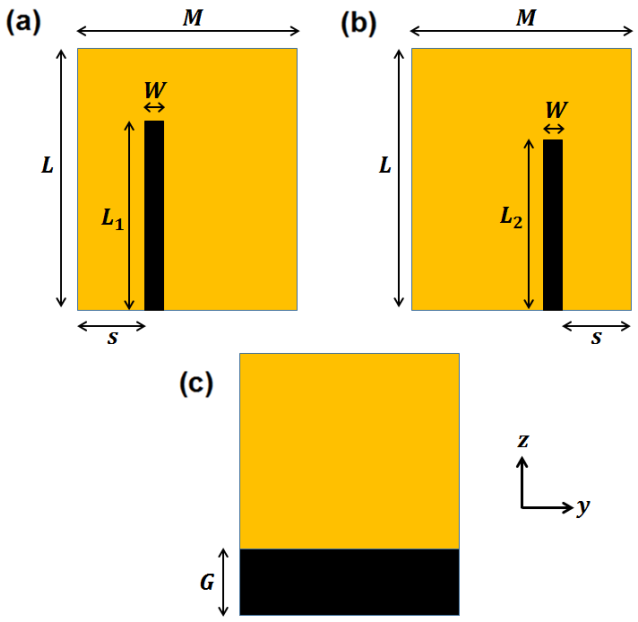

Figure 3.5 Schematics of the top view of (a) the isolated microstrip-fed monopole Antenna I at 3 GHz, and (b) the isolated monopole Antenna II at 3.33 GHz. (c) The bottom view of the antennas.

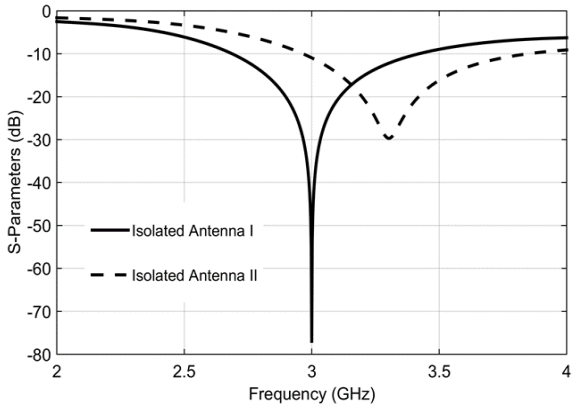

Figure 3.6 Reflection coefficients at the input ports of Antenna I and Antenna II for the isolated case.

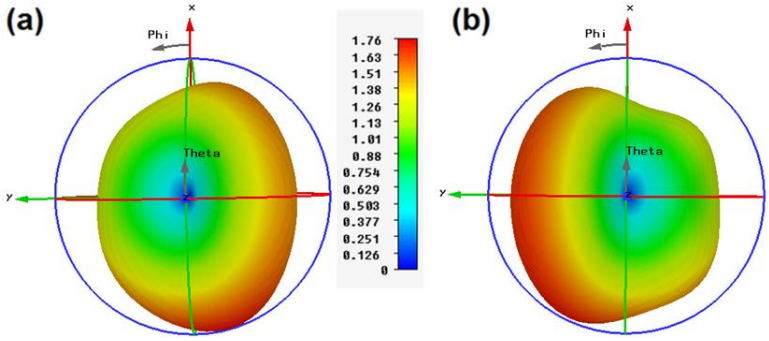

Figure 3.7 3-D linear gain patterns of the isolated (a) Antenna I at 3 GHz and (b) Antenna II at 3.33 GHz.

To study the coupling effect, we place the aformentioned planar monopole antennas close to each other with a short distance of $d = 0.16\,\lambda_1$ (λ_1 is the wavelength related to Antenna I) at $f = 3$ GHz (Figure 3.8(a)). As expected, in the coupled but uncloaked case, the presence of each antenna changes the radiation pattern of the other one drastically, and thus, they no longer provide their original radiation patterns as illustrated in Figures 3.8(b) and 3.8(c).

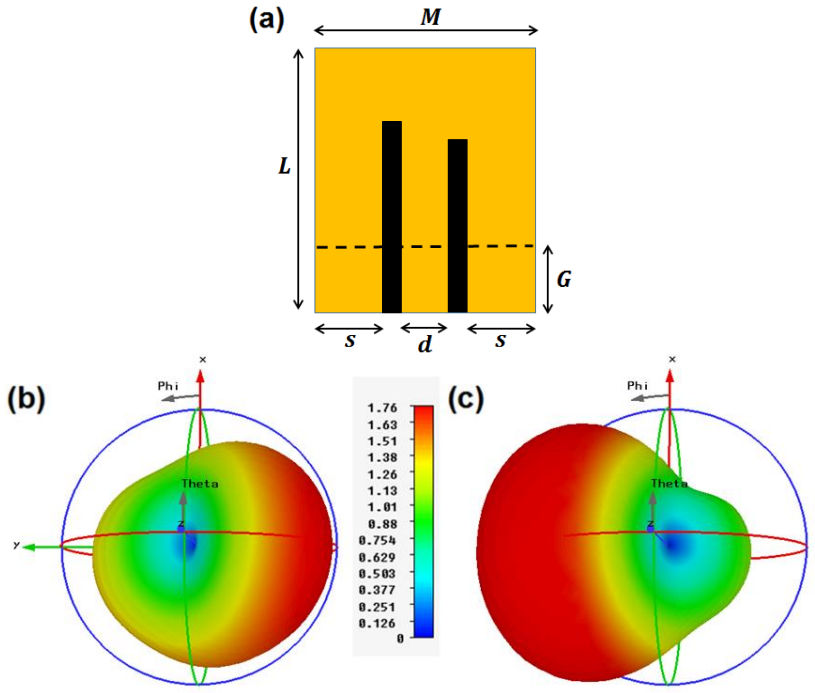

Figure 3.8 Schematics of microstrip-fed monopole Antenna I (left) and Antenna II (right) for the coupled but uncloaked case. 3-D linear gain patterns of (b) Antenna I at 3 GHz and (c) Antenna II at 3.33 GHz.

Now, in order to surmount the issue mentioned above and overcome the blockage effect of the near-field coupling between the antennas, we propose to cover the radiating part of each antenna with its respective conformal elliptical metasurface formed by confocal printed arrays of sub-wavelength periodic elements, partially embedded in the substrate. The configuration of the

antennas with the proposed cloak structures are shown in Figure 3.9 with the parameters: $R_1 = 20.65$ mm and $R_2 = 18.4$ mm.

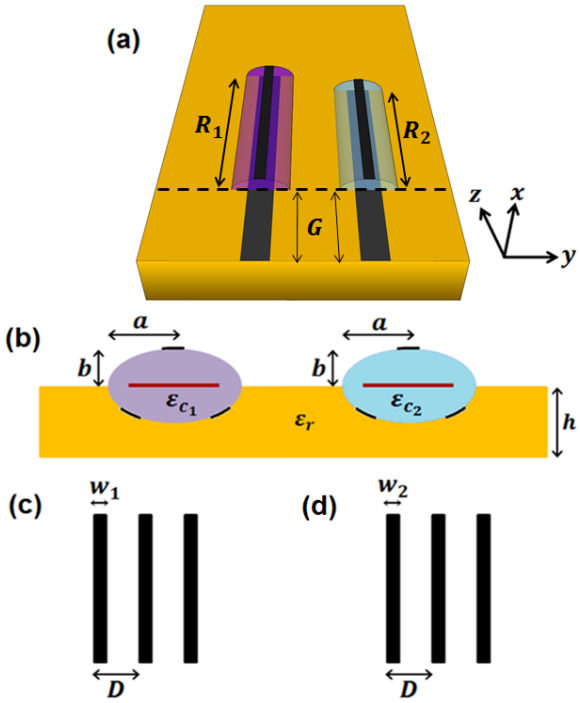

Figure 3.9 Schematics of Antenna I and Antenna II for the cloaked case. Cross-section view of the antennas in the cloaked case. The metasurface cloak for (c) Antenna I and (d) Antenna II in the cloaked case.

To achieve an appropriate cloak design for the antennas, according to the design procedure mentioned in the previous section, we consider to have $N = 3$ as the total number of vertical strips of the cloak structure, which implies to have $D = 3.4034$ mm due to the perimeter of the dielectric spacer with $a = 2.2$ mm and $b = 0.9165$ mm. In order to find optimum values for the parameters of the cloak structures, initially, we consider the dimensions mentioned in the previous section for the free-standing monopole antennas and the printed dipole ones, exactly the same as the parameters given in [67]. Based on these initial values and following the procedure explained in Section II, we perform a careful case study to find the optimum values for which the interaction

and coupling between the antennas will be minimized, and at the same time, their input impedances will be recovered. The optimum values of the elliptically shaped metasurface cloaks obtained by numerical simulations are: $\varepsilon_{c_1} = 5.55$, $\varepsilon_{c_2} = 9.8$, $w_1 = 0.35$ mm, and $w_2 = 0.3$ mm. It can be clearly seen that the same metasurfaces as the ones mentioned in the previous section can be applied to the microstrip-fed antennas here, only with a slight change in ε_{c_1} from $\varepsilon_{c_1} = 6.15$ to $\varepsilon_{c_1} = 5.55$. The 3-D linear gain patterns of the antennas along with their S-parameters are shown in Figure 3.10. The results imply the fact that covering the radiating parts of each antenna by its respective properly designed cloak leads to the restoration of the radiation patterns of the antennas and recovering their input impedance characteristics qualitatively. To compare the uncloaked and cloaked cases quantitatively in terms of the mutual scattering parameter (S_{12}), it should be mentioned that at $f = 2.97$ GHz, the S_{12} is reduced about 25.5 dB, and at $f = 3.35$ GHz, the S_{12} is improved about 29.5 dB, which confirms the applicability of the mantle cloaks for suppressing the near-field coupling between these monopole antennas. In addition, it can be observed that the 3-D patterns of the antennas are very much similar to the isolated case shown in Figures 3.7(b) and 3.7(c). Here, to provide a fair comparison between the radiation patterns, the 2-D linear gain patterns of the antennas for the isolated, coupled but uncloaked, and cloaked cases are illustrated in Figure 3.11 in the H-plane (xy-plane) and E-plane (xz-plane). It is obvious that the radiation patterns of the antennas are recovered remarkably by applying the metasurfaces formed by inductive vertical strips. Actually, the presence of each antenna forces the pattern of the other one to become highly directive in the absence of the cloak structures, while in case of their presence, the antennas radiate in a very much similar way to the isolated case.

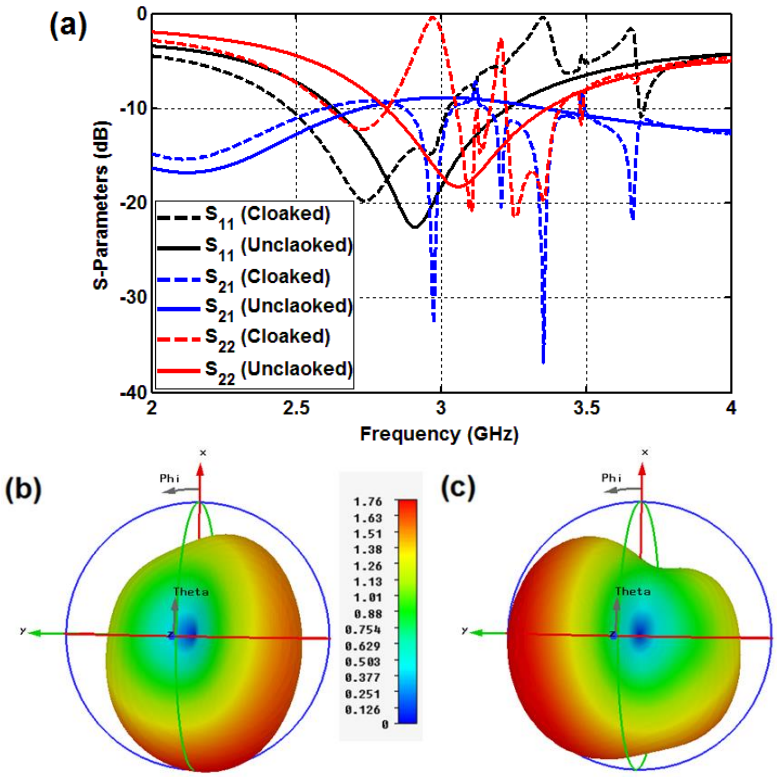

Figure 3.10 (a) S-parameters of the antennas for the coupled but uncloaked case and the cloaked case. 3-D linear gain patterns of (b) Antenna I at 2.95 GHz and (c) Antenna II at 3.35 GHz.

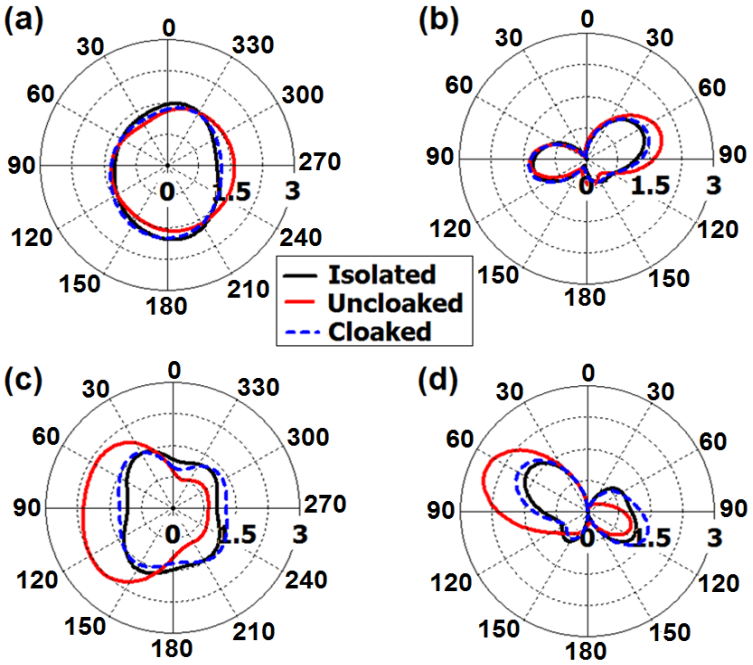

Figure 3.11 Linear gain patterns of Antenna I at 2.95 GHz (a) in the H-plane and (b) in the E-plane. Linear gain patterns of Antenna II at 3.35 GHz (c) in the H-plane and (d) in the E-plane.

To clarify further the concept of mutual coupling reduction based on the proposed design, the time snapshots of the electric field distributions of the antennas are shown for the top view in Figure 3.12. For the uncloaked case, the electric fields of each antenna is intensively perturbed due to the presence of the other antenna in its near-field region, and the power is coupled to the port of the neighboring antenna through the microstrip feed line. On the other hand, the presence of the mantle cloaks reduces the field interaction between the antennas by making the radiating parts of the antennas invisible to each other, and thus, the electric fields produced by each antenna are not sensed by the input port of the other antenna. Also, in Figure 3.13, a cross-section view of the electric field distribution at $z = 25$ mm is provided, in which Antenna I is excited but Antenna II is passive. It can be clearly seen that in the cloaked case, the radiator part of Antenna II is invisible to the incoming near fields originated from Antenna I, while in the uncloaked case the electric field is coupled to Antenna II and the radiation power of Antenna I is transferred to Antenna II. In Figure 3.14, the current distributions of the antennas are shown for different cases and the top view. In the uncloaked case, the microstrip-fed antennas are strongly involved in the near-field coupling and each excited antenna induces a surface current on the neighboring antenna. However, when the radiating parts of the antennas are cloaked, due to the nature of the mantle cloaking method, in which anti-phase surface currents are produced by the cloak structure to cancel the induced currents on the object to be cloaked, induced surface currents are canceled by the elliptically shaped metasurfaces and will not reach the input port of the neighboring antenna. Hence, the mutual coupling between the antennas will be lowered drastically in a way that the antennas do not sense the presence of each other.

In addition to the parameters mentioned above, here we consider the results of the total

radiation efficiencies of the antennas, simulated and calculated by using CST Microwave Studio, plotted in Figure 3.15. It can be observed that the total efficiencies of the antennas have been improved in the cloaked case in comparison to the uncloaked case at their resonance frequencies. It should be emphasized that the presence of the metasurfaces not only improves the total efficiency of each antenna at its own frequency, but also reduces its efficiency drastically at the resonance frequency of the other antenna, and thus, makes it a poor radiator at that frequency. Hence, the mutual coupling between the antennas will be lowered remarkably in comparison to the case, wherein the antennas are dramatically coupled with no metasurface cloaks.

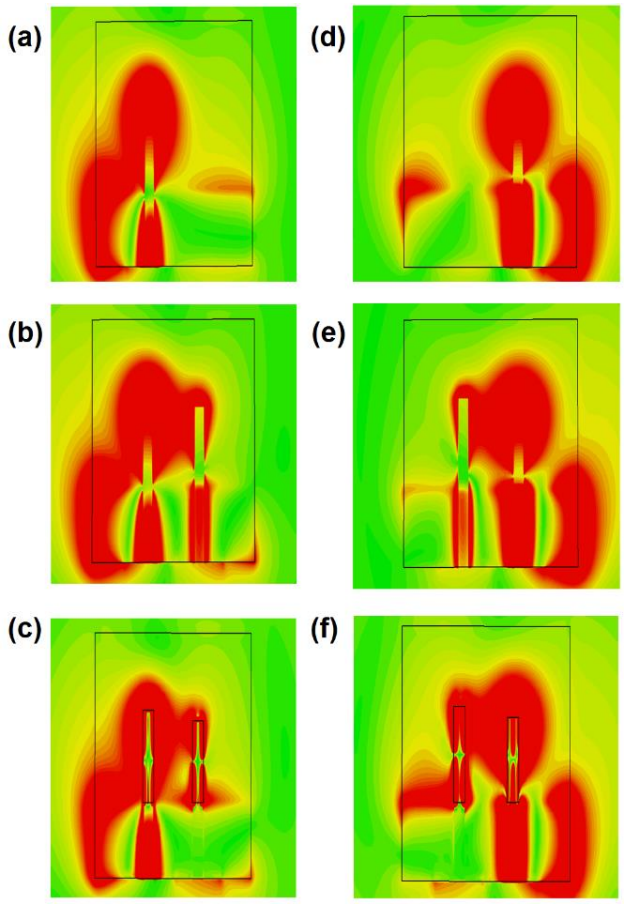

Figure 3.12 Snapshots of the electric field distributions of Antenna I at 2.95 GHz for (a) isolated, (b) uncloaked, and (c) cloaked cases. Snapshots of the electric field distributions of Antenna II at 3.35 GHz for (a) isolated, (b) uncloaked, and (c) cloaked cases.

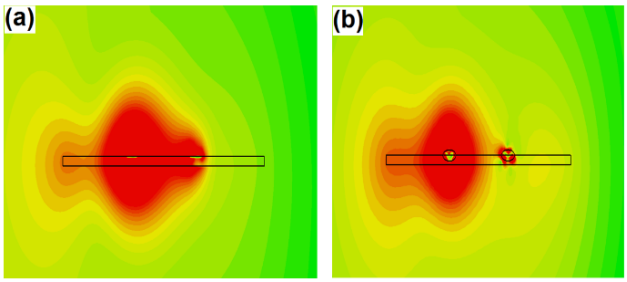

Figure 3.13 Cross-section view of the snapshots of the electric field distributions of Antenna I at 2.95 GHz and $z = 25$ mm for (a) uncloaked and (b) cloaked cases.

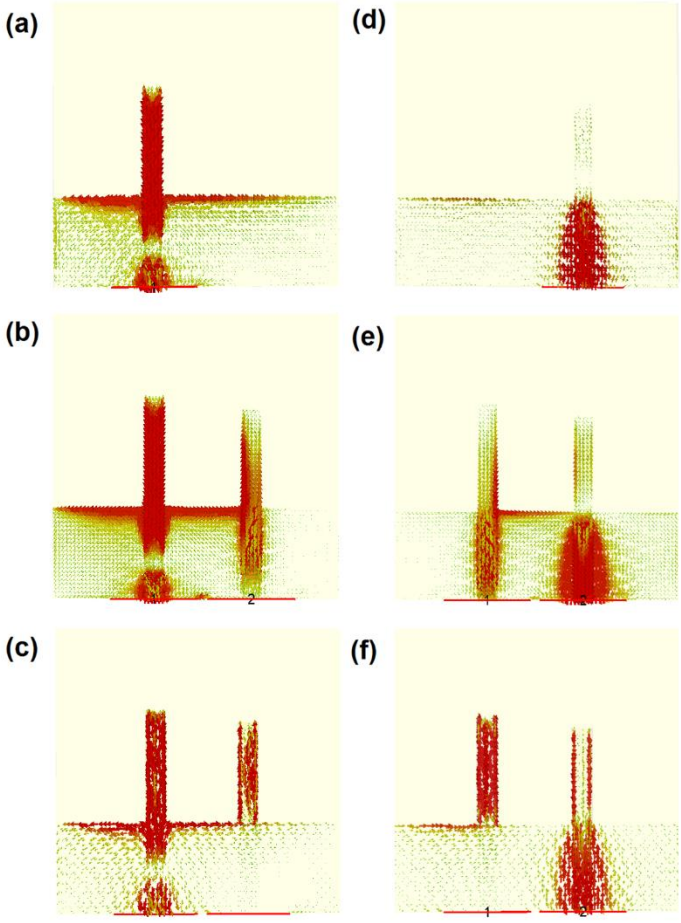

Figure 3.14 Current distributions of Antenna I at 2.95 GHz for (a) isolated, (b) uncloaked, and (c) cloaked cases. Current distributions of Antenna II at 3.35 GHz for (a) isolated, (b) uncloaked, and (c) cloaked cases.

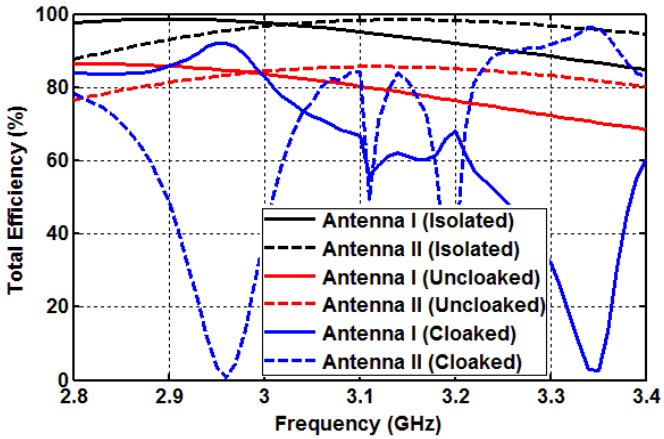

Figure 3.15 Total efficiencies of the antennas for the isolated, uncloaked, and cloaked cases.

3.3.2 Scenario II – Reduction of Far-field Coupling

In this sub-section, our objective is to investigate the coupling effect between the antennas located in the far-field region of each other, and present the applicability of the same cloak structures introduced previously and show how these confocal and conformal elliptical metasurfaces are able to lower the far-field coupling between the antennas and their presence leads to the restoration of the radiation patterns of the microstrip-fed monopole antennas. In a similar way to Section A, initially, we supposed to have the antennas in the isolated case (Figure 3.16) with $M = 97$ mm, and all other parameters are the same as the ones mentioned in Scenario I. Due to the change in the size of the non-symmetric ground plane structure of the antennas, their S-parameters and radiation patterns will be different from the ones presented in the previous section as shown in Figure 3.17 and Figure 3.18.

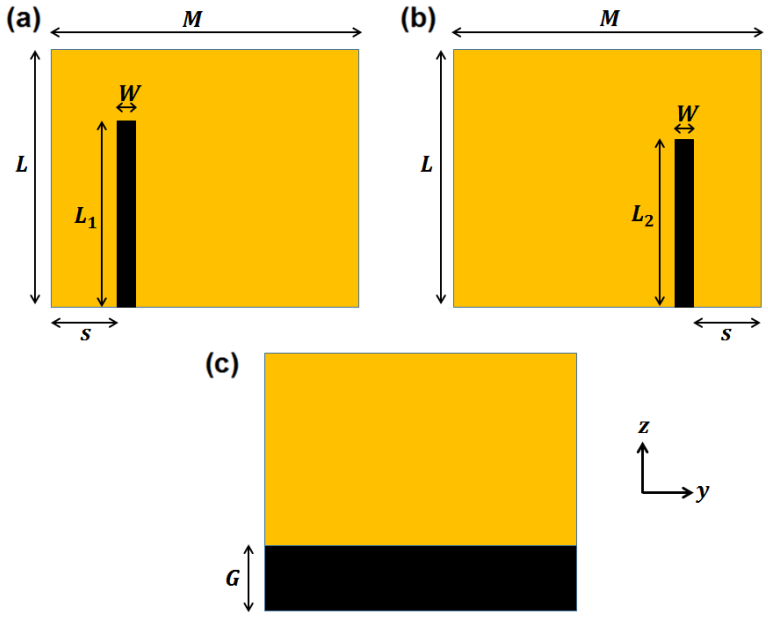

Figure 3.16 Schematics of (a) the isolated microstrip-fed monopole Antenna I at 3 GHz, and (b) the isolated monopole Antenna II at 3.33 GHz. (c) The bottom view of the antennas.

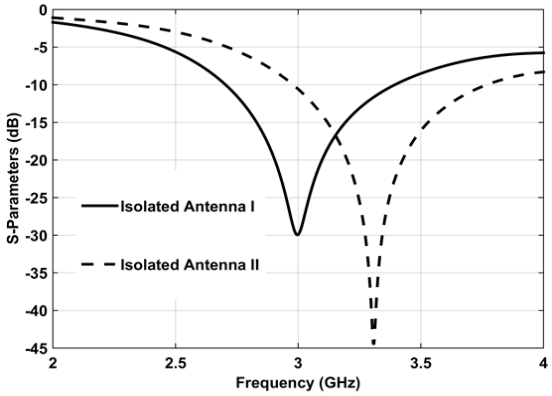

Figure 3.17 Reflection coefficients at the input ports of Antenna I and Antenna II for the isolated case.

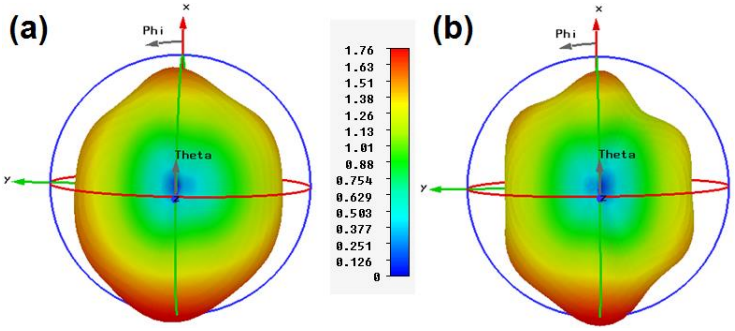

Figure 3.18 3-D linear gain patterns of the isolated (a) Antenna I at 3 GHz and (b) Antenna II at 3.33 GHz.

Now, we place both of the antennas on the same substrate with a separation of $d = 0.5\,\lambda_1$ (λ_1 is the wavelength related to Antenna I) at $f = 3$ GHz (Figure 3.19(a)). To examine the consequence of this configuration in terms of radiation pattern, the 3-D linear gain patterns of the antennas are shown in Figures 3.19(b) and 3.19(c).

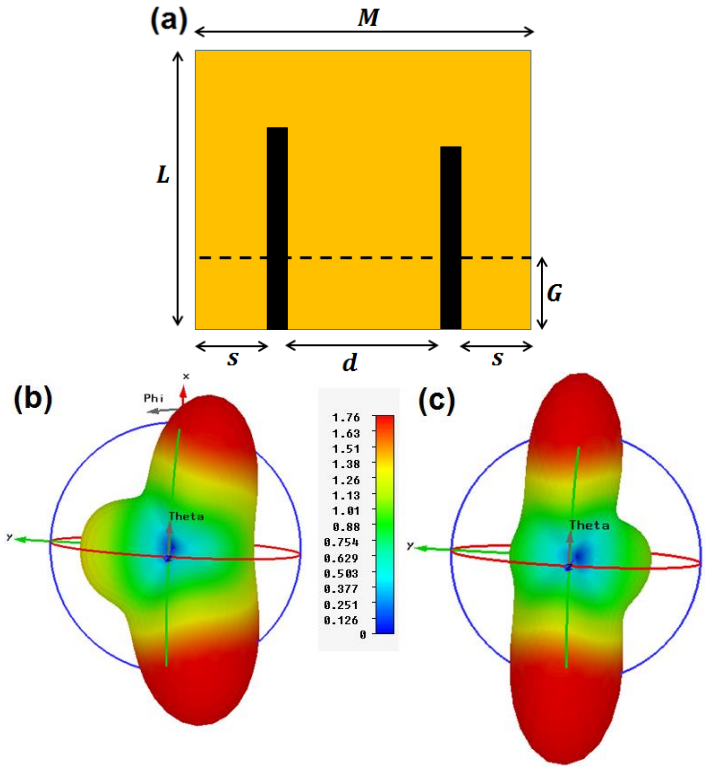

Figure 3.19 Schematics of microstrip-fed monopole Antenna I (left) and Antenna II (right) for the coupled but uncloaked case. 3-D linear gain patterns of (b) Antenna I at 3 GHz and (c) Antenna II at 3.33 GHz.

It can be clearly seen that the presence of the antennas changes the gain pattern of each antenna intensively in such a way that the pattern becomes highly directive. In fact, since the resonance frequencies of the antennas are close to each other, with a separation of half-wavelength for Antenna I and near to half-wavelength for Antenna II, this configuration of the antennas results in an array-type radiation pattern, which is not of interest for these microstrip-fed antennas that are

supposed to operate individually and radiate in such a way that their own radiation patterns encounter no change. To suppress the resulting far-field coupling between the antennas and restore their radiation patterns, we cover each antenna with the same cloak structure in Section A as shown in Figure 3.20 with the parameters of the metaurfaces the same as the ones in Scenario I. The 3-D linear gain patterns of the antennas and their S-parameters are shown in Figure 3.21. Similar to the previous scenario, it is obvious that cloaking the antennas by the conformal metasurfaces provides mutual coupling reduction, and thus, restores their radiation patterns as if they were isolated. It is worth pointing out that the mutual scattering parameter (S_{12}) of the antennas have been improved about 35.6 dB and 29 dB for Antenna I at $f = 2.98$ GHz and Antenna II at $f = 3.36$ GHz, respectively, verifying the fact that the far-field coupling between the microstrip-fed monopole antennas is reduced drastically. In addition, the coupling suppression provides extremely high similarity between the 3-D gain patterns of the antennas in the cloaked case to the isolated case as illustrated in Figures 3.21(b) and 3.21(c). Also, the 2-D linear gain patterns of the antennas for the isolated, coupled but uncloaked, and cloaked cases are plotted in Figure 3.22 in the H-plane (xy-plane) and E-plane (xz-plane) at $f = 2.98$ GHz and $f = 3.36$ GHz for Antenna I and Antenna II, respectively. The 2-D gain plots explicitly demonstrate that each of the antennas is affected by the presence of the other neighboring antenna in the uncloaked case and its radiation pattern is totally perturbed and highly directive, and thus, the antenna no longer can provide the desired radiation pattern as in the isolated case. However, in the cloaked case, the cloaks cancel this effect and make the antennas invisible to each other in a way that their patterns are recovered and improved.

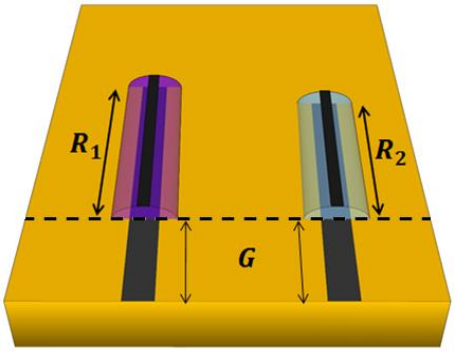

Figure 3.20 Schematics of Antenna I and Antenna II for the cloaked case.

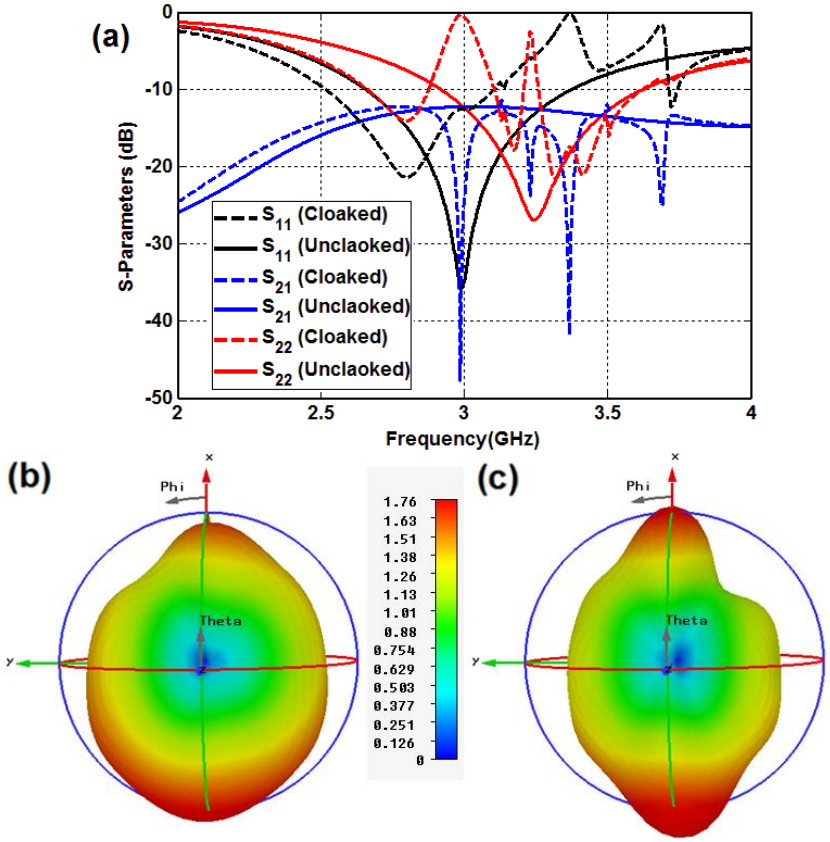

Figure 3.21 (a) S-parameters of the antennas for the coupled but uncloaked case and cloaked case. 3-D linear gain patterns of (b) Antenna I at 2.98 GHz and (c) Antenna II at 3.36 GHz.

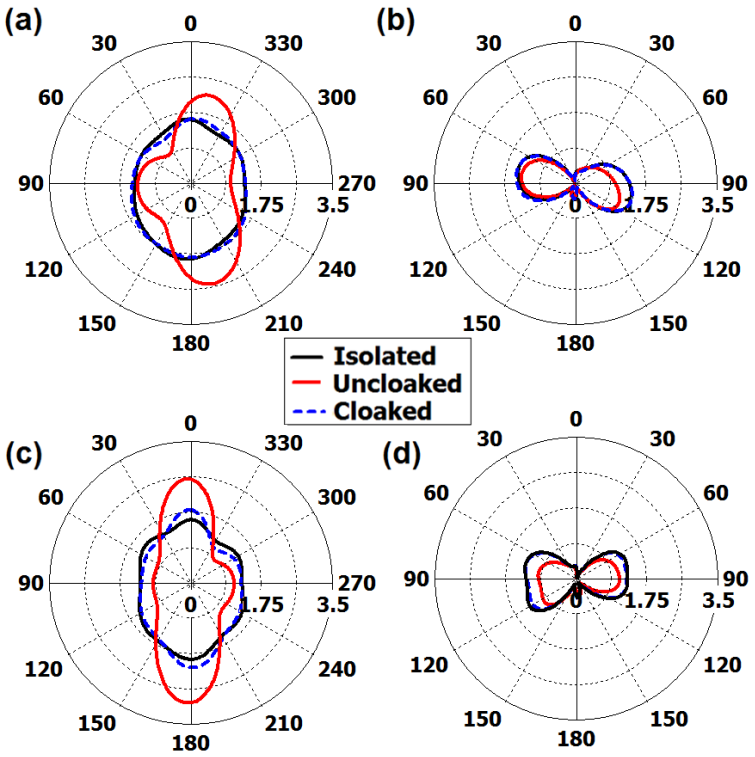

Figure 3.22 2-D linear gain patterns of Antenna I at 2.98 GHz (a) in the H-plane and (b) in the E-plane. Linear gain patterns of Antenna II at 3.36 GHz (c) in the H-plane and (d) in the E-plane.

Here, we present the time snapshots of the electric field distributions of the antennas in Figure 3.23 in order to show how the elliptically shaped metasurfaces change the distribution due to the cloaking phenomenon. A careful study of the distributions reveals the fact that by making the antennas invisible to each other, realized by wrapping the radiators with their own suitable metasurface cloaks, the perturbation of the radiating electric fields of each antenna will be resolved. Consequently, the electric field distribution for each antenna will resemble the one in the isolated case and the antennas do not sense the presence of each other. In contrast to this phenomenon, in the uncloaked case, the fields become intensively disturbed and a high level of mutual coupling will dominate the performance of each antenna. Besides, in Figure 3.24, a cross-section view of the electric field distributions of Antenna I at $z = 25$ mm is shown, wherein

Antenna I is active but Antenna II is passive. It is obvious that, in the cloaked case, Antenna II, which is covered by the conformal cloak designed for the resonance frequency of Antenna I, becomes hidden from the incoming waves originated from the excitation of Antenna I. However, in the uncloaked case, these electric fields will couple to the radiator of Antenna II, and undesirably, it receives the power transmitted by the other antenna.

Also, to conduct an investigation into the current distributions of the antennas and compare their behaviors for different cases in order to understand the effectiveness of the proposed cloaks more profoundly, the currents of the antennas for the top view are shown in Figure 3.25. It is worth noting that the mutual coupling and power interaction between the planar monopole antennas result in the induction of a surface current on the radiating element of the other neighboring antenna in the uncloaked case, and then, this current will be transferred to the port through the feed line and exacerbate the input impedance characteristics of it. On the other hand, the elliptical cloak structure of each antenna compensates the unwanted induced surface current by creating anti-phase surface currents, and thus, the input port of the neighboring antenna will not receive any signal. Accordingly, by suppressing the coupling between the antennas, provided by the mantle cloaks, the surface currents of the antennas will be similar to their currents in the isolated case. Besides, the total radiation efficiencies of the antennas are plotted in Figure 3.26. It is of paramount importance that by cloaking the antennas with the aforementioned properly designed elliptical metasurfaces, the total efficiency of each antenna will be reduced significantly at the resonance frequency of the other antenna and may be improved at its own resonance frequency, and thus, the antenna becomes a poor radiator at the frequency of the neighboring antenna, and at the same time, radiates similarly to the isolated case at its resonance frequency. Consequently, the presence of the

metasurfaces leads to the suppression of the far-field coupling between the antennas.

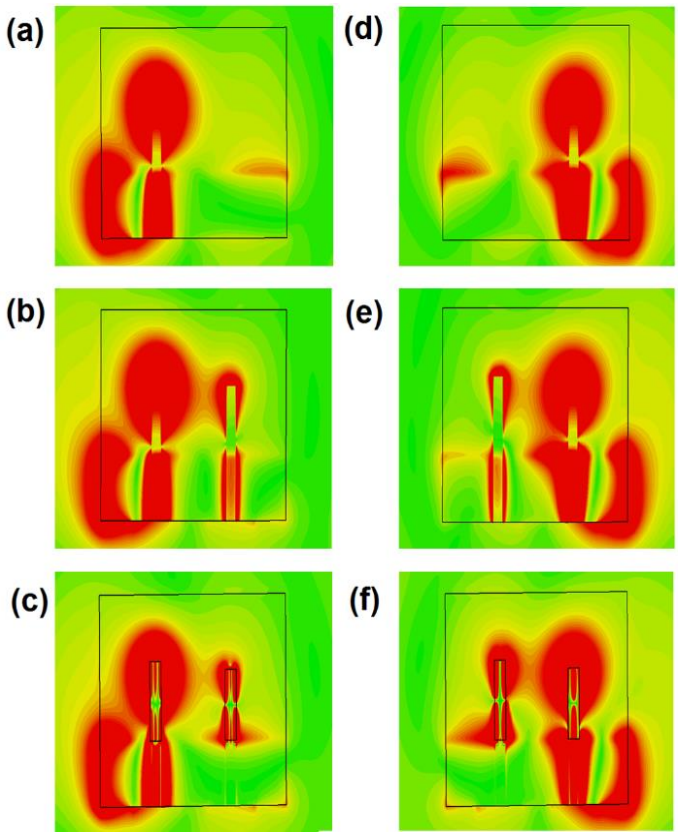

Figure 3.23 Snapshots of the electric field distributions of Antenna I at 2.98 GHz for (a) isolated, (b) uncloaked, and (c) cloaked cases. Snapshots of the electric field distributions of Antenna II at 3.36 GHz for (a) isolated, (b) uncloaked, and (c) cloaked cases.

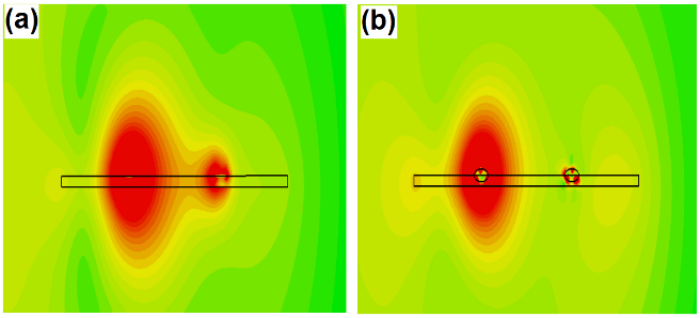

Figure 3.24 Cross-section view of the snapshots of the electric field distributions of Antenna I at 2.98 GHz and $z = 25$ mm for (a) uncloaked and (b) cloaked cases.

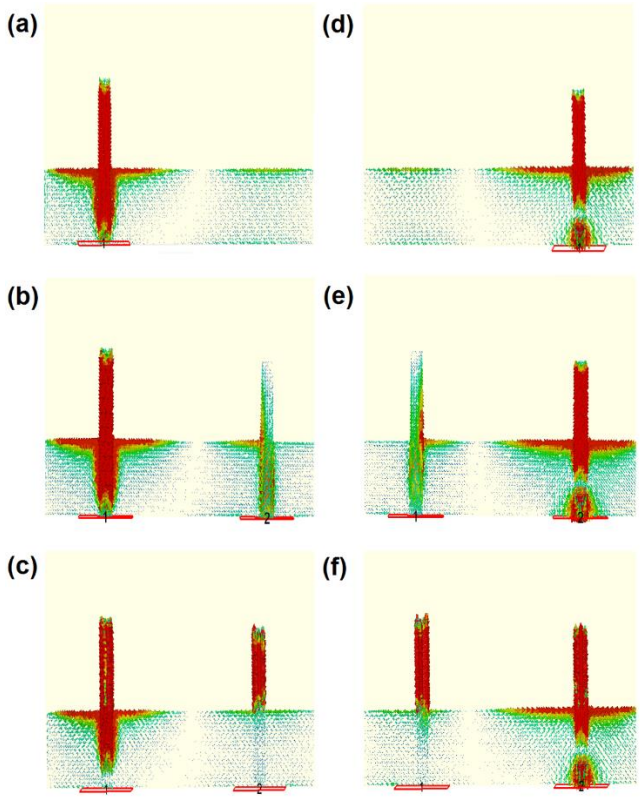

Figure 3.25 Current distributions of Antenna I at 2.98 GHz for (a) isolated, (b) uncloaked, and (c) cloaked cases. Current distributions of Antenna II at 3.36 GHz for (a) isolated, (b) uncloaked, and (c) cloaked cases.

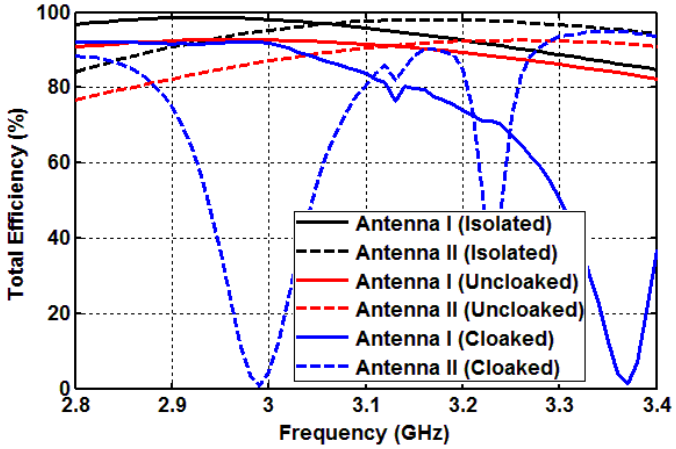

Figure 3.26 Total efficiencies of the antennas for the isolated, uncloaked, and cloaked cases.

3.4 Conclusion

In this chapter, we have proposed the use of the mantle cloaking method in order to make planar antennas invisible to each other, and thus, to suppress the mutual near-field coupling and far-field coupling drastically between two microstrip-fed monopole antennas in printed technology. It has been shown that by covering each antenna with an appropriately designed confocal elliptically shaped metasurface cloak, partially inserted in the substrate, the near-field coupling between the antennas has been reduced 25.5 dB and 29.5 dB, and the far-field coupling has been lowered 35.6 dB and 29 dB in terms of the mutual scattering parameter (S_{12}). Consequently, the matching characteristics and radiation patterns of the antennas have been improved and recovered in a way that the antennas in the cloaked case operate similarly to the isolated case.

REFERENCES

REFERENCES

[1] A. Alù and N. Engheta, "Cloaked near-field scanning optical microscope tip for noninvasive near-field imaging," *Phys. Rev. Lett.*, vol. 105, p. 263906, 2010.

[2] F. Billotti, S. Tricarico, F. Pierini, and L. Vegni, "Cloaking apertureless near-field scanning optical microscopy tips," *Optics Lett.*, vol. 36, pp. 211–213, 2011.

[3] A. Alù and N. Engheta, "Cloaking a sensor," *Phys. Rev. Lett.*, vol. 102, p. 233901, 2009.

[4] D. H. Kwon and D. H. Werner, "Restoration of Antenna Parameters in Scattering Environments Using Electromagnetic Cloaking," *Appl. Phys. Lett.*, vol. 92, p. 113507, 2008.

[5] J. B. Pendry, D. Schurig, and D. R. Smith, "Controlling electromagnetic fields," *Science*, vol. 312, no. 5781, pp. 1780–1782, 2006.

[6] U. Leonhardt, "Optical conformal mapping," *Science*, vol. 312, no. 5781, pp. 1777–1780, 2006.

[7] J. Li and J. B. Pendry, "Hiding under the carpet: A new strategy for cloaking," *Phys. Rev. Lett.*, vol. 101, p. 203901, 2008.

[8] D. Schurig, J. J. Mock, B. J. Justice, S. A. Cummer, J. B. Pendry, A. F. Starr, and D. R. Smith, "Metamaterial electromagnetic cloak at microwave frequencies," *Science*, vol. 314, no. 5801, pp. 977–980, 2006.

[9] P. Sheng, "Waves on the horizon," *Science*, vol. 313, no. 5792, pp. 1399–1400, 2006.

[10] Z. Ruan, M. Yan, C. W. Neff, and M. Qiu, "Ideal cylindrical cloak: Perfect but sensitive to tiny perturbations," *Phys. Rev. Lett.*, vol. 99, p. 113903, 2007.

[11] G. W. Milton and N. A. P. Nicorovici, "On the cloaking effects associated with anomalous localized resonances," *Proc. R. Soc. A.*, vol. 462, pp. 3027–3060, 2006.

[12] P. Alitalo, O. Lukkkonen, L. Jylha, J. Venermo, and S. A. Tretyakov, "Transmission-line networks cloaking objects from electromagnetic fields," *IEEE Trans. Antennas and Propag.*, vol. 56, no. 2, pp. 416–424, 2008.

[13] P. Alitalo and S. A. Tretyakov, "Broadband electromagnetic cloaking realized with transmission-line and waveguiding structures," *Proc. IEEE*, vol. 99, no. 10, pp. 1646–1659, 2011.

[14] S. A. Tretyakov, P. Alitalo, O. Lukkkonen, and C. Simovski, "Broadband electromagnetic cloaking of long cylindrical objects," *Phys. Rev. Lett.*, vol. 103, pp. 103905, 2009.

[15] A. Alù and N. Engheta, "Achieving transparency with plasmonic and metamaterial coatings," *Phys. Rev. E*, vol. 72, p. 016623, 2005.

[16] A. Alù and N. Engheta, "Plasmonic and metamaterial cloaking: physical mechanisms and potentials," *J. Opt. A: Pure Appl. Opt.*, vol. 10, p. 093002, 2008.

[17] S. Tricarico, F. Bilotti, A. Alù, and L.Vegni, "Plasmonic cloaking for irregular objects with anisotropic scattering properties," *Phys. Rev. E*, vol. 81, p. 026602, 2010.

[18] B. Edwards, A. Alù, M. E. Young, M. Silveirinha, and N. Engheta, "Experimental verification of epsilon-near-zero metamaterial coupling and energy squeezing using a microwave waveguide," *Phys.Rev. Lett.*, vol. 100, p. 033903, 2008.

[19] A. Alù, D. Rainwater, and A. Kerkhoff, "Plasmonic cloaking of cylinders: finite length, oblique illumination and cross-polarization coupling," *New. J. Phys.*, vol. 12, pp. 103028, 2010.

[20] F. Bilotti, S. Tricarico, and L.Vegni, "Plasmonic metamaterial cloaking at optical frequencies," *IEEE Trans. Nanotech.*, vol. 9, no. 1, pp. 55–61, 2010.

[21] A. Alù, "Mantle cloak: Invisibility induced by a surface," *Phys. Rev. B*, vol. 80, p. 245115, 2009.

[22] P. Y. Chen and A. Alù, "Mantle cloaking using thin patterned metasurfaces," *Phys. Rev. B.*, vol. 84, p. 205110, 2011.

[23] P. Y. Chen, F. Monticone, and A. Alù, "Suppressing the electromagnetic scattering with an helical mantle cloak," *IEEE Antennas Wireless Propag. Lett.*, vol. 10, pp. 1598–1601, 2011.

[24] P. Y. Chen, C. Argyropoulos, and A. Alù, "Broadening the cloaking bandwidth with non-foster metasurfaces," *Phys. Rev. Lett.*, vol. 111, p. 233001, 2013.

[25] L. Matekovits, T. S. Bird, "Width-modulated microstrip-line based mantle cloaks for thin single- and multiple cylinders", *IEEE Trans. Antennas and Propag.*, vol. 62, no. 5, pp. 2606–2615, 2014.

[26] Y. R. Padooru, A. B. Yakovlev, P. Y. Chen, and A. Alù, "Analytical modeling of conformal mantle cloaks for cylindrical objects using sub-wavelength printed and slotted arrays," *J. Appl. Phys.*, vol. 112, p. 0349075, 2012.

[27] Y. R. Padooru, A. B. Yakovlev, P. Y. Chen, and A. Alù, "Line-source excitation of realistic conformal metasurface cloaks," *J. Appl. Phys.*, vol. 112, p. 104902, 2012.

[28] Z. H. Jiang and D. H. Werner, "Exploiting metasurface anisotropy for achieving near-perfect low-profile cloaks beyond the quasi-static limit," *J. Phys. D: Appl. Phys.*, vol. 46, p. 505306, 2013.

[29] K. S. Novoselov, A. K. Geim, S. V. Morozov, D. Jiang, Y. Zhang, S. V. Dubonos, I. V. Grigorieva, and A. A. Firsov, "Electric field effect in atomically thin carbon films," *Science*, vol. 306, no. 5696, pp. 666–669, 2004.

[30] I. F. Akyildiz, and J. M. Jornet, "The internet of nano-things," *IEEE Wirel. Commun. Mag.*, vol. 17, no. 6, pp. 58–63, 2010.

[31] Q. Bao, H. Zhang, B. Wang, Z. Ni, C. Haley, Y. X. Lim, Y. Wang, D. Y. Tang, and K. P. Loh, "Broadband graphene polarizer," *Nature Photon.*, vol. 5, pp. 411–415, 2011.

[32] M. Liu, X. B. Yin, E. Ulin-Avila, B. S. Geng, T. Zentgraf, L. Ju, F. Wang, and X. Zhang, "A graphene-based broadband optical modulator," *Nature*, vol. 474, no. 7349, pp. 64–67, 2011.

[33] P. Y. Chen, C. Argyropoulos, and A. Alù, "Terahertz antenna phase shifters using integrally-gated graphene transmission-lines," *IEEE Trans. Antennas and Propag.*, vol. 61, no. 4, pp. 1528–1537, 2013.

[34] E. Carrasco and J. Perruisseau-Carrier, "Reflectarray antenna at terahertz using graphene," *IEEE Antennas Wireless Propag. Lett.*, vol. 12, pp. 253–256, 2013.

[35] G. W. Hanson, "Dyadic Green's functions and guided surface waves for a surface conductivity model of graphene," *J. Appl. Phys.*, vol. 103, p. 064302, 2008.

[36] P. Y. Chen and A. Alù, "Atomically-thin surface cloak using graphene monolayers," *ACS Nano*, vol. 5, pp. 5855–5863, 2011.

[37] Y. R. Padooru, A. B. Yakovlev, C. S. R. Kaipa, G. W. Hanson, F. Medina, and F. Messa, "Dual capacitive-inductive nature of periodic graphene patches: Transmission characteristics at lowterahertz frequencies", *Phys. Rev. B*, vol. 87, pp. 115401, 2013.

[38] P. Y. Chen, J. Soric, Y. R. Padooru, H. M. Bernety, A. B. Yakovlev, and A. Alù, "Nanostructured graphene metasurface for tunable terahertz cloaking," *New. J. Phys*., vol. 15, pp. 123029, 2013.

[39] V. P. Chumachenko, "Domain product technique solution for the problem of electromagnetic scattering from multiangular composite cylinders," *IEEE Trans. Antennas and Propag.*, vol. 51, no. 10, pp. 2845–2851, 2003.

[40] H. M. Bernety and A. B. Yakovlev, "Reduction of mutual coupling between neighboring strip dipole antennas using confocal elliptical metasurface cloaks," *IEEE Trans. Antennas and Propag.*, vol. 63, no. 4, pp. 1554–1563, 2015.

[41] P. M. Morse and H. Feshbach, *Methods of Theoretical Physics*. New York, McGraw-Hill, 1953.

[42] Computer Simulation Technology (CST) Microwave Studio 2012 (www.cst.com)

[43] A. Alù and N. Engheta, "Cloaking and transparency for collections of particles with metamaterial and plasmonic covers," *Opt. Express*, vol. 15, pp. 7578–7590, 2007.

[44] Cojocaru E (arXiv:0808.2123v1)

[45] A. Monti, F. Bilotti, and A. Toscano, "Optical cloaking of cylindrical objects by using covers made of core-shell nanoparticles," *IEEE Trans. Nanotech.*, vol. 9, no. 1, pp. 55–61, 2010.

[46] A. Monti, F. Bilotti, A. Toscano, and L. Vegni, "Possible implementation of epsilon-near-zero metamaterials working at optical frequencies," *Opt. Commun.*, vol. 285, pp. 3412–3418, 2012.

[47] R. C. Mitchell-Thomas, T. M. McManus, O. Quevedo-Teruel, S. A. R. Horsley, and Y. Hao, "Perfect surface wave cloaks," *Phys. Rev. Lett.*, vol. 111, p. 213901, 2013.

[48] J. Wang, S. Qu, Z. Xu, H. Ma, J. Zhang, Y. Li, and X. Wang, "Super-thin cloaks based on microwave networks," *IEEE Trans. Antennas and Propag.*, vol. 61, no. 2, pp. 748–754, 2013.

[49] C. A. Valagiannopoulos, P. Alitalo, and S. A. Tretyakov, "On the minimal scattering response of PEC cylinders in a dielectric cloak," *IEEE Antennas Wireless Propag. Lett.*, vol. 13, pp. 403–406, 2014.

[50] H. M. Bernety and A. B. Yakovlev, "Conformal and confocal mantle cloaking of elliptical cylinders using sub-wavelength metallic meshes and patches," *IEEE APS Int. Symp.*, pp. 1433–1434, 2014.

[51] H. M. Bernety and A. B. Yakovlev, "Cloaking of dielectric and metallic elliptical cylinders with a nanostructured graphene metasurface," *IEEE APS Int. Symp.*, pp. 890–891, 2014.

[52] H. M. Bernety and A. B. Yakovlev, "Metasurface cloaks for dielectric and metallic elliptical cylinders and strips," *IEEE International Conference on Electromagnetics in Advanced Applications (ICEAA 2014)*, pp. 496–499, 2014.

[53] A. B. Yakovlev and H. M. Bernety, "Nanostructured graphene metasurface for terahertz cloaking of elliptical cylinders and metallic strips," *IEEE 8thInternational Congress on Advanced Electromagnetic Materials in Microwaves and Optics (Metamaterials 2014)*, 2014.

[54] P. S. Kildal, A. A. Kishk, and A. Tengs, "Reduction of forward scattering from cylindrical objects using hard surfaces," *IEEE Trans. Antennas and Propag.*, vol. 44, no. 11, pp. 1509–1520, 1996.

[55] M. Riel, Y. Brand, Y. Demers, and P. D. Maagt, "Performance improvement of center-fed reflector antennas using low scattering struts," *IEEE Trans. Antennas and Propag.*, vol. 60, no. 3, pp. 1269–1280, 2012.

[56] P. Alitalo, C. Valagiannopoulos, and S. A. Tretyakov, "Simple cloak for antenna blockage reduction," *Proc. IEEE APS Int. Symp.*, pp. 669–672, 2011.

[57] P. Alitalo, J. Vehmas, and S. A. Tretyakov, "Reduction of antenna blockage with a transmission-like cloak," *Proc. 5th EuCAP*, pp. 2399–2402, 2011.

[58] F. Yang and Y. Rahmat-Samii, "Microstrip antennas integrated with electromagnetic band-gap (EBG) structures: A low mutual coupling design for array applications," *IEEE Trans. Antennas and Propag.*, vol. 51, no. 10, pp. 2936–2946, 2003.

[59] C. A. Valagiannopoulos and N. L. Tsitsas, "Integral equation analysis of a low-profile receiving planar microstrip antenna with a cloaking superstrate," *Radio Sci.*, vol. 47, 2012.

[60] J. Soric, R. Fleury, A. Monti, A. Toscano, F. Bilotti, and A. Alù, "Controlling scattering and absorption with metamaterial covers," *IEEE Trans. Antennas and Propag.*, vol. 62, no. 8, pp. 4220–4229, 2014.

[61] A. Monti, J. Soric, A. Alù, F. Bilotti, A. Toscano, and L. Vegni, "Overcoming mutual blockage between neighboring dipole antennas using a low-profile patterned metasurface," *IEEE Antennas Wireless Propag. Lett.*, vol. 11, pp. 1414–1417, 2012.

[62] A. Monti, J. Soric, R. Fleury, A. Alù, A. Toscano, and F. Bilotti, "Mantle cloaking and related applications in antennas," *IEEE International Conference on Electromagnetics in Advanced Applications (ICEAA 2014)*, pp. 878–881, 2014.

[63] O. Luukkonen, C. Simovski, G. Granet, G. Goussetis, D. Lioubtchenko, A. V. Räisänen, and S. A. Tretyakov, "Simple and accurate analytical model of planar grids and high-impedance surfaces compromising metal strips or patches," *IEEE Trans. Antennas and Propag.*, vol. 56, no. 6, pp. 1624–1632, 2008.

[64] J. Soric, P. Y. Chen, A. Kerkhoff, D. Rainwater, K. Melin, and A. Alù, "Demonstration of an ultralow profile cloak for scattering suppression of a finite-length rod in free space," *New. J. Phys.*, vol. 15, pp. 033037, 2013.

[65] H. M. Bernety and A. B. Yakovlev, "Cloaking of single and multiple elliptical cylinders and strips with confocal elliptical nanostructured graphene metasurface," *J. Phys.: Condens. Matter*, vol. 18, p. 185304, 2015.

[66] S.-S. Lee, H.-S. Park, J.-G. Bang, and H.-T. Kim, "Coupling reduction between slanted shipboard antennas," *Microw. Opt. Technol. Lett.*, vol. 33, pp. 37–40, 2002.

[67] H. M. Bernety and A. B. Yakovlev, "Reduction of mutual coupling between neighboring strip dipole antennas using confocal elliptical metasurface cloaks," *IEEE Trans. Antennas and Propag.*, vol. 63, no. 4, pp. 1554–1563, 2015.

[68] M. M. Nikolic, A. R. Djordjevic, and A. Nehorai, "Microstrip antennas with suppressed radiation in horizontal directions and reduced coupling," *IEEE Trans. Antennas and Propag.*, vol. 53, pp. 3469–3476, 2005.

[69] M. A. Khayat, J. T. Williams, D. R. Jackson, and S. A. Long, "Mutual coupling between reduced surface-wave microstrip antennas", *IEEE Trans. Antennas and Propag.*, vol. 48, no. 10, 2000.

[70] Yu, A. and X. Zhang, "A novel method to improve the performance of microstrip antenna arrays using a dumbbell EBG structure," *IEEE Antennas Wireless Propag. Lett.*, vol. 2, no. 1, 170–172, 2003.

[71] Z. Iluz, R. Shavit, and R. Bauer, "Microstrip antenna phased array with electromagnetic band gap substrate," *IEEE Trans. Antennas Propag.*, vol. 52, no. 6, 1446–1453, 2004.

[72] E. Rajo-Iglesias, O. Quevedo-Teruel, and L. Inclan-Sanchez, "Mutual coupling reduction in patch antenna arrays by using a planar EBG structure and a multilayer dielectric substrate," *IEEE Trans. Antennas Propag.*, vol. 56, no. 6, 1648–1655, 2008.

[73] H. S. Farahani, M. Veysi, M. Kamyab, and A. Tadjalli, "Mutual coupling reduction in patch antenna arrays using a UC-EBG superstrate," *IEEE Antennas Wireless Propag. Lett.*, vol. 9, 57–59, 2010.

[74] M. Coulombe, S. F. Koodiani, and C. Caloz, "Compact elongated mushroom (EM)-EBG structure for enhancement of patch antenna array performances," *IEEE Trans. Antennas Propag.*, vol. 58, no. 4, pp. 1076–1086, 2010.

[75] S. Assimonis, T. Yioultsis, and C. Antonopoulus, "Design and optimization of uniplanar EBG structures for low profile antenna applications and mutual coupling reduction," IEEE Trans. Antennas Propag., vol. 60, no. 10, pp. 4944–4949, 2012.

[76] M. salehi and A. Tavakoli, "A novel low mutual coupling microstrip antenna array design using defected ground structure," *Int. J. Electron Commun.*, vol. 60, no. 10, pp. 718–723, 2006.

[77] Mandal, M. K. and S. Sanyal, "A novel defected ground structure for planar circuits," *IEEE Microw. Wireless Comp. Lett.*, vol. 16, no. 2, 93–95, 2006.

[78] F.-G. Zhu, J.-D. Xu, and Q. Xu, "Reduction of mutual coupling between closely-packed antenna elements using defected ground structure," *Electron. Lett.*, vol. 45, no. 12, pp. 601–602, 2009.

[79] J. Ou Yang, F. Yang, and Z. M. Wang, "Reducing mutual coupling of closely spaced microstrip MIMO antennas for WLAN application," *IEEE Antennas Wireless Propag. Lett.*, vol. 10, pp. 310–312, 2011.

[80] C. K. Ghosh, B. Mandal, and S. K. Parui, "Mutual coupling reduction of a dual-frequency microstrip antenna array using U-shaped DGS and inverted U-shaped microstrip resonator," *Progress In Electromagnetic Research C*, vol. 48, 61–68, 2014.

[81] D. Guha, M. Biswas, and Y. M. M. Antar, "Microstrip patch antenna with defected ground structure for cross polarization suppression," *IEEE Antennas and Wireless Propag. Lett.*, vol. 4, pp. 455–458, 2005.

[82] R. Dehdasht-Heydari and M. Naser-Moghadasi, "Introduction of a novel technique for the reduction of cross polarization of rectangular microstrip patch antenna with elliptical DGS," *Journal of Electromagnetic Waves and Applications*, vol. 22, no. 8-9, pp. 1214–1222, 2008.

[83] F. Y. Zulkifli, E. T. Rahardjo, and D. Hartanto, "Mutual coupling reduction using dumbbell defected ground structure for multiband microstrip antenna array," *Progress In Electromagnetic Research Letters*, vol. 5, pp. 29–40, 2010.

[84] J. Zhu and G. V. Eleftheriades, "A simple approach for reducing mutual coupling in two closely spaced metamaterial-inspired monopole antennas," *IEEE Antennas and Wireless Propag. Lett.*, vol. 9, pp. 379–382, 2010.

[85] C.Y. Chiu, C.H. Cheng, R.D. Murch, and C.R. Rowell, "Reduction of mutual coupling between closely-packed antenna elements," *IEEE Trans. Antennas Propag.*, vol. 55, no. 6, pp. 1732–1738, 2007.

[86] M. M. Bait-Suwailam, O. F. Siddiqui, and O. M. Ramahi, "Mutual coupling reduction between microstrip patch antennas using slotted-complementary split-ring resonators," *IEEE Antennas Wireless Propag. Lett.*, vol. 9, 876–878, 2010.

[87] A. Habashi, J. Nourinia, and C. Ghobadi, “Mutual coupling reduction between very closely spaced patch antennas using low-profile folded split-ring resonators,” *IEEE Antennas Wireless Propag. Lett.*, vol. 10, 862–865, 2011.

[88] S. Farsi, H. Aliakbarian, B. Nauwelaers, and G. A. E. Vandenbosch, “Mutual coupling reduction between planar antenna by using a simple microstrip U-section,” *IEEE Antennas Wireless Propag. Lett.*, vol. 11, 1501–1503, 2012.

[89] C. K. Ghosh and S. K. Parui, “Reduction of mutual coupling between E-shaped microstrip antenna array by using a simple microstrip I-section,” *Microwave and Optical Technology Letter*, vol. 55, no. 11, 2544–2549, 2013.

APPENDIX

APPENDIX

Here, we present the analytical formulation of the electromagnetic scattering problem in detail. For the sake of brevity, we present the analytical expressions only for the metallic elliptical cylinder shown in Figure 1.1(c). The boundary conditions are as following:

$$E_z^t|_{u=u_1} = 0 \tag{A.1}$$

$$E_z^i\big|_{u=u_0^+} + E_z^s|_{u=u_0^+} = E_z^t|_{u=u_0^-} \tag{A.2}$$

$$E_z^t|_{u=u_0^-} = Z_s\left[H_v^i\big|_{u=u_0^+} + H_v^s|_{u=u_0^+} - H_v^t|_{u=u_0^-}\right]. \tag{A.3}$$

Then, by considering the electric and magnetic fields presented in equations (1.4), (1.5), (1.6), (1.7), and the boundary conditions we obtain:

$$b_{pm}J_{pm}(q_1,u_1,n) + c_{pm}Y_{pm}(q_1,u_1,n) = 0 \tag{A.4}$$

$$\sqrt{8\pi}\sum_n j^{-n}\left[\frac{J_{pm}(q_0,u_0,n)}{N_{pm}(q_0,n)} + a_{pm}H_{pm}^{(1)}(q_0,u_0,n)\right] \times S_{pm}(q_0,v,n)\,S_{pm}(q_0,\varphi,n) =$$

$$\sqrt{8\pi}\sum_n j^{-n}\left[b_{pm}J_{pm}(q_1,u_0,n) + c_{pm}Y_{pm}(q_1,u_0,n)\right] \times S_{pm}(q_1,v,n)\,S_{pm}(q_0,\varphi,n) \tag{A.5}$$

$$Z_s\left\{\frac{j\sqrt{8\pi}}{\omega\mu h}\sum_n j^{-n}\left[\frac{J'_{pm}(q_0,u_0,n)}{N_{pm}(q_0,n)} + a_{pm}H_{pm}^{(1)'}(q_0,u_0,n)\right] \times S_{pm}(q_0,v,n)\,S_{pm}(q_0,\varphi,n) -\right.$$

$$\left.\frac{j\sqrt{8\pi}}{\omega\mu h}\sum_n j^{-n}\left[b_{pm}J'_{pm}(q_1,u_0,n) + c_{pm}Y'_{pm}(q_1,u_0,n)\right] \times S_{pm}(q_1,v,n)S_{pm}(q_0,\varphi,n)\right\}$$

$$= \sqrt{8\pi}\sum_n j^{-n}\left[b_{pm}J_{pm}(q_1,u_0,n) + c_{pm}Y_{pm}(q_1,u_0,n)\right] \times S_{pm}(q_1,v,n)S_{pm}(q_0,\varphi,n)\,. \tag{A.6}$$

It should be noted that the prime indicates the derivative of the functions with respect to

the variable u.

Then, we multiply both sides in equations (A.5) and (A.6) by the Mathieu angular function $S_{pm'}(q_0, v, n)$ and use the orthogonality relations of angular Mathieu functions in order to obtain three independent equations by considering the normalization and correlation factors provided in Ref. [44] as below:

$$\int_0^{2\pi} S_{pm'}(q_0, v, n)\, S_{pm}(q_0, v, n) = N_{pm}(q_0, n)\, \delta_{mm'} \tag{A.7.1}$$

$$\int_0^{2\pi} S_{pm'}(q_0, v, n)\, S_{pm}(q_0, v, n) = \gamma_{pm}(n)\, \delta_{mm'}. \tag{A.7.2}$$

where $\delta_{mm'}$ equals 1 if $m = m'$ and equals 0 otherwise. On the other hand, by considering the scale factor equal to $h = F\sqrt{\cosh^2 u - \cos^2 v}$, we define two more co- and cross- factors $N^*_{pm}(q_0, n)$ and $\gamma^*_{pm}(n)$ as follows:

$$\int_0^{2\pi} \frac{S_{pm}(q_0,v,n)\, S_{pm'}(q_0,v,n)}{\sqrt{\cosh^2 u_0 - \cos^2 v}}\, dv = N^*_{pm}(q_0, n)\, \delta_{mm'} \tag{A.7.3}$$

$$\int_0^{2\pi} \frac{S_{pm}(q_1,v,n)\, S_{pm'}(q_0,v,n)}{\sqrt{\cosh^2 u_0 - \cos^2 v}}\, dv = \gamma^*_{pm}(n)\, \delta_{mm'} \tag{A.7.4}$$

Finally, we come to a matrix equation for each order n:

$$A\, X = B \tag{A.8.1}$$

where the matrices X (the matrix of unknown coefficients to be found) and B are,

$$X = \begin{bmatrix} a_{pm} \\ b_{pm} \\ c_{pm} \end{bmatrix},\ B = \begin{bmatrix} 0 \\ -\frac{J_{pm}(q_0,u,n)}{N_{pm}} \\ -\frac{J'_{pm}(q_0,u,n)}{N_{pm}} \end{bmatrix} \tag{A.8.2}$$

and the matrix A can be written as:

$$A = \begin{bmatrix} A_{11} & A_{12} & A_{13} \\ A_{21} & A_{22} & A_{23} \\ A_{31} & A_{32} & A_{33} \end{bmatrix} \tag{A.8.3}$$

with

$$A_{11} = 0 \tag{A.8.4}$$

$$A_{12} = J_{pm}(q_1, u_1, n) \tag{A.8.5}$$

$$A_{13} = Y_{pm}(q_1, u_1, n) \tag{A.8.6}$$

$$A_{21} = H_{pm}^{(1)}(q_0, u_0, n) \tag{A.8.7}$$

$$A_{22} = -\frac{\gamma_{pm}}{N_{pm}} J_{pm}(q_1, u_0, n) \tag{A.8.8}$$

$$A_{23} = -\frac{\gamma_{pm}}{N_{pm}} Y_{pm}(q_1, u_0, n) \tag{A.8.9}$$

$$A_{31} = H_{pm}^{(1)'}(q_0, u_0, n) \tag{A.8.10}$$

$$A_{32} = -\frac{\gamma_{pm}^*}{N_{pm}^*} J'_{pm}(q_1, u_0, n) + \frac{\gamma_{pm}}{N_{pm}^*} \frac{j\omega\mu F}{Z_s} J_{pm}(q_1, u_0, n) \tag{A.8.11}$$

$$A_{33} = -\frac{\gamma_{pm}^*}{N_{pm}^*} Y'_{pm}(q_1, u_0, n) + \frac{\gamma_{pm}}{N_{pm}^*} \frac{j\omega\mu F}{Z_s} Y_{pm}(q_1, u_0, n). \tag{A.8.12}$$

VITA

Hossein Mehrpourbernety (Hossein M. Bernety) was born in Sary, Iran, in September 1987. He received his B.Sc. degree in Electrical Engineering-Communications from the Ferdowsi University of Mashhad, Mashhad, Iran, in 2010, and the M.Sc. degree in Electrical Engineering-Communications from Babol Noshirvani University of Technology, Babol, Iran, in 2013.

From 2013 to 2015, he worked as a research assistant at the University of Mississippi, where he pursued his M.Sc. degree in Electrical Engineering-Electromagnetics. His main research interests include electromagnetic scattering, cloaking, antennas, and antenna arrays.

Mr. Mehrpourbernety is a student member of Institute of Electrical and Electronics Engineers (IEEE). He was the recipient of the Honorable Mention Award in the student paper competition held at the 2014 IEEE International Symposium on Antennas and Propagation (APS), Memphis. In recognition of his active research work, Mr. Mehrpourbernety received the University of Mississippi Graduate Research Award in 2015.

JOURNAL PUBLICATIONS:

- H. M. Bernety, R. Chinnambeti, and A. B. Yakovlev, "Elliptical Metasurface Cloaks in Printed Technology – Reduction of Mutual Coupling between Microstrip-fed Monopole Antennas," *IEEE Transactions on Antennas and Propagation*, ***under review***.
- A. Forouzmand, H. M. Bernety, and A. B. Yakovlev, "Graphene Loaded Wire Medium for Tunable Broadband Subwavelength Imaging," *Physical Review B,* **under review.**
- H. M. Bernety and A. B. Yakovlev, "Cloaking of Single and Multiple Elliptical Cylinders and Strips with Confocal Elliptical Nanostructured Graphene Metasurface," *Journal of Physics: Condensed Matter*, vol. 27, p. 185304, April 2015.
- H. M. Bernety and A. B. Yakovlev, "Reduction of Mutual Coupling between Neighboring Strip Dipole Antennas Using Confocal Elliptical Metasurface Cloaks," *IEEE Transactions on Antennas and Propagation*, vol.63, no. 4, pp. 1554–1563, April 2015.
- P. Y. Chen, J. Soric, Y. R. Padooru, H. M. Bernety, A. B. Yakovlev, and A. Alú, "Nanostructured Graphene Metasurface for Tunable Terahertz Cloaking," *New Journal of Physics*, vol. 15, p. 123029, December 2013.
- R. Gholami, B. Zakeri, and H. M. Bernety, "Design and Analysis of New Ultra-wideband Antenna Linear Array Antenna for Wireless Applications," *Amirkabir International Journal of Science and Research*, vol.44, no. 2, pp. 11–19, 2012.
- H. M. Bernety, B. Zakeri, and R. Gholami, "Design of A Novel Directional Microstrip-fed Superwideband Antenna," *Modares Journal of Electrical Engineering*, vol.11, no. 3, pp. 13–18, 2011.
-

CONFERENCE PUBLICATIONS AND PRESENTATIONS:

- H. M. Bernety, R. Chinnambeti, and A. B. Yakovlev, "Elliptical Metasurface Cloaks in Printed Technology – Reduction of Mutual Coupling in Closely Spaced Planar Antennas," *IEEE 9th International Congress on Advanced Electromagnetic Materials in Microwaves and Optics (METACongress 2015),* ***accepted***.

- H. M. Bernety and A. B. Yakovlev, "Mutual Coupling Reduction between Neighboring Strip Dipole Antennas Using Confocal Elliptical Metasurfaces," *IEEE 9th European Conference on Antennas and Propagation (EuCAP 2015),* April 2015, ***accepted***.

- H. M. Bernety and A. B. Yakovlev "Mutual Coupling Reduction Between Neighboring Strip Monopole Antennas Using Confocal Elliptical Cloak Metasurfaces," *Poster Presentation at BWAC Workshop,* January 2015.

- B. Yakovlev and H. M. Bernety "Reduction of Mutual Coupling in Closely Spaced Strip Dipole Antennas with Elliptical Metasurfaces," ***Keynote Talk*** *at BWAC Workshop,* January 2015.

- B. Yakovlev and H. M. Bernety, "Nanostructured Graphene Metasurface for Terahertz Cloaking of Elliptical Cylinders and Metallic Strips," *IEEE 8thInternational Congress on Advanced Electromagnetic Materials in Microwaves and Optics (METACongress),* pp. 298–300*, 2014 (****Invited Paper****).*

- H. M. Bernety and A. B. Yakovlev, "Metasurface Cloaks for Dielectric and Metallic Elliptical Cylinders and Strips," *IEEE International Conference Electromagnetic Advanced Applications (ICEAA 2014),* pp. 496–499, 2014 *(****Invited Paper****).*

- H. M. Bernety and A. B. Yakovlev, "Cloaking of Dielectric and Metallic Elliptical Cylinders with a Nanostructured Graphene Metasurface," *IEEE AP-S International Symposium on Antennas and Propagation*, pp. 890–891, 2014 ***(Honorable Mention Award)***.

- H. M. Bernety and A. B. Yakovlev, "Conformal and Confocal Mantle Cloaking of Elliptical Cylinders using Sub-Wavelength Metallic Meshes and Patches," *IEEE AP-S International Symposium on Antennas and Propagation*, pp. 1433–1434, 2014.

- H. M. Bernety, R. Gholami, B. Zakeri, and M. Rostamian, "Linear Antenna Array Design for UWB Radar," *IEEE RADAR Conference (RADARCON 2013)*, pp. 1–4, May 2013.

- H. M. Bernety, B. Zakeri, and R. Gholami, "A Compact Directional Super-wideband Antenna," *IEEE 21st Iranian Conference on Electrical Engineering (ICEE2013)*, pp. 1–4, May 2013.

- R. Gholami, H. Mehrpourbernety, and B. Zakeri, "UWB Phased Array Antennas for High Resolution Radars," *Proceedings of the 2013 International Symposium on Electromagnetic Theory (URSI-EMTS 2013)*, pp. 532–535, May 2013.

- H. M. Bernety, B. Zakeri, and A. Ebrahimzadeh, "A Novel Partially Grounded Super-wideband Antenna," *Proceedings of IEEE International Conference on Ultra-Wideband (ICUWB 2012)*, pp. 435–438, September 2012.

- H. M. Bernety and B. Zakeri, "A New Partially Grounded Slotted Ultra-Wideband Antenna with WLAN Band-rejection," *IEEE 20th Telecommunication Forum (TELFOR 2012)*, pp. 1153–1155, November 2012.

- H. M. Bernety, B. Zakeri, and I. Kalantari, "A Novel Frog-eye Band-notched Ultra-wideband Antenna," *IEEE Radar Conference (RADARCON 2012)*, pp. 0676 –0680, May 2012.
- A. S. Rostami, H. M. Bernety, and A. R. Hosseinabadi, "A Novel and Optimized Algorithm to Select Monitoring Sensors by GSA," *IEEE 2nd International Conference on Control, Instrumentation, and Automation (ICCIA)*, pp. 829–834, December 2011.
- A. S. Rostami, K Nosrati, and H. M. Bernety, "Optimizing the Parameters of Active Sensor Selection and Using GA to Decrease Energy Consumption in Point Coverage Wireless Sensor Networks," *IEEE 6th International Conference on Wireless Communication and Sensor Networks (WCSN)*, pp. 1–6, December 2010.
- A. S. Rostami, M. R. Tanhatalab, and H. M. Bernety, "Decreasing the Energy Consumption by a Distribution Classification New Algorithm in Choosing the Best Sensor Node in Wireless Sensor Network with Point Coverage," *IEEE International Conference on Computational Intelligence and Communication Networks (CICN)*, pp. 269–274, November 2010.
- A. S. Rostami, M. R. Tanhatalab, and H. M. Bernety, "Novel Algorithm of Energy-Aware in Asymmetric Wireless Sensor Networks Routing for In-Point Coverage," *IEEE International Conference on Computational Intelligence and Communication Networks (CICN)*, pp. 308–313, November 2010.